Addis Ababa University

Addis Ababa Institute of Technology

School of Mechanical & Industrial Engineering

The Analysis of Creepage at the Wheel-Rail Interface for Light Rail Transit

A Thesis Submitted to the School of Graduate Studies of Addis Ababa Institute of Technology, Addis Ababa University in partial fulfillment of the Requirement for the Degree of Master of Science in Mechanical Engineering (Mechanical Design)

By: Gemechis Edosa

Advisor: Dr. Samuel Tesfaye

Addis Ababa, Ethiopia

Oct, 2023

Addis Ababa University

Addis Ababa Institute of Technology
School of Graduate Studies

School of Mechanical and Industrial Engineering

The Analysis of Creepage at the Wheel-Rail Interface for Light Rail Transit

By

Gemechis Edosa

Approved by the Board of Examiners:

Dr. Samuel Tesfaye	____________________	_____________
Advisor Name	Signature	Date
Dr. Araya Abera	____________________	_____________
Internal Examiner	Signature	Date
Mr. Behailu Mamo	____________________	_____________
External Examiner	Signature	Date
Dr. Araya Abera	____________________	_____________
School Dean	Signature	Date
Dr. Sosina Mengistu	____________________	_____________
Associate Director for PG Program	Signature	Date

Declaration

I affirm that the content discussed in this thesis titled "The Analysis of Creepage at the Wheel-Rail Interface for Light Rail Transit" is exclusively my own work, never submitted to any other educational institution. Additionally, I duly acknowledge all the resources and materials utilized during the completion of this thesis.

_________________________ __________________________

Gemechis Edosa Date

I confirm that, to the best of my understating, the declaration made by the candidate above is accurate.

________________________________ __________________________

Dr. Samuel Tesfaye (Advisor) Date

ACKNOWLEDGMENTS

First of all, I would like to express my gratitude to Almighty God for providing assistance in all aspects of my journey, from beginning to end.

Next, I would like to extend a special thanks to my advisor, Dr. Samuel Tesfaye, for his invaluable advice and guidance throughout my research.

Thirdly, I would like to express my sincere appreciation to the members of the Addis Ababa Railway Light Transit technician team for their understanding and exceptional assistance during the course of my study.

I would also like to thank Mr. Kejela T. and his staff members for their support and help throughout this endeavor.

Finally, I would like to express my heartfelt appreciation to my family and friends for their unwavering encouragement, tolerance, and endless support during the time I dedicated to my studies.

Abstract

This study focuses on the analysis of creepage at the wheel-rail interface in railway systems. Creepage refers to the relative motion between the wheel and rail when the sliding force exceeds the adhesion force. A multi-body system dynamic simulation approach using Simpack software is employed to capture the dynamics of the wheel-rail system, including interaction forces, contact patch behavior, and resulting creepage. The objectives of this analysis are to investigate the effects of rail irregularity, velocity variation, and adhesion coefficients on creepage and creep forces. The study first examines the impact of rail irregularities on creepage and creep forces by analyzing their presence in the wheel-rail interaction. Subsequently, creepage and creep forces are studied in the absence of rail irregularities to isolate their effects on the overall system dynamics. The influence of velocity variation on creepage and creep forces is also investigated, considering variations in vehicle speed that can significantly affect the behavior and forces at the wheel-rail interface. The results indicate that rail irregularities increase creepage and creep forces, while their absence leads to lower values. Higher velocities generally generate greater creepage and creep forces compared to lower velocities, highlighting the importance of considering velocity variation in the analysis. Furthermore, the adhesion coefficient plays a crucial role in determining the level of creepage and creep forces. Higher adhesion coefficients are associated with lower creepage and creep forces, emphasizing the influence of adhesion on the wheel-rail interface. The study concludes by analyzing creepage and creep force considering different adhesion coefficients. Analytical simulations are conducted to assess the effects of varying adhesion coefficients on creepage and creep force, providing valuable insights into the influence of adhesion on the wheel-rail interface. Overall, this research contributes to a better understanding of creepage at the wheel-rail interface by considering various conditions such as rail irregularity, velocity variation, and adhesion coefficients. The findings have implications for improving the performance and safety of railway systems.

Key words

Creepage, Creep force, Adhesion coefficients, Rail irregularity, Velocity variation

Nomenclature

Wr	wear rate	V	wear volume
f_T	tangential force	ξ_x	Longitudinal creepage
$R\omega$	Actual forward velocity	V	Pure rolling forward velocity
v_x	longitudinal creep	v_y	lateral creep
f_i	adhesion coefficient for each wheelset	φ	spin creep
$F_{x,i}$	longitudinal forces	N_i	normal forces
v	translational velocity of the vehicle	d_w	diameter of the wheel
ω	Angular velocity around the normal axis of contact patch	F	normal load
v_ξ , v_η	velocities in the direction of (ξ , η)	A_n	normal contact area
T_b	braking torque applied on each wheelset	v_{sli}	relative sliding velocity
T_y	torque applied on each wheelset	A	thermal diffusivity
ρ	density of the material [kg/m^3]	P	the contact pressure [N/m^2]
k_i	wear coefficient [-]	W	wear rate [Kg/m]
ΔZ	the depth of the wear [m	A	vehicle acceleration
r_o	nominal contact radius	R	wheel radius
H_o	material hardness	T_{tb}	total braking torque
$\dot{\omega}_{w,i}$	the angular acceleration of the i wheelset	T_t	total torque
$I_{w,yy}$	the polar momentum of inertia of the wheelset	M	mass of the vehicle
$T_{b,i}$	the braking torque acting on braked wheelset		

List of Tables

Tabel 3. 1 Conditions about the vehicle.. 26

Tabel 3. 2 Main parameters 26

Tabel 3. 3 Parameters from literature 27

Table 4. 1 Input parameters for the analysis [37][34]……………………………….………………..29

Table 4. 2 Rigid body inertia 29

Table 4. 3 Vehicle data information and standard specifications taken from literatures and AALTR documents[34], [37]... 30

Table 4. 4 Main parameters of wheelset[34],[38]... 31

Table 4. 5 Main parameters for bogie modeling[34] 32

Table 4. 6 Main parameters for Vehicle modeling[34]... 33

List of Figures

Figure 1. 1 Positive longitudinal creepage 5
Figure 1. 2 Negative longitudinal creepage[14] 5
Figure 1. 3 Lateral creepage[14] 5
Figure 1. 4 Spinning the coin on the table top 6
Figure 1. 5 Spin creepage[14] 6
Figure 1. 6 Lateral and Spin creepage[15] 6
Figure 1. 7 The longitudinal creep, lateral creep and spin moment at wheel-rail interface[15] 7
Figure 1. 8 (a) Curving of a wheelset and (b) Spin creepage, with rotational speed and contact angle[16]. 8
Figure 1. 9 Radial position of a wheelset in a curve with in (a) the longitudinal creepages and (b) the longitudinal creep forces[16]. 9
Figure 1. 10 Under-radial position of a wheelset in a curve with in (a) the lateral creepages and (b) the lateral creep forces[16]. 9
Figure 2. 1 Equilibrium of forces on the wheel in the moments prior to derailment [21] 14
Figure 2. 2 Equilibrium of momentum of the braked wheelset [24] 16
Figure 2. 3 Different wear mechanism [25] 17
Figure 2. 4 Parameters of wheel wear [26] 19
Figure 2. 5 Wheel-rail creep and normal forces and typical rail wear for a wheelset in a curve[26] 19
Figure 3. 1 The coordinates of the wheel and rail 25
Figure 3. 5 Methods of modeling and simulation 28
Figure 3. 2 Typical shape of a worn wheel[16] 34
Figure 3. 3 Equilibrium of momentum of the braked wheelset 36
Figure 4. 1 Wheelset 31
Figure 4. 2 Bogie model 32
Figure 4. 3 Vehicle modeling 33
Figure 5. 1 The graph of vertical load vs time without the application of preload 40
Figure 5. 2 The graph of derailment coefficient before wheel-rail defects 40
Figure 5. 3 Longitudinal creep force at 40km/h with the presence of rail irregularity 41

Figure 5. 4 Lateral creep force at 40km/h with the presence of rail irregularity 41
Figure 5. 5 Longitudinal creep force, lateral creep force and creep torque 42
Figure 5. 6 Longitudinal creepage at 40km/h with the presence of rail irregularity 42
Figure 5. 7 Lateral creepage at 40km/h with the presence of rail irregularity.............................. 43
Figure 5. 8 Spin creepage at 40km/h with the presence of rail irregularity................................. 43
Figure 5. 9 Longitudinal and lateral Adhesion coefficients at 40km/h with the presence of rail irregularity.. 44
Figure 5. 10 Longitudinal and lateral creep forces at 40km/h with the presence of rail irregularity 44
Figure 5. 11 Longitudinal and lateral creepage at 40km/h with the presence of rail irregularity. 45
Figure 5. 12 Longitudinal and lateral creepage at 40km/h with the presence of rail irregularity. 45
Figure 5. 13 Creep force at 20km/h with presence of rail irregularity 46
Figure 5. 14 Longitudinal creepage at 20km/h of vehicle speed with presence of rail irregularity 46
Figure 5. 15 Lateral creepage at 20km/h of vehicle speed with presence of rail irregularity....... 47
Figure 5. 16 Spin creepage at 20km/h of vehicle speed with presence of rail irregularity........... 47
Figure 5. 17 Adhesion coefficients at 20km/h with presence of rail irregularity 48
Figure 5. 18 Creep forces without the presence of rail irregularity 49
Figure 5. 19 Creepage without the presence of rail irregularity 50
Figure 5. 20 Adhesion coefficients without the presence of rail irregularity 51
Figure 5. 21 Creep forces and creep torque when the adhesion coefficient is 0.3........................ 52
Figure 5. 22 Longitudinal creepage when the adhesion coefficient is 0.3................................... 52
Figure 5. 23 Lateral creepage when the adhesion coefficient is 0.3 53
Figure 5. 24 The result of spin creepage generated with the adhesion coefficients of 0.3 53

Table of Contents

ACKNOWLEDGMENTS I

Abstract II

Nomenclature III

List of Tables IV

List of Figures V

CHAPTER ONE 1

INTRODUCTION 1

1.1 Background 1

1.1.1 Creepage at Wheel-Rail Interface 4

1.1.2 Wheel-rail interaction 7

1.1.3 Contact Forces at Wheel-Rail Interface 10

1.2 Statement of the Problem 11

1.3 Objective 11

1.3.1 Main objective 11

1.3.2 Specific objective 11

1.4 Scope of the Study 12

1.5 Significance of the Study 12

1.6 Limitation of the Study 12

CHAPTER TWO 13

LITERATURE REVIEW 13

2.1 Introduction 13

2.2 Numerical Analysis 13

2.2.1 Archard's Wear Model and Energy Approach 14

2.3 Wear Mechanism 17

2.3.1 The Wheel Wear ... 18
2.3.1 Wear of Rail ... 19
2.4 Dynamic Analysis ... 20
2.5 Experimental Analysis ... 20
2.6 Numerical simulations based on software analysis ... 22
2.7 Adhesion Conditions ... 23
2.8 Summary of the Literature Review ... 24
CHAPTER THREE ... 25
MATERIALS, CONDITIONS AND METHODS ... 25
3.1 Materials ... 25
3.1.1 Literature Review ... 25
3.1.2 Software ... 25
3.1.3 Wheel and Rail Geometry ... 25
3.2 Conditions ... 26
3.3 Expected Results ... 27
3.4 Methods ... 27
CHAPTER FOUR ... 29
MODELING AND ANALYSIS ... 29
4.1.1 Main Parameters ... 29
4.1.2 Wheelset modeling ... 31
4.1.3 Bogie modeling ... 32
4.1.4 Vehicle body modeling ... 33
4.1.5 Wear Volume Calculation for Wheel and Rail ... 34
4.1.6 Archard's Wear Model ... 34
3.4 Adhesion Coefficient ... 35

4.2 Braking and Traction System 36

4.4 Creepage/Creep Force at Wheel-Rail Interface 37

4.5 Multi-body System Dynamic Simulation 38

CHAPTER FIVE 39

RESULT AND DISCUSSION 39

5.1 Result Validation 39

5.2 The Generated Result 41

CHAPTER SIX 55

CONCLUSION AND RECOMMENDATION 55

6.1 Conclusion 55

6.1.2 Recommendations 56

Future Work 56

Appendices 62

CHAPTER ONE

INTRODUCTION

1.1 Background

The occurrence of creepage between the wheel and rail interface significantly affects the performance and safety of railway systems. Creepage happens when the force of sliding between the wheel and rail exceeds the adhesion force, resulting in relative motion. This phenomenon can happen during various operating conditions such as acceleration, deceleration, braking, and encounters with rail irregularities. Analyzing creepage and its associated parameters, like creep force, is vital for understanding the behavior and interaction between the wheel and rail. By studying these factors, valuable insights can be gained about the performance and safety of the railway system. Ultimately, comprehending the phenomenon of creepage and its impact on the wheel-rail interface is crucial for ensuring optimal performance and safety in railway operations[1], [2].

The analysis of creepage and creep force when encountering rail irregularities is highly important as it enables us to understand how the system responds to unevenness and imperfections on the track. Rail irregularities, such as bumps, dips, or corrugation, have a significant impact on creepage behavior, which in turn affects vehicle stability and ride quality. This understanding is crucial for designing railway infrastructure and implementing appropriate maintenance practices to ensure passenger comfort and safety. On the other hand, analyzing creepage and creep force without rail irregularities provides valuable insights into the underlying mechanisms governing creepage behavior. By isolating external factors like rail irregularities, this analysis allows us to focus on the inherent characteristics of the wheel-rail interface. It helps us evaluate the effectiveness of adhesion forces and comprehend the contributing factors to creepage and creep force. By conducting both analyses, one with rail irregularity and one without, we can gain a comprehensive understanding of the wheel-rail interface. This understanding serves as a guide for developing strategies to minimize the impact of rail irregularities and optimize the performance and safety of railway systems[3].

Examining creepage and creep force in relation to changes in velocity enables the exploration of how velocity impacts the occurrence of creepage at the wheel-rail interface. Varying velocities can lead to alterations in contact forces between the wheel and rail, resulting in different creepage behaviors. Understanding the effect of velocity on creepage is vital for optimizing train operations, identifying efficient and safe operating speeds, and managing energy consumption. Minimizing energy losses caused by creepage and enhancing overall energy efficiency can be achieved by comprehending how velocity influences creepage. Moreover, considering velocity variation in relation to creepage and creep force helps in reducing wear and tear on the wheel and rail surfaces. High velocities combined with excessive creepage can generate increased friction and wear, impacting the durability and maintenance requirements of the wheel and rail components. By comprehending the correlation between velocity and creepage, maintenance practices can be optimized to minimize wear and ensure the longevity of the wheel-rail interface. In conclusion, taking into account creepage and creep force alongside velocity variation provides valuable insights into enhancing train operations, managing energy consumption, and mitigating wear and tear on the wheel and rail surfaces. This understanding contributes to the overall efficiency, safety, and maintenance of railway systems[4].

By considering the factors of creepage and creep force and their correlation with adhesion coefficients, one can analyze how the adhesive properties affect the behavior of creepage. The adhesion coefficient plays a crucial role in determining the friction level between the wheel and rail, which in turn affects the occurrence and degree of creepage. Examining the impacts of various adhesion coefficients offers valuable knowledge for enhancing train control systems, especially during braking and acceleration stages.[5].

The lifespan of wheels and rails in a railway can be affected by several factors such as adhesion, braking, corrugations, thermal defects, rolling contact fatigue, wheel and rail wear, curving force, and vehicle steering. These factors can also impact the performance of the train. The movement of the rail, known as creep, can be caused by the acceleration, deceleration, or sudden stopping of the train. During acceleration, the lateral thrust of the wheels can cause the rail to move. Similarly, when the train suddenly stops, the braking effect can push the rail forward, causing creep in that direction. The shapes of the wheel and rail profiles are designed to support the load of the train, resulting in high contact stresses at the interface between the wheel and rail. These stresses can lead to material loss on the surfaces of both the wheel and rail, ultimately changing their dimensions and orientations. These changes in profile geometry can significantly impact the dynamics and stability of the train.[6].

When a train encounters curves, accelerates, or brakes, it produces a phenomenon known as creep forces between the wheels and rails. As the train travels over a stretch of track, dynamic forces are generated on both the train and the track. This interaction and non-linear phenomenon. [7]. Applying brakes leads to increased traction compared to vehicle acceleration. The shape of wheel profiles can impact the overall performance of the vehicle. This includes factors such as dynamic stability, ride comfort, derailment safety, and the durability of wheels with significant wear on their profiles. [8].

The interaction between wheels and rails can have an impact on how railway vehicle behave. Understanding the theory behind this contact is crucial for railways, as it affects like wear, fatigue, friction, and track irregularities. When designing intelligent condition monitoring systems for railways, it is important to study the forces that occur at the wheel-rail contact. modeling this contact allows us to examine the stability and dynamics of the vehicle as it moves along the track. Two key parameters that can affect the vehicle's motion are its lateral displacement and yaw angle. [9].

When bodies in railways make contact, such as steel on steel, there is very little resistance when the wheels are freely rolling. However, friction occurs when external torques or forces cause the wheels to move slowly, taking them out of their free rolling state. The quality of traction, braking, and overall performance of high-speed trains depends on the characteristics of the adhesion between the wheels and rails. Factors like speed, weight on the wheels, the angle at which the wheels hit the rails, and the condition of the wheel-rail contact surface can all affect this adhesion. If the adhesion is not sufficient, the wheels may slip during train operations, causing the train to fall in its ability to move, start, and accelerate. Similarly, excessive braking can lead to the wheels sliding and the train exceeding the intended stopping distance. [10]. Low adhesion at the wheel-rail interface can have negative consequences on both safety and track and vehicle performance. In braking situations, it can result in station overruns, while in traction scenarios, it can result delays[11].

If the amount of grip between a train's wheel s and the rail Is not enough to handle the momentum when transitioning from curve section of track to a straight section, there is a higher risk of derailment accidents occurring on the curved parts of the track. Therefore, it is important to study the interaction between the wheel and rail at these curved sections. Factors such as the smoothness and wear of the wheel and rail, as well as the stability and safety of the train, can all impact the grip between the wheel and rail. [12]. There are two light railway lines in addis ababa, one running from east to west and the other from the south to north. The combined length of these lines is 31.6km, with the south to north line measuring 16.9km and the east to west line measuring 14.7 km. the south to north line consists of 22 stops, including a section that is shared with the east to west line [13].

1.1.1 Creepage at Wheel-Rail Interface

The phenomenon known as creep occurs when there is a difference between the overall forward velocity and the velocity around the circumference of an object. This discrepancy is caused by frictional forces at the contact point. If the circumferential velocity is higher than the forward velocity, the wheel experiences a net forward force which speeds up the object. Conversely, if the wheel is braking, the circumferential velocity is lower than the forward velocity. Creep occurs when two rigid bodies make contact, press against each other, and roll. According to Hertzian theory, the contact surface between these bodies will have an elliptical shape. Creepage is a term used to describe the deviations from pure rolling conditions. In the case of wheel-rail interaction, there are three types of creepage: longitudinal creepage, lateral creepage, and spin creepage[14].

The following figures show the longitudinal creepage at wheel-rail interface.

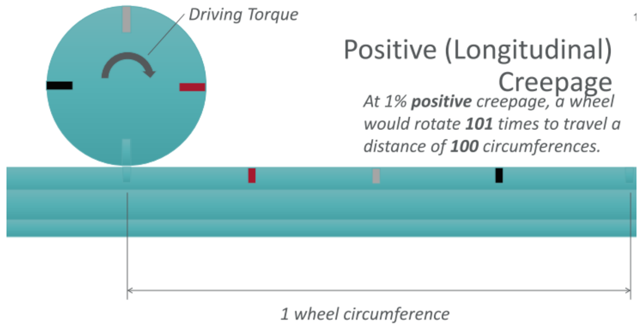

Figure 1. 1 Positive longitudinal creepage

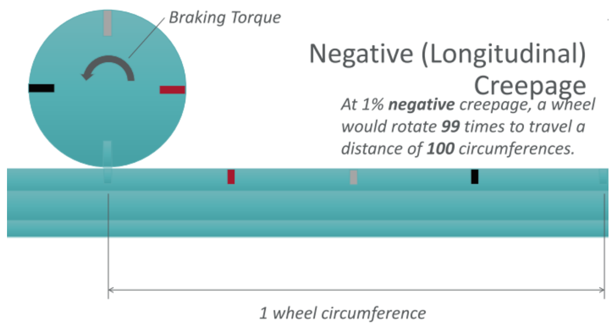

Figure 1. 2 Negative longitudinal creepage[14]

The lateral creepage mostly occurs when the vehicle negotiates curve.

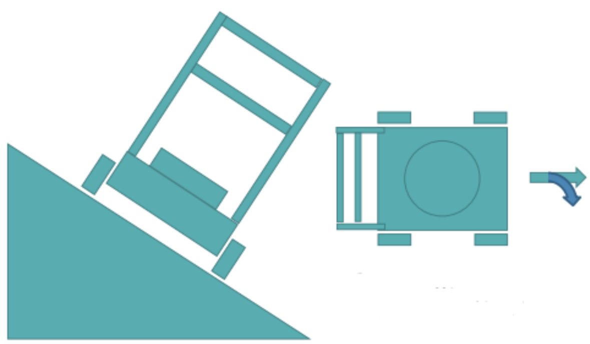

Figure 1. 3 Lateral creepage[14]

The following figure shows the spinning of the coin on the top of table. The concept is related to the wheel spin on the rail.

Figure 1. 4 Spinning the coin on the table top

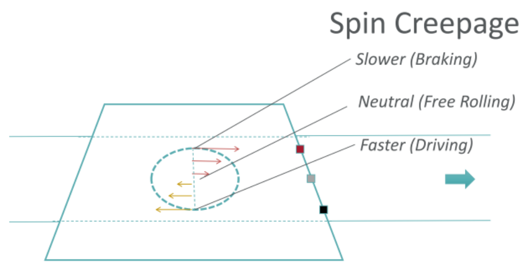

Figure 1. 5 Spin creepage[14]

The mathematical expression for the longitudinal creepage is given as follows:

Longitudinal creepage = $\frac{actual\ forward\ velocity - pure\ rolling\ forward\ velocity}{pure\ rolling\ forward\ velocity}$

$$\boldsymbol{\xi_x} = \frac{\boldsymbol{R\omega - V}}{\boldsymbol{V}} \qquad (1.\ 1)$$

The below figures shows the lateral and spin creepage at wheel-rail interface.

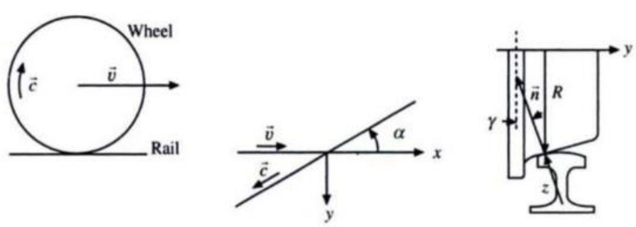

Figure 1. 6 Lateral and Spin creepage[15]

From the figures above, the lateral creepage is the same with the angle of attack. The lateral creepage and spin creepage is mathematical expressed as the following equations respectively[15].

$$\boldsymbol{\xi_y} = \boldsymbol{\alpha} \qquad (1.\ 2)$$

$\xi_{sp} = \boldsymbol{R} \sin \boldsymbol{\gamma} / |\boldsymbol{c}| \boldsymbol{\gamma}$ (1. 3)

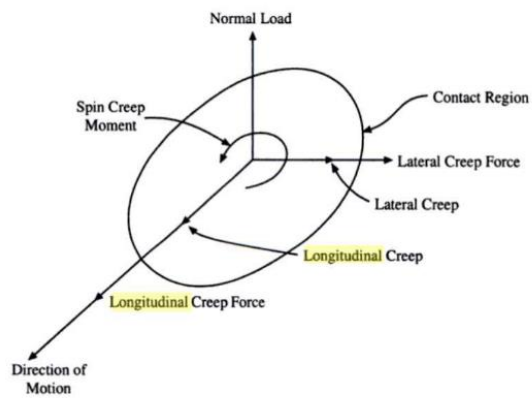

Figure 1. 7 The longitudinal creep, lateral creep and spin moment at wheel-rail interface[15]

1.1.2 Wheel-rail interaction

Understanding the forces and sliding motions that occur in the contact between the wheel and rail is important. When a vehicle encounters a curve, one of the wheelsets will move sideways towards the outer side of the curve. This causes the outer wheel to have a larger rolling radius, while the inner wheel has a smaller rolling radius because of the conical shape of the wheels. As a result, the outer wheel can roll further than the inner wheel at the same rotational speed. When the wheelset moves far enough towards the outer side of the curve, the difference in rolling radius compensates for the difference in rail lengths. In this situation, the wheelset achieves "pure rolling" without generating any friction forces between the wheel and rail. However, in most cases, the wheelset is unable to position itself perfectly radially in a curve [16][17].

As shown in the figure below the wheelset is yawed in a direction relative to the track or angle of attack (φ). Creepage or sliding motion is occurring when the contact surface of the wheel moves relative to the rail. Creepage in this case is the quotient of sliding velocity (v) and vehicle speed (V).

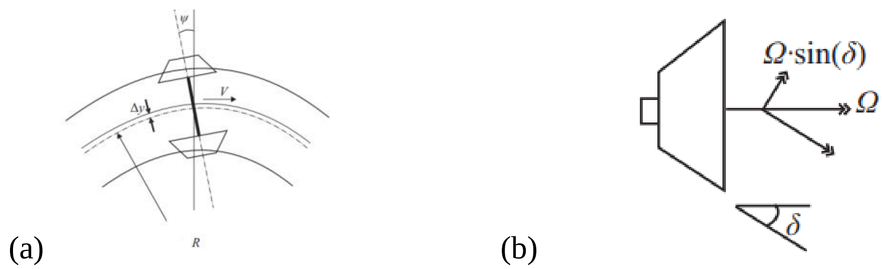

Figure 1. 8 (a) Curving of a wheelset and (b) Spin creepage, with rotational speed and contact angle[16].

$$\boldsymbol{v_x = \frac{v_x}{V}} \qquad (1.1)$$

$$\boldsymbol{v_y = \frac{v_y}{V}} \qquad (1.2)$$

$$\boldsymbol{\varphi = \frac{\omega}{V}} \qquad (1.3)$$

Where

v_x = longitudinal creep

v_y = lateral creep

φ = spin creep

Longitudinal creep is primarily influenced by the sideways movement of the wheelset and the conicity of the wheels. Lateral creep is directly linked to the angle at which the wheelset moves. As mentioned earlier, spin creepage refers to the relative angular velocity between the wheel and the rail. It consists of two components: the yaw velocity of the wheelset and the rotational speed. When the contact surface is not parallel to the wheel's axis of rotation, the rotational speed can be divided into a component that moves parallel to the contact surface, known as pure rolling, and a component that moves perpendicular to the contact surface[16].

Creepage at the interface between the wheel and rail leads to the emergence of creep forces. These forces act both longitudinally and laterally, opposing the relative motion of the wheel and rail. As a result, the relationship between creepage and creep force is nonlinear, although for small creepage values, it can be approximated as linear. At certain areas of contact between the wheel and rail, there may be relative motion in the form of sliding or slipping. In the case of slipping, the tangential stress is equal to the product of the coefficient of friction and the contact pressure. Conversely, when there is no slip between the contact surfaces, the tangential stress is minimal[16].

The on the edges of the contact point differs, with lower stress at the front and higher stress at the back. Sliding occurs at the rear of the contact, creating a sliding zone. In the rest of the contact, known as the adhesion area, there is no sliding. The overall friction force transmitted increases as the sliding area expands. When the entire contact area slides, the total friction force equals thecoefficient of friction multiplied by the normal force on the contact.

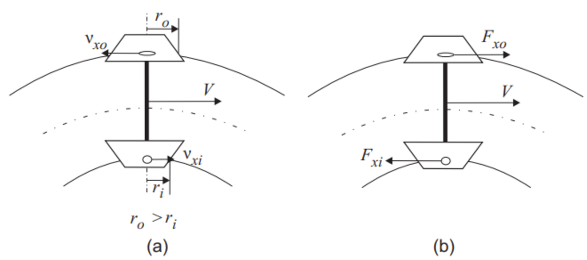

Figure 1. 9 Radial position of a wheelset in a curve with in (a) the longitudinal creepages and (b) the longitudinal creep forces[16].

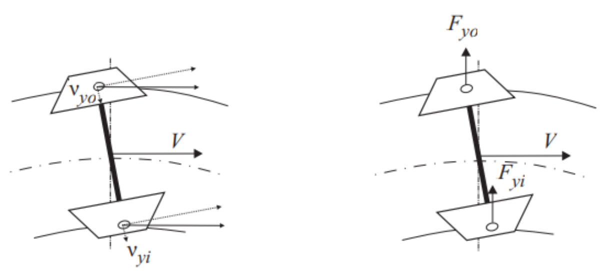

Figure 1. 10 Under-radial position of a wheelset in a curve with in (a) the lateral creepages and (b) the lateral creep forces[16].

To improve the position of a wheelset in a curve, the longitudinal creep forces cause a yaw moment that forces the wheelset to yaw. This results in a smaller yaw angle for wheelsets that are not radially positioned. However, the lateral creep force on the outer and inner wheels in an under-radial steering situation points outwards in the curve, which is in the same direction as the centrifugal forces. The lateral component of the normal force on the wheels needs to compensate for these forces. In order for a wheelset to steer radially in a curve, the yaw moment caused by the longitudinal creep forces must be greater than the resisting forces of the primary suspension.

To achieve a more radial position of a wheelset in a curve, the primary suspension can be made 'soft'. However, a softer primary suspension will result in lower stability on straight tracks at higher speeds. If a bogie with a very rigid primary suspension and wheelbase 2a approaches a curve with radius R, the angle of attack (ψ) can be determined as [16].

$$\Psi = \frac{\boldsymbol{a}}{\boldsymbol{R}} \qquad (1.\ 4)$$

Bogies with a larger wheelbase therefore experience higher creep forces in curves. This can result in more damage to the wheels and rails in terms of wear or rolling contact fatigue (RCF). [16].

1.1.3 Contact Forces at Wheel-Rail Interface

Analyzing the forces produced where the wheel meets the rail is critical for understanding how a train behaves. These forces have a major impact on the vehicle's dynamics, particularly during acceleration and braking. However, calculating these forces is challenging because they are influenced by factors such as variable contact conditions and the presence of various contaminants[18].

The locomotive's overall dynamic behavior can be greatly influenced by the forces exerted at the interface between the wheel and rail. Thus, the wheel-rail interface holds great importance in railway dynamics. The behavior exhibited at this interface is nonlinear, and two methods that are commonly suggested for studying it are the Heuristic non-linear contact model and Kalker's linear theory[9].

Previous papers have introduced three models for the contact between a wheel and rail: Hertz contact theory, non-Hertzian contact models, and finite element methods. Hertz's contact theory assumes that the contact area between the wheel and rail is elliptical and that they do not conform perfectly to each other. As a result, there is no friction between the wheel and rail, and the contact area is significantly smaller in size compared to the overall dimensions of the wheel and rail[19][9].

Non-Hertzian contact models, such as semi-Hertzian contact theory and CONTACT, are employed to analyze the interaction between a wheel and rail. These models focus on determining the shape of the contact patch, which is the region where the wheel and rail intersect. The shape of the contact patch is non-elliptical when subjected to high normal contact forces, whereas it is represented as elliptical under low contact forces. To simulate the dynamics of the wheel-rail interface, the finite element method was utilized[20]. Finite element methods, which demand significant computational resources, are seldom employed in railway vehicle dynamic simulations due to the extensive time they consume [9].

1.2 Statement of the Problem

The creepage phenomenon occurring at the wheel-rail interface poses significant challenges in the efficient and safe operation of railway systems. Creepage refers to the relative slip or sliding motion between the wheel and rail surfaces. The creepage can occur due to velocity variations during stops and starts of the vehicle at stations. This creepage can cause the low adhesion at wheel-rail interface. The large creepage and low adhesion may lead the wheel to slide over the rail. Due to insufficient adhesion, the vehicle wheel can slide on the rail and can move beyond the limited distance after the brake is applied. The movement of the wheel beyond a limited distance can cause unexpected damage. It can lead to reduced adhesion, and compromised vehicle stability. Another critical concern is the reduced adhesion caused by creepage. Adequate adhesion between the wheel and rail is essential for safe and efficient vehicle operations. The complex nature of creepage and the numerous factors influencing its occurrence, including rail irregularity, wheel-rail contact pressure and vehicle speed.

1.3 Objective

1.3.1 Main objective

- To analysis creepage at the wheel-rail interface of light rail transit.

1.3.2 Specific objective

- To analysis creepage and creep forces with rail irregularity

- To analysis creepage and creep forces without rail irregularity
- To analysis creepage and creep forces with velocity variation
- To analysis adhesion coefficients with creepage and creep forces

1.4 Scope of the Study

The analysis is conducted based on the numerical simulation with the help of the Simpack 2020.1 software tool. The study focused on the analysis of creepage and creep forces with the presence of rail irregularity, without the rail irregularity, with velocity variations and adhesion coefficients occurring at the wheel-rail interface.

1.5 Significance of the Study

There are many complicated problems, which can influence the performance of the vehicle in different aspects. Among of them, creepage at the wheel-rail interface is one of the factors that can affect the performance of the vehicle. The dynamic behavior of the vehicle has a direct relationship with the creepage. In general, understanding and identifying the effect of the creepage at the wheel-rail interface during the stop/start of the vehicle at stations helps to estimate the damage that occurs on the wheel and rail with what kind of maintenance is needed.

1.6 Limitation of the Study

The main limitation of the study is: - the study considered the new wheel and rail, worn wheel and rail are not considered in the analysis. The amount of materials removed from the wheel and rail is also not included. The third body layer between the wheel and rail is not considered.

CHAPTER TWO

LITERATURE REVIEW

2.1 Introduction

Many research papers can relate to the wheel and rail in the case of the railway. The most recent papers related to the work are reviewed. As a recent paper indicates, creepage can relate to the dynamic behavior of the vehicle since there is wheel-rail contact. The understanding of the wheel-rail contact mechanism and the force generated on the wheel and rail can have a vital role in the railway. So, there are some parameters for the interaction of the wheel and rail that can influence the vehicle's dynamic characteristics and can cause material removal from both wheel and rail during contact occurs between them. Those parameters are contact patch, wheel and rail profile, lateral displacement, lateral force, longitudinal force, spin moment and vehicle speed. The light rail vehicles at low speeds run over a line and have many stops where they are stops and starts. The analysis of the start/stop rail vehicle effects on the rail and wheel is supported by some related papers and they are listed below.

2.2 Numerical Analysis

The study by Michael Thompson and Linda Davis in 2018, examined the creepage behavior that takes place at the wheel-rail interface when braking occurs. By conducting tests in a laboratory setting and collecting measurements in the field, the authors identified various aspects that affect creepage, including the condition of the track, the force applied during braking, and the adhesion between the wheel and the rail. The review concludes by suggesting potential strategies for The study by Santamaria, Vadillo, and Gomez in 2009 examined how to effectively manage creepage in order to improve braking performance. They analyzed Nadal's equation, which describes the relationship between lateral and vertical forces that can cause a wheel to derail. According to Nadal, the worst-case scenario occurs when the tangential force Ty is at its highest as this contributes to derailment. Using Coulomb's theory, it is stated that the maximum tangential force Ty cannot exceed the product of the static friction coefficient μ and the normal force[21].

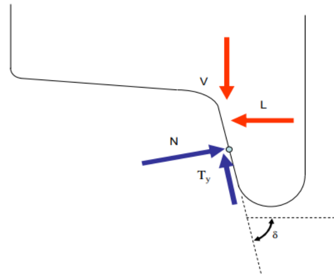

Figure 2. 1 Equilibrium of forces on the wheel in the moments prior to derailment [21]

2.2.1 Archard's Wear Model and Energy Approach

Aceituno and colleagues (2017), conducted a study to examine how the flexibility of railway tracks influences the wear and tear on wheels and rails. They developed an energy-based model to predict the loss of material as the wheel-rail system wears. To analyze the wear, they proposed a simplified mixed wear hypothesis based on the frictional energy loss at the contact patch. They used advanced techniques such as three-dimensional contact formulations and nonlinear multi-body systems to calculate the wear distribution on the wheel-profiled surface, the contact forces, creepages, and location of the wheel-rail contact points considering the flexibility of the rail. They found that the contact point locations, contact forces, and creepages are nonlinearly affected by rail deformations, and the wear distribution is directly proportional to the normal force in the contact area. The track was represented as a rigid body in their numerical simulations. They compared the results obtained from their simplified wheel-rail wear model with those from Archard's wear model. The comparison showed that the wear distribution was similar for both models. However, the energy-based approach predicted slightly larger magnitudes of wear, which were considered acceptable. Additionally, there were some differences in the wear distribution shape between the two models[6].

In 2018, Fourie, conducted a study on the analysis of railway wheel-squeal. The focus was on the effects of unsteady longitudinal creepage on the occurrence of squealing. Longitudinal creepage refers to the energy that leads to squealing, and the lateral displacement of the wheelset contributes to high levels of longitudinal creepage at the contact point between the wheel and rail. This displacement is considered a significant factor in squeal, particularly in 1000 m radius test curves. The combination of worn wheel and rail profiles results in self-steering bogies underneath empty freight wagons oversteering in these curves. This oversteering causes both wheelsets of the bogie to move laterally towards the outside of the curve, leading to increased levels of longitudinal creepage. It should be noted that the squealing wheels mainly experience longitudinal creepage, with minimal lateral creepage[22].

Wu, Cole, and Spiryagin (2020), conducted an analysis of train braking simulation using a wheel-rail adhesion model. They observed that creepage occurs at the wheel-rail interface when there is a difference in speed between the circumferential wheel and the translational speed. The ratio of this speed difference to the translational speed quantifies the creepage value. This creepage value is influenced by the coefficient of adhesion, which is dependent on the actual friction conditions between the wheel and rail. The coefficient of adhesion serves as an indicator of the actual friction coefficient, enabling the generation of frictional forces at the wheel-rail interface. By multiplying the normal contact force between the wheel and rail by the coefficient of adhesion, a brake force can be generated. In summary, the combination of creepage and the normal contact force at the wheel-rail interface plays a crucial role in generating the brake force during train braking simulations[23].

Dirks (2015), conducted an analysis of the fatigue and wear experienced by wheels on rails using two main models: frictional work models and Archard wear models. Frictional work models relate the wear rate to the energy expended in the contact between the wheel and rail, while Archard wear models are based on wear rate in relation to factors such as sliding distance, normal force, and material hardness. In the Archard wear model, wear does not occur in the adhesion zone of the contact, where the sliding distance or slip velocity is zero. To determine the wear distribution, the wear depth along the longitudinal direction is added for each cell element for every revolution of the wheel (dz).........[16].

Dependent on the energy dissipation in the contact of bodies Pearce and Sherratt developed a method to calculate wear. For this model, three regimes can relate the wear and energy dissipation.

The mild regime

$$\boldsymbol{T\gamma < 100N: A_w = 0.25\frac{T\gamma}{D}} \quad (2.\ 1)$$

The transition regime

$$\mathbf{100 \leq NT\gamma < 200N}: \boldsymbol{A_w = \frac{25.0}{D}} \quad (2.2)$$

The severe regime

$$\boldsymbol{T\gamma \geq 200N}: \boldsymbol{A_w = \frac{1.19\,T\gamma - 154}{D}} \quad (2.3)$$

Where

T is the total creep force [N],

γ = the creepage, D = the wheel diameter [mm] and

A_w = the worn-off area per travelled kilometer [mm^2].

In this case, the value is treated as an index to obtain the appropriate the wear rate[16].

The following equation can help to calculate the adhesion coefficient for each wheelset (fi). The relationship is expressed as the ratio between the longitudinal forces (Fx, i) and normal forces (Ni) acting on the wheel-rail interface[24].

$$\boldsymbol{f_i = \frac{F_{x,i}}{N_i}} \quad (2.4)$$

To determine the longitudinal force, the equilibrium of momentum for a braked wheelset can help as the following expression.

$$\boldsymbol{F_{x,i} = \frac{2}{d_w}(T_{b,i} - I_{w,yy}\dot{\omega}_{w,i})} \quad (2.5)$$

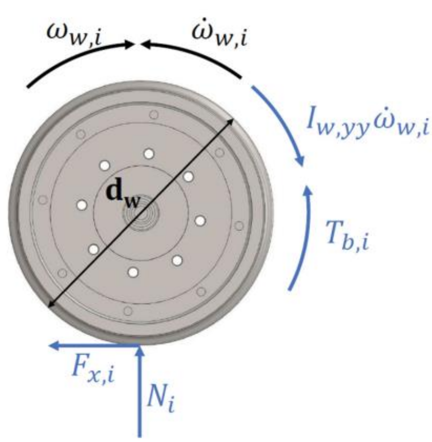

Figure 2. 2 Equilibrium of momentum of the braked wheelset [24]

Where d_w is diameter of the wheel, $T_{b,i}$ is the braking torque acting on braked wheelset, $I_{w,yy}$ is the polar momentum of inertia of the wheelset and $\dot{\omega}_{w,i}$ is the angular acceleration of the i wheelset[24].

2.3 Wear Mechanism

Wear-rate transitions and their correlation with wear mechanisms were addressed by Lim, Ashby, and Brunton in a study conducted in 1987. It is crucial to comprehend the wear mechanisms in order to quantify the wear rate. The type of wear mechanism relied upon the temperature at the contact interface. Specifically, the sliding velocity and contact pressure played a significant role in this regard. A visual representation, such as the accompanying graph, can serve as a concise summary of the various wear mechanisms based on normalized pressure and slip[25].

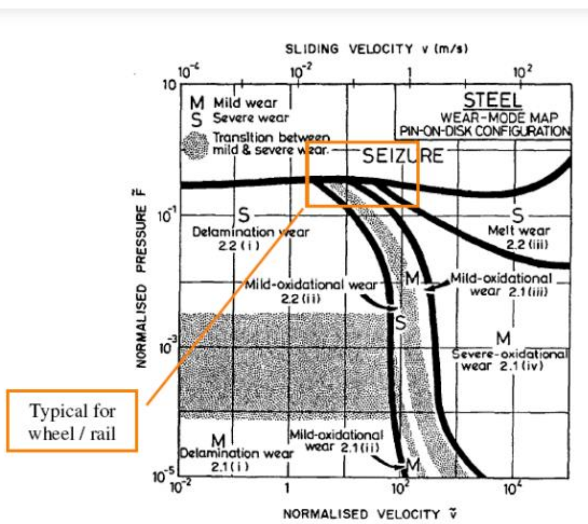

Figure 2. 3 Different wear mechanism [25]

The normalized parameters are defined as the following expressions:

$$\bar{F} = \frac{F}{A_n \cdot H_o} \quad (2.6)$$

$$\bar{V} = \frac{v_{slip} \cdot r_o}{a} \quad (2.7)$$

Where

F is normal load

A_n is normal contact area

H_o is material hardness

v_{slip} is relative sliding velocity

r_o is nominal contact radius and

a is thermal diffusivity.

2.3.1 The Wheel Wear

The primary factors considered for predicting wheel wear include flange thickness (t_f), flange height (h_t), and flange inclination (q_R). In a study conducted by Robla Sánchez in 2010 on the wear simulation of the A32 light rail vehicle, it was observed that wheel wear can be caused by both flange wear (leading to reduced thickness and increased inclination) and tread wear (resulting in increased height and thickness). Flange wear occurs when the curve radius is smaller and there is a larger angle of attack between the wheel and rail, leading to higher creepage and creep forces. Increased friction coefficient also intensifies creep forces, resulting in more material removal. The running gear of the vehicle can also influence flange wear, especially if the angle of attack between the wheel and rail is high, as this leads to higher creepage, creep forces, and material removal. Tread wear, on the other hand, can be influenced by the normal forces between the wheel tread and the top surface of the rail, as well as the levels of creepage and creep forces. Braking and traction activities can generate a high amount of creepage, thereby contributing to tread wear[26].

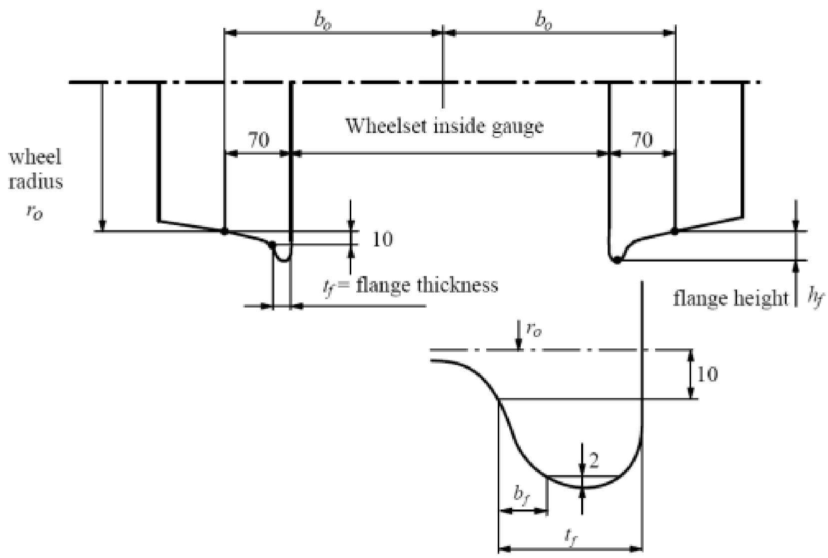

Figure 2. 4 Parameters of wheel wear [26]

2.3.1 Wear of Rail

The rail wear takes place at the same time as wheel wear. So, the worn parts of the rail affect the wheel wear when they are in contact. The gauge corner wear (outer rail in curves) and top surface wear (inner rail) are two components of rail wear[26].

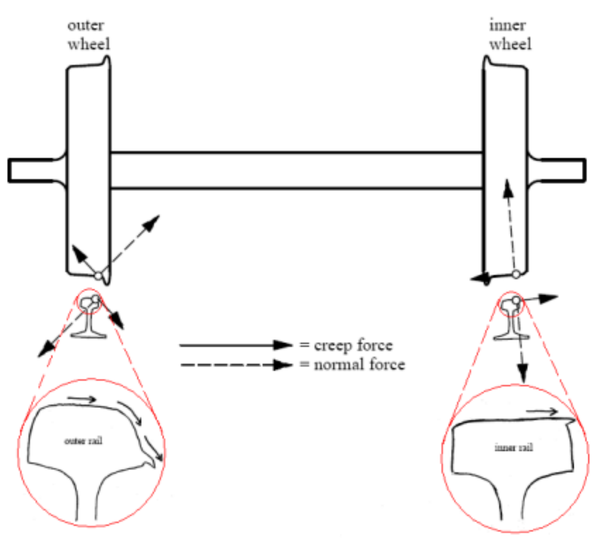

Figure 2. 5 Wheel-rail creep and normal forces and typical rail wear for a wheelset in a curve[26]

2.4 Dynamic Analysis

Lei and Wang's analysis in 2021, focused on the contact and creep characteristics of the wheel-rail system, specifically examining the phenomenon of corrugation with unique wavelengths and wave-like wear. They posited that these phenomena could be represented as continuous harmonic vibrations with three different wavelengths and wave depths, and developed a dynamic model to study the interaction between the vehicle and the track. In their study, they found that when the wavelength was kept constant and the wave depth increased, there was an increase in the average values of rail-wheel vertical vibration acceleration and wheel-rail longitudinal creepage/creep force. Conversely, when the wave depth was fixed, the average value of transverse creepage/creep force decreased. This indicated that there was a positive relationship between the changes in longitudinal creepage/creep force and wave depth.Additionally, Lei and Wang observed a positive relationship between the changes in transverse creepage/creep force and wavelength[27].

Tao focused his study in 2021, on investigating the specific irregularities experienced by locomotive wheels. The measurement of wheel roughness at various field sites revealed that wheels suffer from distinct irregularities like wheel flats or local defects. To understand the impact of these irregularities on the polygonization of locomotive wheels, a model of wheel wear was utilized. This model included a calculation to predict wear and a flexible-rigid dynamics model that considered the interaction between the locomotive and the track through the frictional work of the wheel-rail contact patch. The model incorporated discrete irregularities with different wavelengths as initial inputs. The simulation results demonstrated that these irregularities could induce elastic vibrations in the wheelset, particularly causing lateral vibrations in the wheels. Consequently, this led to oscillations in both lateral creepage and creep force at specific frequencies. Ultimately, the fluctuation in wheel-rail creepages and creep forces resulted in wheel polygonization.[28].

2.5 Experimental Analysis

Liu, Xiao, and Meehan 2019, in their investigation a rolling contact two-disk test rig is used to measure the lateral adhesion ratio in the case of both dry and wet conditions. The result indicates that the lateral adhesion ratio reduces after the application of water. The influence is reasonable at a large angle of attack for low speed, and the reduction rate is almost up to fifty percent. On the lateral adhesion ratio at high speed, the influence of water application is almost negligible. So, this study investigates the influence of rolling speed on the lateral adhesion ratio in the case of wet and dry conditions. The lateral adhesion ratio reduces with rolling speed under dry conditions; while after the application of water, the measured result indicates an opposite mode. Based on experimental measurements a model of wheel-rail contact mechanics is developed and using the model, with the increase of rolling speed the simulated friction creep curves shift down[12].

Chang et al. 2019, in their study take experiments under the wet condition on a high-speed full-scale roller rig of the wheel-rail interface to simulate the low adhesion problem of a high-speed railway. The adhesion characteristics at high speed under water lubrication tests are conducted in this study. The effect of wheel-rail adhesion coefficient factors on the high-speed are investigated, this embraces water spray amount, the roughness of wheel-rail contact surface, running speed, water temperature and axle load. To investigate the adhesion coefficient between rail and wheel under a water-lubricated condition the full-scale high-speed wheel-rail interface test rig is applicable. As the author proposed, the water spray amount, the wheel-rail contact of the roughness of the surface and running speed have more significant influence than the water spray temperature and axle load on the adhesion coefficient under wet conditions. Therefore, to raise the wheel-rail adhesion coefficient under wet conditions, increase the roughness of the wheel-rail contact surface[10].

Vollebregt, Six, and Polach 2021, discussed in their study the modeling and understanding of wheel–rail creep forces. It more focuses on tribological aspects. They show the importance of the role played by the surface conditions, which means the presence of liquid and solid layers, surface roughness, and near-surface plastic deformation. As the surface conditions change over time, transient changes may be obtained in the creep force characteristic. This brings feedback into the picture, with consequences and opportunities for optimized adhesion recovery, traction control, and braking systems[29].

2.6 Numerical simulations based on software analysis

Yang. 2022, investigates the influence of polygonal wear of heavy-haul locomotive wheels on the performance of dynamic and wheel-rail interactions through site tests and numerical simulations. The vehicle vibrations and dynamic wheel-rail tangential forces are considered. Two vehicle measurement results are compared including the characteristics of wheel polygonal wear and vehicle vibrations in vertical, longitudinal and lateral directions. To investigate wheel-rail dynamic interaction produced by polygonal wear of vehicle wheels, a 3D heavy-haul train-track coupled dynamic model was formulated. A low adhesion zone and a PI-based anti-slip control algorithm were embedded into the dynamic model to analyze the effects of wheel polygonal wear on wheel/rail longitudinal and lateral interactions under normal and low adhesion conditions. So, the wheel high-order polygonal wear influences longitudinal, lateral, and vertical vibrations of vehicle system components[30].

Teshome M. 2020, investigated wear resistance analysis by comparing two materials Manganese and Pearlite steels. He assessed the level of wear and wear resistance exhibited by different materials in the contact between wheels and rails. This involved comparing the wear and wear resistance of the current material, manganese steel, with the new material, Pearlite Steel. Specifically, he looked at the rate of wear and the ability of both Manganese Steel and Pearlite Steel to withstand wear[31].

Zemenu B.2013, The theoretical foundation for understanding how the curved radius of a rail line and the speed of a vehicle affect rail tribology was developed. Mathematical equations were by considering the geometrical relation of the curved rail, the conic shape of the wheels, and speed and mass of vehicle. This analysis involved two parts: a kinematic analysis and dynamic analysis. The study on the UIC 60 standard carbon steel material commonly used in rails and incorporated wear coefficients obtained existing literature. All calculation and analysis were performed using MATLAB software[32].

Atalay 2018, The aim was to minimize the wearing of the wheel and rail by optimizing the wheel’s shape and conducting a dynamic performance analysis of both the original and improved wheel profiles. Using the Simpack software, the newly optimized profile was evaluated for stability, wear, and safety requirements [33].

Dula Fekadu 2014, The author presents a logical approach to understanding the causes of wheel wear at the AALRT system. He conducted an analysis of actual wheel data collected from AALRT depots to determine the type of wear and compared vehicles from the North-South and East-West lines to identify which line was more affected. It was found that the tight curves on the North-South line were a major contributor to high flange wear, based on the analysis of wheel data. He proceeded to use SIMPACK software to conduct a multi-body simulation analysis of the AALRT vehicle's performance on curves and straight tracks, validating it against vehicle standards such as the coefficient of derailment, ride index, and lateral force. through literature review, parameters like critical speed coefficient of friction, and passenger loading were identified, and their impact on wear was determined based on the current track infrastructure of AARLT. The simulation results provided data on longitudinal/lateral creepage and creep forces, which were then used to calculate the wear index. [34].

Negash 2012 He conducts research to find the best wheel/rail contact and determine where the contact occurs, which is crucial for understanding how loads are distributed on the contact interface. The study relies on the Hertz contact theory assumptions and mathematical to identify the contact between the wheel and rail as point contact.[35].

Aklilu 2021 Examines cracks and fatigue in railroad wheels by utilizing a Finite Element Model. He assess the performance of rail vehicles in crucial areas where the rail and wheel meet, with a focus on various damage mechanisms such as surface and sub-surface cracks, plastic deformation, and wear. Investigating the highly stressed interface is essential in understanding these mechanisms. Additionally, the researcher investigates how different factors like wheel diameter, friction, and vertical loads impact the wheel's fatigue life. [36].

2.7 Adhesion Conditions

Alturbeh et al. 2020 discussed the low adhesion conditions of the wheel-rail interface, and develop the model MATLAB/Simulink is used. Still, the sliding of the long train occurs. The complexity of the components of the braking system and their effects on the whole braking system characteristics is included in the model. The occurrence of low adhesion at the wheel-rail interface influences the performance of the vehicle by leading to run the vehicle stations overrun.

To improve the performance of the braking system of the vehicle used modern simulation software to model the components of the braking system. The result generated here is vehicle speed, vehicle acceleration, wheel-rail force, wheel rotational speed, load, adhesion, gradient, wheel-rail force/load and wheel slide protection status[11].

2.8 Summary of the Literature Review

Based on the above literature reviews, it is evident that creepage at the wheel-rail interface during velocity variation of a vehicle plays a vital role in railway system. Experimental and numerical techniques are commonly employed to investigate and quantify creepage behavior. Factors such as wheel-rail adhesion, longitudinal force, track condition, and train weight have been identified as significant contributors to creepage. Understanding these factors and their interplay is essential for developing accurate models and control strategies.

In conclusion, creepage at the wheel-rail interface during velocity variation is a critical aspect of railway systems that requires thorough analysis and understanding. The reviewed literature provides valuable insights into the factors influencing creepage, its impact on various parameters, and possible strategies for managing and controlling it.

CHAPTER THREE

MATERIALS, CONDITIONS AND METHODS

3.1 Materials

3.1.1 Literature Review

Literature is the primary input to the work, since current related studies are reviewed to begin the work and helps to take some important data from the papers. The current studies that related to the creepage at the wheel-rail interface and its effects on the rail and vehicle performance are reviewed and some necessary data has been taken. The result is also validated based on the literatures.

3.1.2 Software

Simpack software is used for the multi-body dynamic simulation of the vehicle. So, the Simpack2020.1 software tool helps to model and simulate the rail vehicle wheel-rail interface.

3.1.3 Wheel and Rail Geometry

Wheels are used to support the whole part of the vehicle and run over the rail. The following figure shows wheel and rail profile coordinates. On the coordinate, the z-axis points downward and the y-axis is a lateral position.

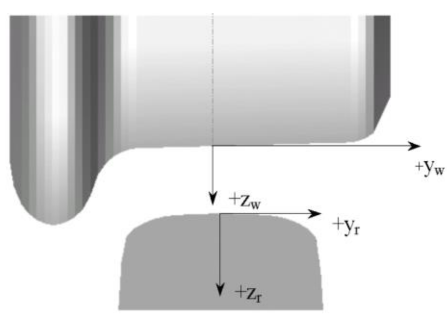

Figure 3. 1 The coordinates of the wheel and rail

3.2 Conditions

The analysis is considered the effects of creepage at wheel-rail interface for light rail transit. The model is considered new wheel and rail with dry condition contact between wheel and rail. The multi-body system dynamic simulation considered the wheel/rail interaction with the defects, track irregularity, rail corrugation, wheel polygon, and wheel flat and the dynamic response highly influenced. Therefore, to study the creepage and creep force, multi-body system dynamic simulation is considered in order to analysis the dynamic response effects.

Tabel 3. 1 Conditions about the vehicle

Velocity variation	40km/h and 20km/h
Lubrication condition	Dry condition
Rail type	UIC60
Wheel type	S1002

The following parameters are taken from the AALTR documents

Tabel 3. 2 Main parameters

Parameters	Units
Maximum velocity	m/s
Operating velocity	m/s
Average acceleration for starting	m/s^2
Average deceleration for braking	m/s^2
Total weight of the vehicle	Kg

Tabel 3. 3 Parameters from literature

Parameters	Unites
Area of contact	cm^2
Sliding velocity during braking and traction	m/s
Wear coefficient	-
Density of material	kg/m^3
Material hardness	MPa
Longitudinal element length	m

3.3 Expected Results

The expected results from these different analyses would provide valuable insights into the factors influencing creepage and creep force at the wheel-rail interface, helping in enhancing the understanding of rail vehicle behavior and guiding the development of mitigation measures or maintenance strategies for improved rail system performance and safety.

3.4 Methods

To analyze the creepage and creep force multi-body system dynamics simulation with defects should be considered in order to analyze the dynamic response effects. When the multi-body dynamic system simulation considered the wheel/rail interaction and track irregularity rail-related highly influenced the dynamic response effects.

The comparison of the creepage and creep force must be based on the:

- Vehicle speed variation (40km/h and 20km/h)
- Consideration of track with irregularity
- Consideration of the track without irregularity
- Adhesion coefficients (0.3 and 0.4)

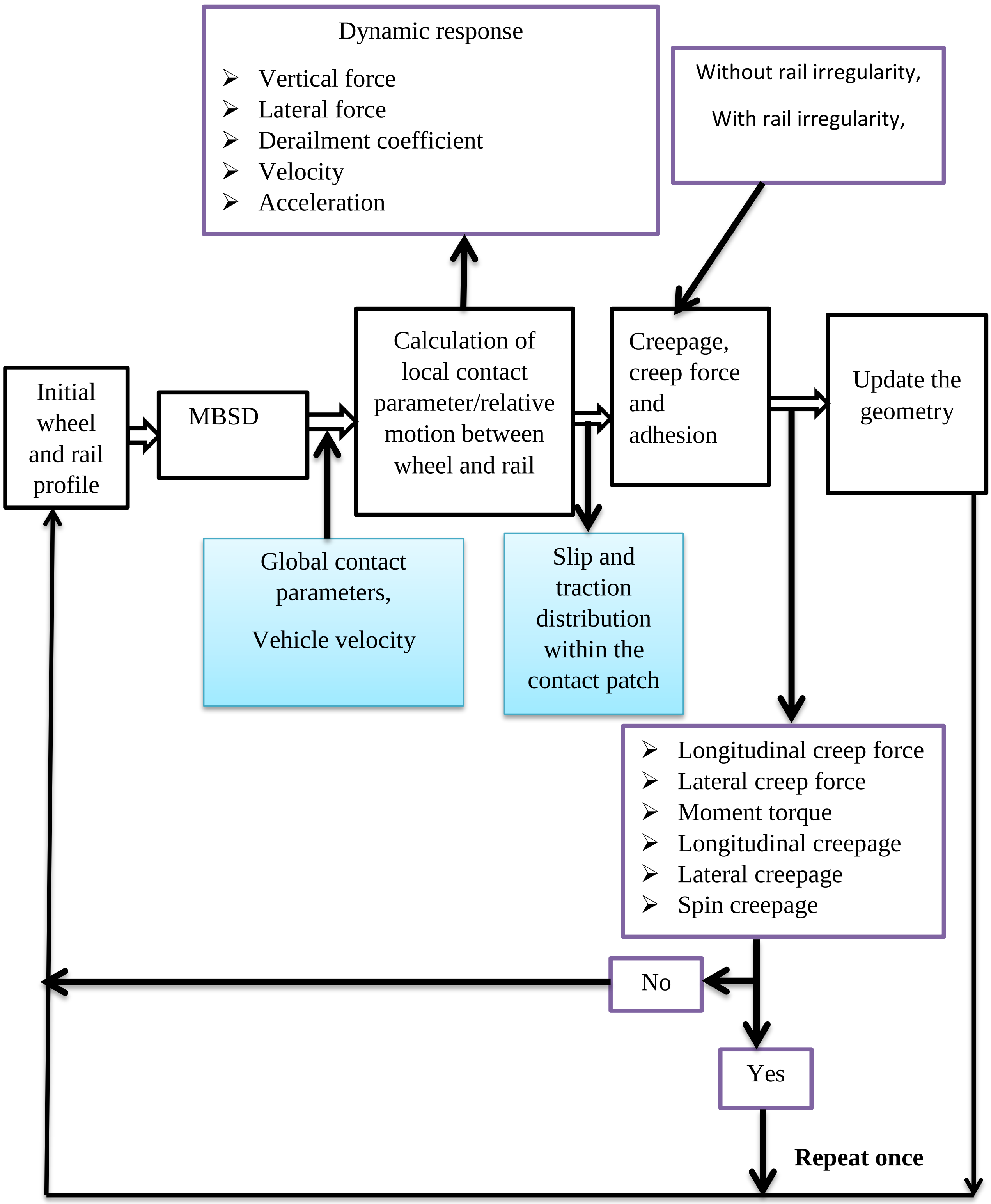

Figure 3. 2 Methods of modeling and simulation

CHAPTER FOUR

MODELING AND ANALYSIS

4.1.1 Main Parameters

The model is analyzed based on the multi-body system dynamics simulation and the main parameters used for the simulation are listed as the following tables.

Table 4. 1 Input parameters for the analysis [37][34]

Parameters	Symbols	Unites
Coefficient of friction	F	0.4
Average acceleration for starting up	a_s	$1m/s^2$
Average deceleration for braking	a_b	$0.9m/s^2$
Density of material	ρ	$7200kg/m^3$
Youngs modulus	E	2.1×10^{11}
Material hardness	HB	2943MPa (BHN300)

Table 4. 2 Rigid body inertia

Rigid body	I_{xx} (Kgm^2)	I_{yy} (Kgm2)	I_{zz} (Kgm2)
Wheelset Inertia	625.7	133.92	625.7
Bogie Inertia	1722	1476	3076
vehicle Inertia	56800	19700000	19700000

The vehicle information and standard specifications are taken from related literatures and AALRT documents. So the following table summarized the standard specifications used in the analysis.

Table 4. 3 Vehicle data information and standard specifications taken from literatures and AALTR documents[34], [37]

Parameters	Values	Units
Max. running speed	80	Km/h
Max. operating speed	20 and 40	Km/h
Max. width of car body	2650	mm
Height of Car body	3025	mm
Flange angle	70^0	Degree
Flange thickness	21.21	mm
Rail type	UIC60	-
Wheel type	S1002	-
Track gauge	1435	mm
Minimum radius of vertical curve	1000(auxiliary line)	m
Minimum radius of horizontal curve	25	m
Total vehicle weight	63	Ton
Wheel diameter (new)	660	mm
Wheel diameter(fully worn wheel)	580	mm
Track gauge	1435	mm
Wheel base (for power bogie)	1900	mm
Wheel base (for driven bogie)	1600	mm

4.1.2 Wheelset modeling

For the modeling of wheelset the main parameters summarized on the table are used.

Table 4. 4 Main parameters of wheelset[34],[38]

Material property	Density(ρ)	Hardiness (HBN)	Youngs modulus(E)
	7200kg/m^3	2943MPa (BHN300)	2.1×10^{11}
Inertia (I)	I_{xx} (Kgm^2)	I_{yy} (Kgm^2)	I_{zz} (Kgm^2)
	625.7	133.92	625.7
Wheelset mass (m_w)	880kg	-	-
Wheel diameter (d_w)	660mm	-	-
Axle diameter (d_a)	180mm	-	-
Axle length (l)	2200mm	-	-
Axle load	$\leq$ 11 (1+3%) t	-	-
Coefficient of friction (μ)	0.4	-	-

Based on the above parameters the following wheelset is modeled.

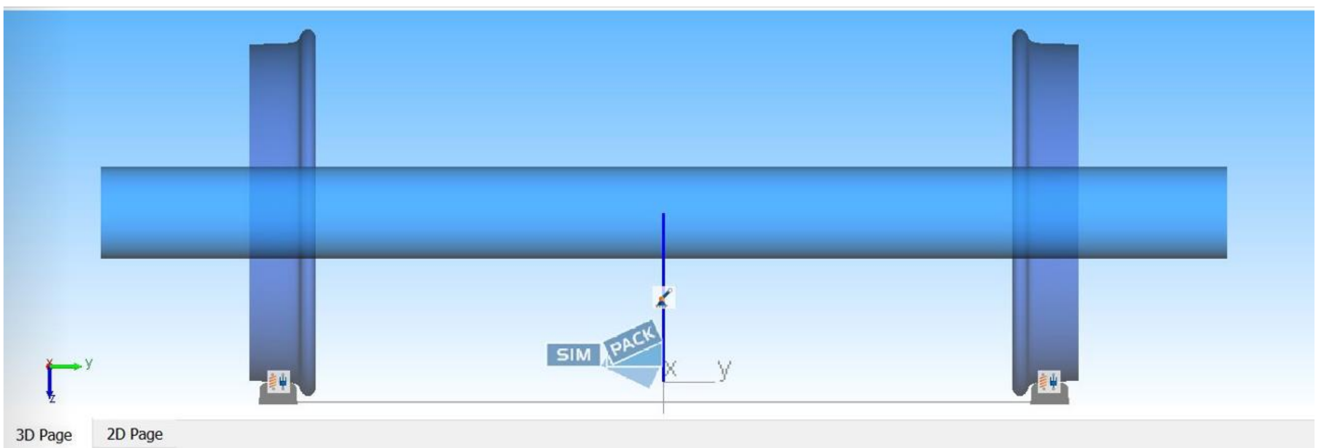

Figure 4. 1 Wheelset

4.1.3 Bogie modeling

To model the bogie the main parameters are listed on the below table.

Table 4. 5 Main parameters for bogie modeling[34]

Inertia (I)	I_{xx} (Kgm^2)	I_{yy} (Kgm^2)	I_{zz} (Kgm^2)
	1215	1875	2182
Bogie frame mass(B_m)	4200	-	-
Suspension system	k_x(N/m)	K_y(N/m)	K_z(N/m)
Primary suspension	613000	613000	1415000
Secondary suspension	150000	150000	500000
	d_x(N/m)	d_y(N/m)	d_z(N/m)
Primary damping	-	-	8000
Secondary damping	-	200000	400000

Based on the above parameters the following bogie is modeled.

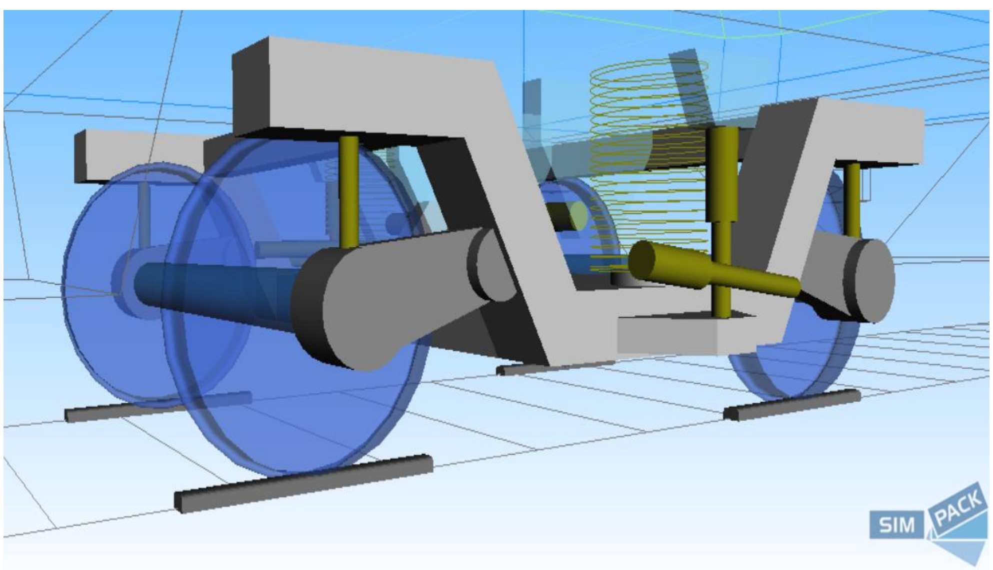

Figure 4. 2 Bogie model

4.1.4 Vehicle body modeling

The vehicle is modeled based on the parameters listed on the below table.

Table 4. 6 Main parameters for Vehicle modeling[34]

Car body Inertia (I)	I_{xx} (Kgm^2)	I_{yy} (Kgm^2)	I_{zz} (Kgm^2)
	4375	8750	8750
Car body mass(C_m)	17500kg	-	-

The following vehicle model is modeled based on the above parameters mentioned on the table.

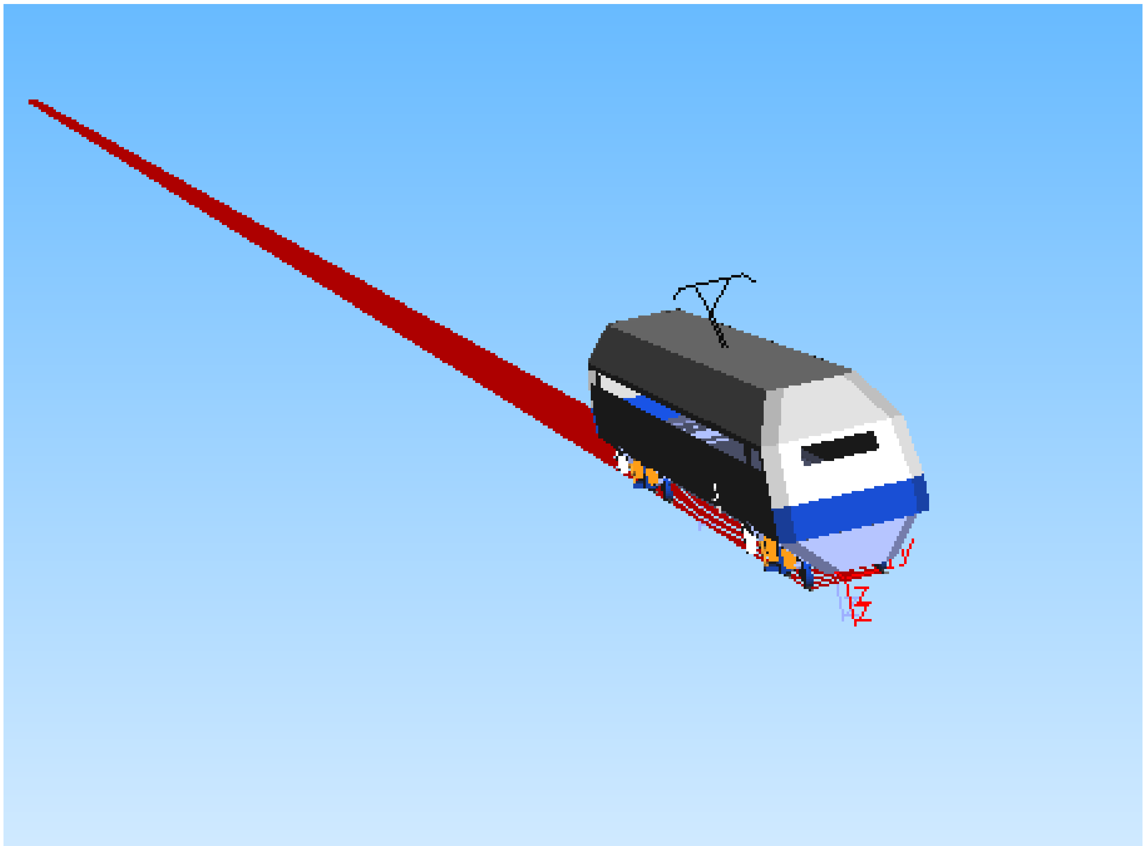

Figure 4. 3 Vehicle modeling

4.1.5 Wear Volume Calculation for Wheel and Rail

The frictional energy (work) models and Archard wear models (sliding) models can help to model the wear. In the case of frictional energy models the wear rate is related to the work done in the wheel-rail contact. Archard wear model is based on the wear rate is related to the sliding distance, normal force and hardness of the material[16]. The following figure shows the new and worn profile of the wheel.

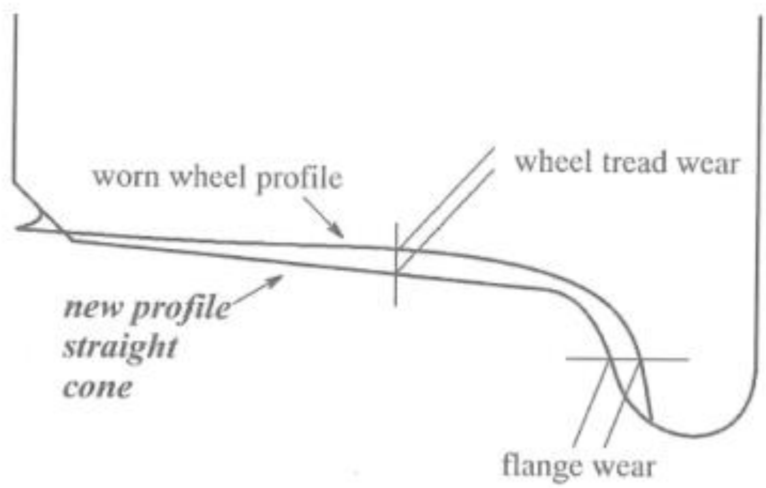

Figure 3. 3 Typical shape of a worn wheel[16]

4.1.6 Archard's Wear Model

To calculate the wear volume V_{wear} [m^3] the following relation can help depend on Archard model[16].

$$\boldsymbol{V_{wear} = k_i \frac{sN}{H}} \qquad (4.1)$$

Where

k_i = wear coefficient [-]

s = sliding distance [m]

N = normal force [N]

H = hardness of the material [N/m^2].

Replace the normal force with the product of the contact pressure and area of an element to determine wear by discretizing the contact patch with a grid of elements. In this case, the depth of the wear for each element can be obtained.

$$\Delta Z = k_i \frac{sPA}{H} \tag{4. 2}$$

Where

ΔZ = the depth of the wear [m]

P = the contact pressure [N/m^2]

A = the area of an element ($\Delta x \Delta y$) [m^2]

The Archard's wear model is based on the wear will not occur in the adhesion zone of the contact, because of the sliding distance is zero or the slip velocity is zero. The wear distribution is obtained for each wheel revolution (dz) [m]by adding the wear depth along the longitudinal direction for each cell element.

$$k_i = \frac{(\frac{W}{\rho})H}{F} \tag{4. 3}$$

Where

W = wear rate [Kg/m]

ρ = density of the material [kg/m^3]

F = applied load [N]

3.4 Adhesion Coefficient

To calculate the adhesion coefficient for each wheelset (f_i) the relationship expressed as the relation between the longitudinal forces ($F_{x,i}$) and normal forces (N_i) acting on the wheel-rail interface can help. (3)

$$f_i = \frac{F_{x,i}}{N_i} \tag{4. 4}$$

To determine the longitudinal force, the equilibrium of momentum for braked wheelset expressed as follow:

$$\boldsymbol{F_{x,i}} = \frac{\mathbf{2}}{\boldsymbol{d_w}}(\boldsymbol{T_{b,i}} - \boldsymbol{I_{w,yy}}\dot{\boldsymbol{\omega}}_{\boldsymbol{w,i}}) \quad (4.\ 5)$$

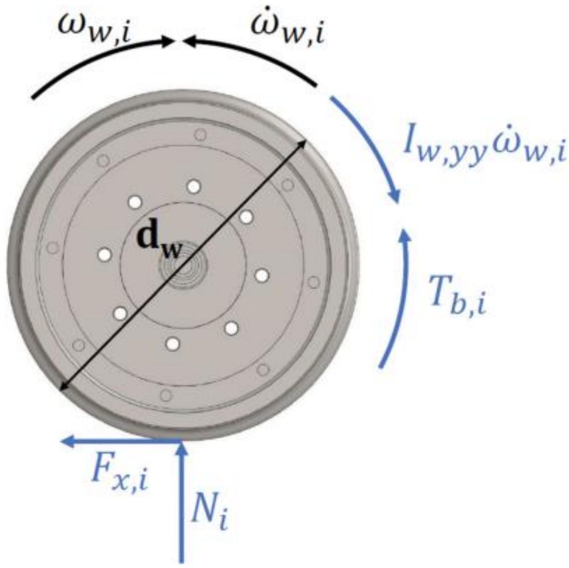

Figure 3. 4 Equilibrium of momentum of the braked wheelset

Where,

d_w = diameter of the wheel

$T_{b,i}$ = the braking torque acting on braked wheelset

$I_{w,yy}$ = the polar momentum of inertia of the wheelset

$\dot{\omega}_{w,i}$ = the angular acceleration of the i wheelset

4.2 Braking and Traction System

The motor bogies of the vehicle have traction motors, one per wheelset. When the vehicle is accelerating a constant traction torque is applied. Equipment's of brake system can be divided into 3 categories by its method to produce braking force.

1. Electrical brake control equipment (such brake equipment is used together with traction equipment).
2. Hydraulic brake control equipment and actuating equipment,
3. Magnetic track brake equipment.

In addition, there is also auxiliary compressed air equipment set for coupler and sanding.

The following expression is given to calculate total torque. In the expression the equivalent mass, running resistance and track gradient is neglected[26].

$$\mathbf{T_t = m \cdot a \cdot r = 4T_y} \qquad (4.\ 6)$$

Where

m = mass of the vehicle

a = vehicle acceleration

r = wheel radius

T_t = total torque and

T_y = torque applied on each wheelset

Braking torque

$$\mathbf{T_{tb} = m \cdot a \cdot r = 4T_b} \qquad (4.\ 7)$$

Where

T_{tb} = total braking torque and

T_b = braking torque applied on each wheelset

4.4 Creepage/Creep Force at Wheel-Rail Interface

This theory is about the tangential contact force of the two bodies. The slip must be occurring when forces transmitted between two bodies in rolling contact. During traction or brake the velocity at the contact point on the wheel must be greater or smaller than the transitional velocity of the vehicle. The sliding velocity is known as creep or creepage. There are three component of the creepage; and these are longitudinal, lateral and spin.

$$\boldsymbol{v}_{\boldsymbol{\xi}} = \frac{\boldsymbol{v}_{\boldsymbol{\xi}}}{\boldsymbol{v}} \qquad (4.\ 8)$$

$$\boldsymbol{v}_{\boldsymbol{\eta}} = \frac{\boldsymbol{v}_{\boldsymbol{\eta}}}{\boldsymbol{v}} \qquad (4.\ 9)$$

$$\emptyset = \frac{\boldsymbol{\omega}}{\boldsymbol{v}} \qquad (4.\ 10)$$

Where,

v_{ξ} and v_{η} = velocities in the direction of (ξ, η)

$\omega =$ Angular velocity around the normal axis of contact patch

v = translational velocity of the vehicle

Then, to sum up these creepage into the resulting translational creep the following relation can describe.

$$\boldsymbol{v} = \sqrt{\boldsymbol{v}_{\boldsymbol{\xi}}^{2} + \boldsymbol{v}_{\boldsymbol{\eta}}^{2}} \qquad (3.\ 11)$$

4.5 Multi-body System Dynamic Simulation

The multi-body system dynamic simulation follows Newton's 2nd law of motion. The total force generated during the dynamic motion is given as the following equations.

$$F_T = (M_c + 2M_B + 8M_w).g \qquad (4.\ 12)$$

To calculate the contact force at individual wheel/rail interaction, divided the total force by the number of the wheels.

$$F_w = T_T/8 \qquad (4.\ 13)$$

CHAPTER FIVE

RESULT AND DISCUSSION

5.1 Result Validation

The results can be validated based on the standard derailment coefficient, vehicle ride index, vertical force (Q), and lateral force. Therefore, the simulated result should maintain a coefficient of derailment for the vehicle of $Y/Q < 0.8$, a ride quality of the vehicle of < 2.5, a graph of the vertical load (Q) vs time (s) as a straight line, and a lateral force less than 60KN ($Y < 60$ KN). The results are validated against the standard vertical force (Q)[34].

For the analysis

- For the analysis 40km/h and 20km/h velocity variation is used.
- The effect of rail irregularity is considered.
- The absence of rail irregularity is considered
- Adhesion coefficients used of the simulation is 0.3 and 0.4.

The results are validated against the standard vertical force (Q).

To validate the result, the simulation is carried out with the standard vertical force (Q). Before applying any preload and initial conditions, the model is simulated under static conditions. At this point, the simulated model represents the vehicle condition without any wheel/rail defects (new wheel and rail). Then, the graph of vertical force (N) vs time (s) is observed without the application of preload and initial conditions, resulting in a straight line.

Therefore, the time integration for the velocity of the vehicle at 40km/h is generated, showing a graph of vertical load vs time as a straight line, as depicted in the following graph. The calculated value for the derailment coefficient also satisfies the standard derailment coefficient, as shown in the following graphs. This indicates that the result generated by Simpack is valid.

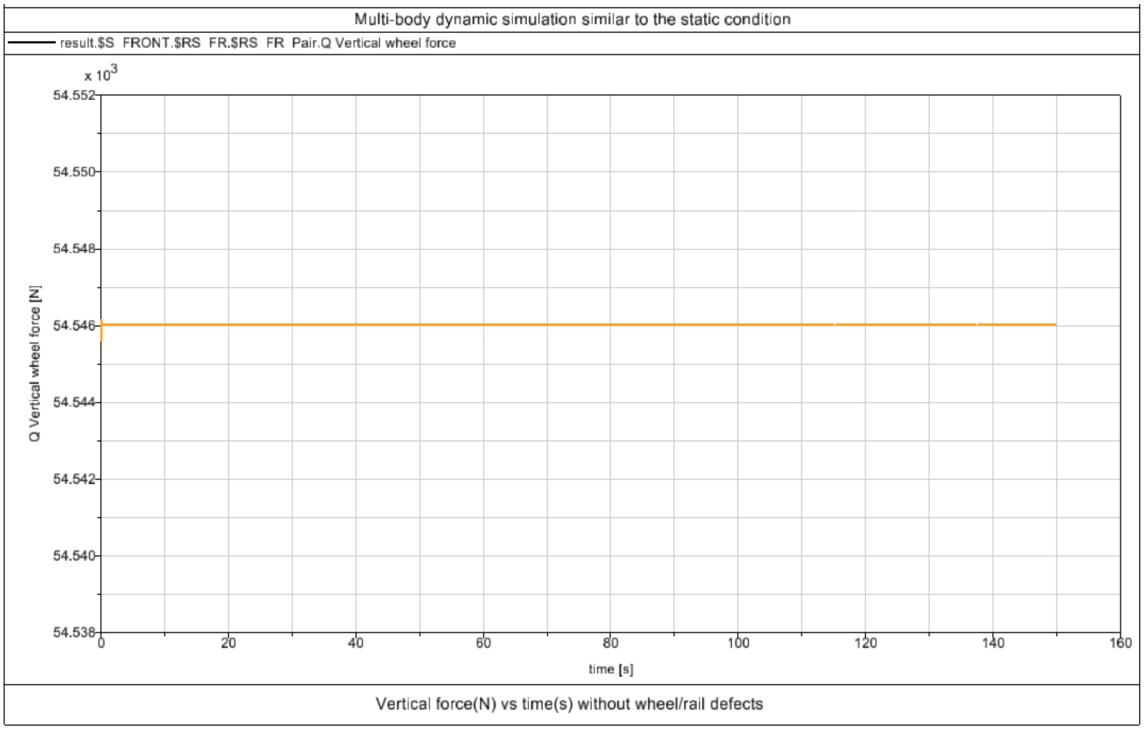

Figure 5. 1 The graph of vertical load vs time without the application of preload

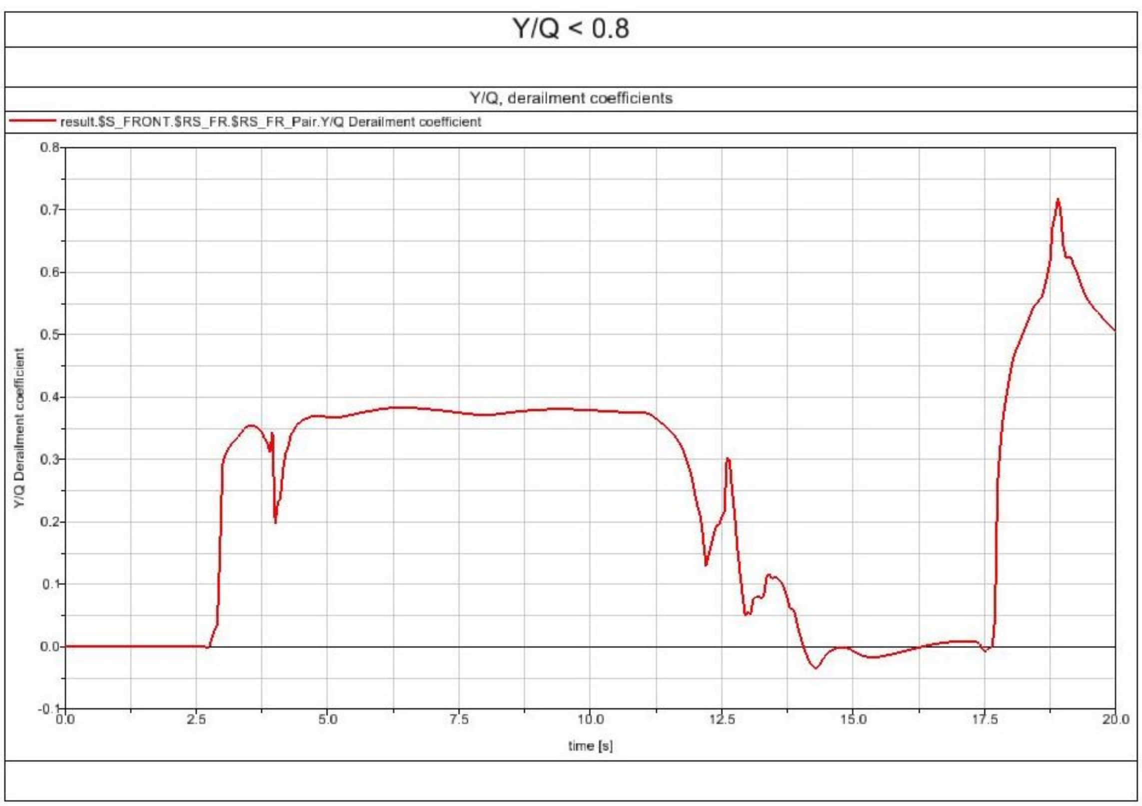

Figure 5. 2 The graph of derailment coefficient before wheel-rail defects

5.2 The Generated Result

The result generated at the vehicle speed of 40km/h with the presence of rail irregularity

The following figures are the result of creep forces generated at the vehicle speed of 40km/h with the presence of rail irregularity. The graph of longitudinal and lateral creep forces are shown as follow.

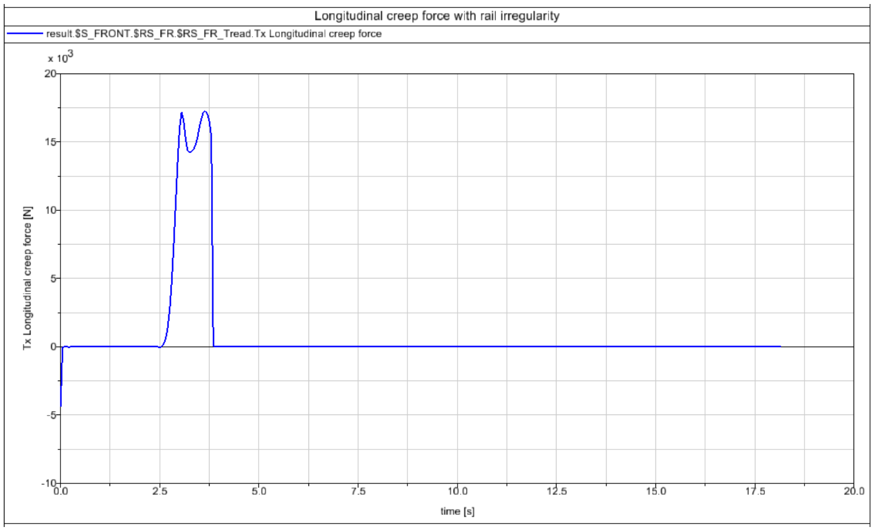

Figure 5. 3 Longitudinal creep force at 40km/h with the presence of rail irregularity

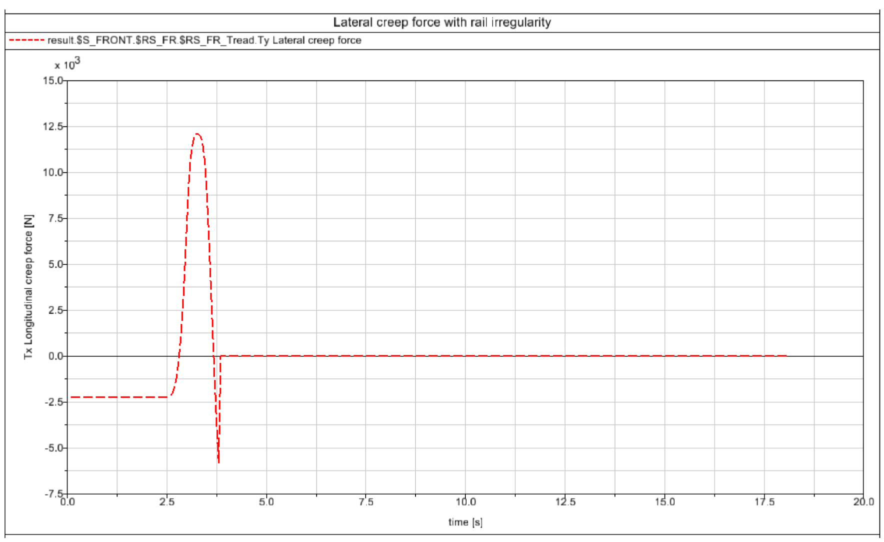

Figure 5. 4 Lateral creep force at 40km/h with the presence of rail irregularity

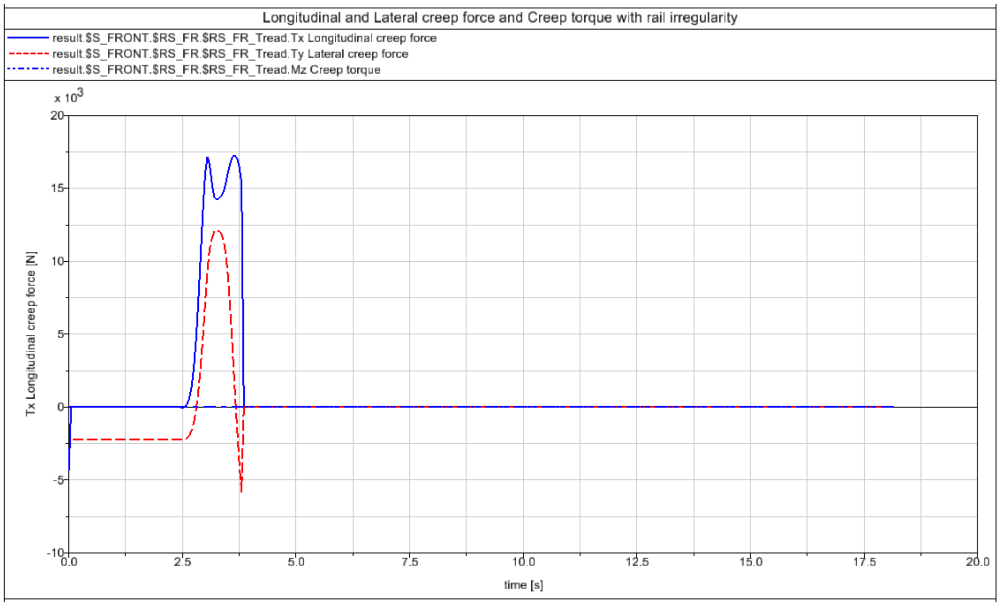

Figure 5. 5 Longitudinal creep force, lateral creep force and creep torque

Creep torque is zero since the wheel spin over the rail instead of sliding.

The following graphs are the results of the longitudinal, lateral and spin creepage at the vehicle speed of 40km/h with presence of rail irregularity.

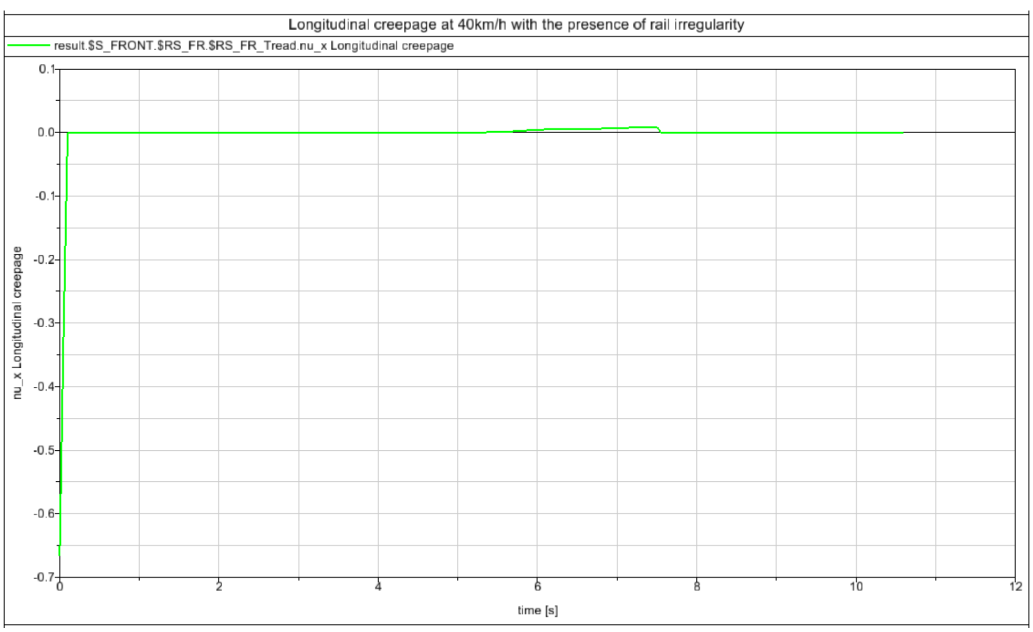

Figure 5. 6 Longitudinal creepage at 40km/h with the presence of rail irregularity

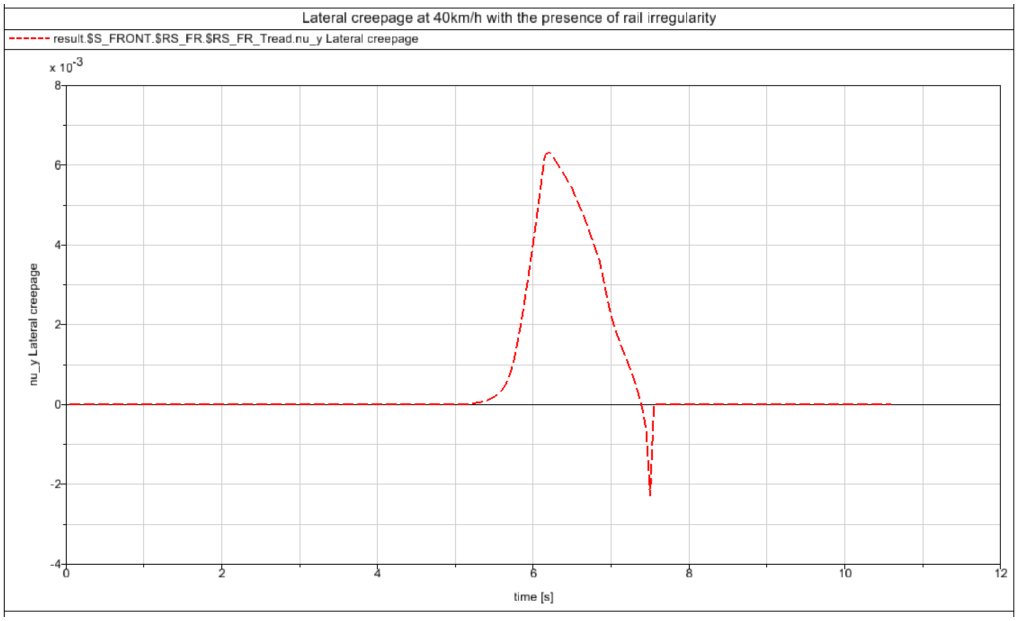

Figure 5. 7 Lateral creepage at 40km/h with the presence of rail irregularity

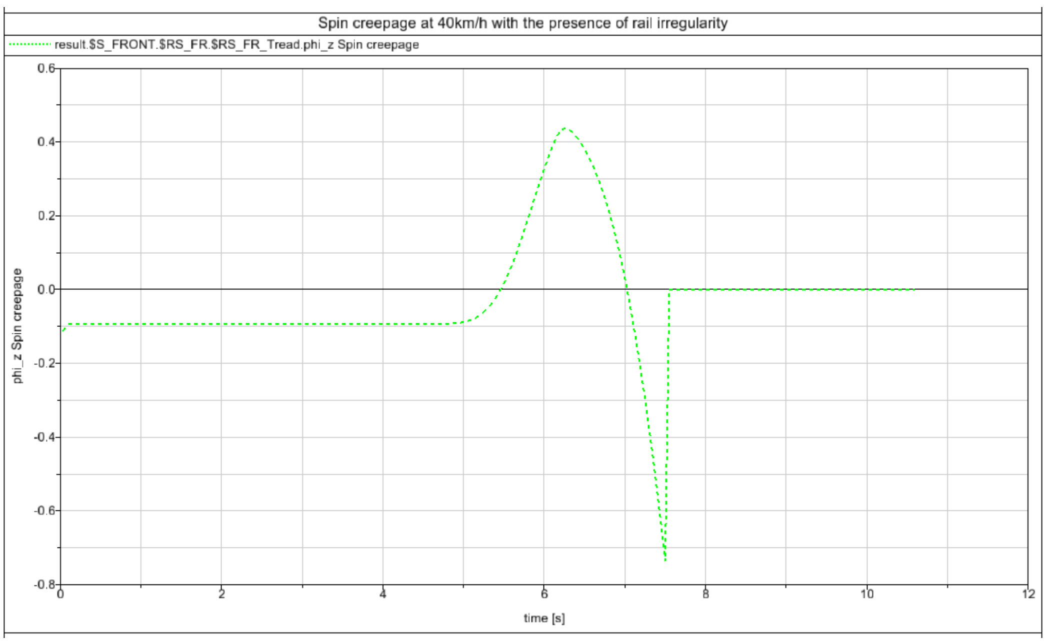

Figure 5. 8 Spin creepage at 40km/h with the presence of rail irregularity

The result generated for the adhesion coefficients at the 40km/h with presence of rail irregularity is shown on the following graphs.

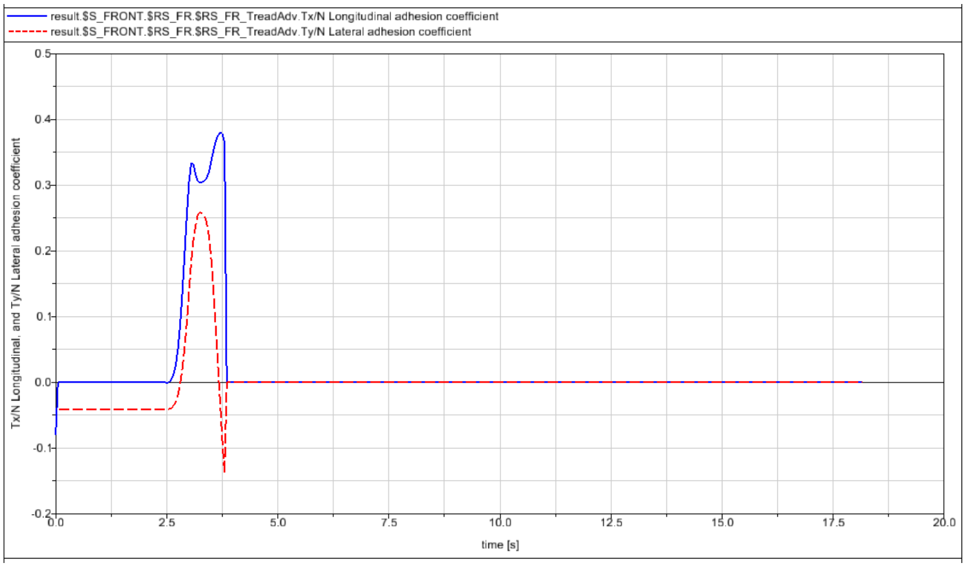

Figure 5. 9 Longitudinal and lateral Adhesion coefficients at 40km/h with the presence of rail irregularity

For the rear wheel-rail pair almost the results are the same. So, for the rear wheel-rail pair the results are discussed as the following graphs.

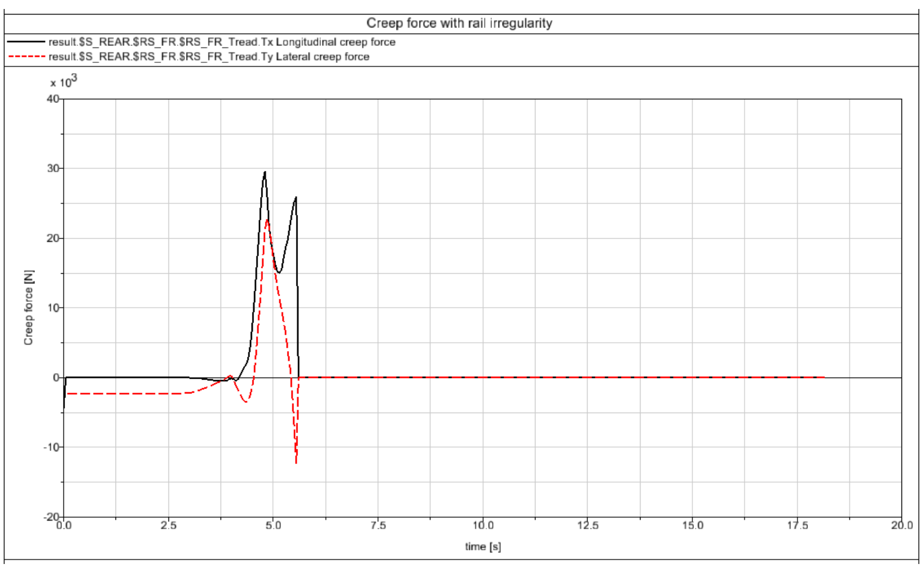

Figure 5. 10 Longitudinal and lateral creep forces at 40km/h with the presence of rail irregularity

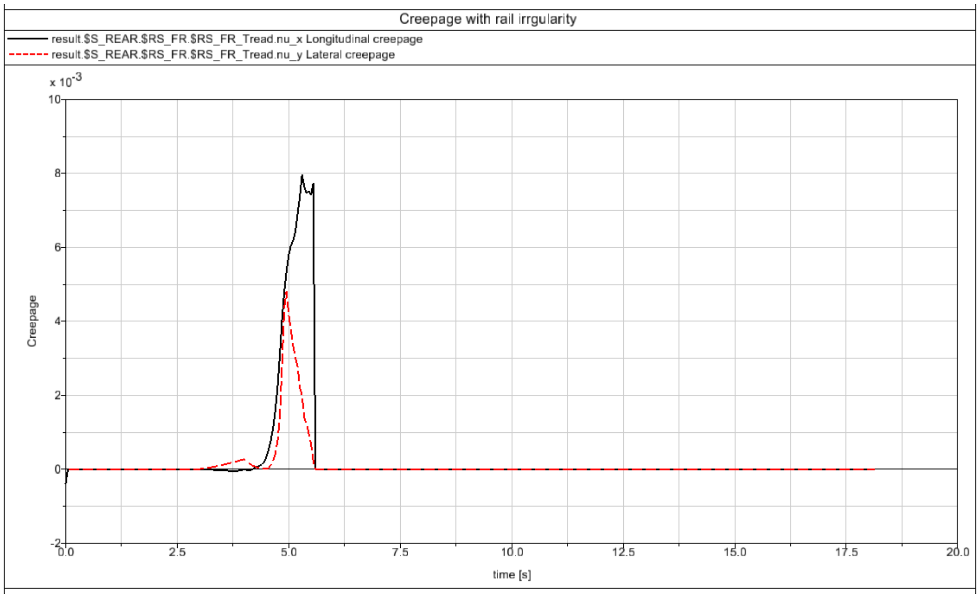

Figure 5. 11 Longitudinal and lateral creepage at 40km/h with the presence of rail irregularity

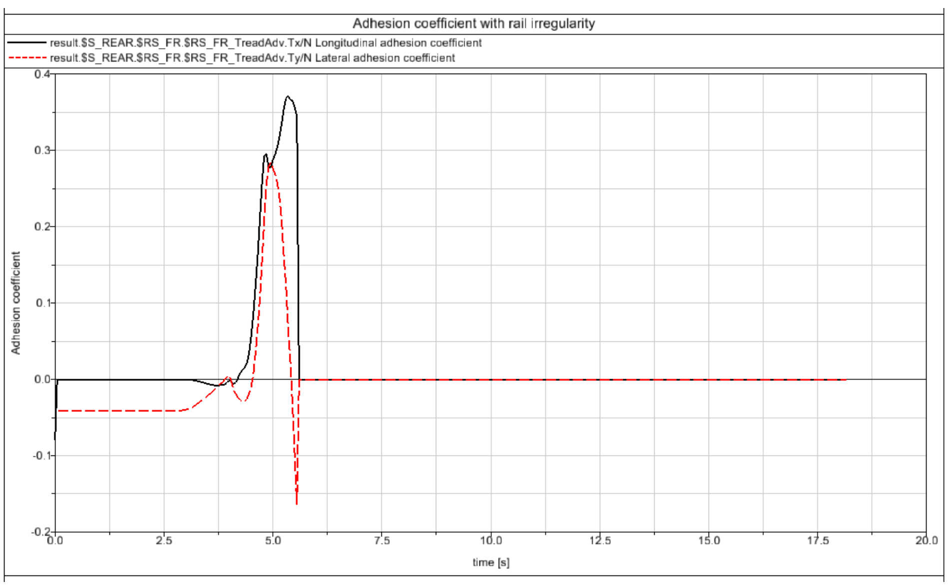

Figure 5. 12 Longitudinal and lateral creepage at 40km/h with the presence of rail irregularity

The above results are generated at the vehicle speed of 40km/h with effect of rail irregularity and compared with result generated at the vehicle speed of 20km/h with presence of rail irregularity.

For the 20km/h speed of vehicle with the presence of rail irregularity, the results are generated as following graphs.

The following graph is the result of creep forces at 20km/h.

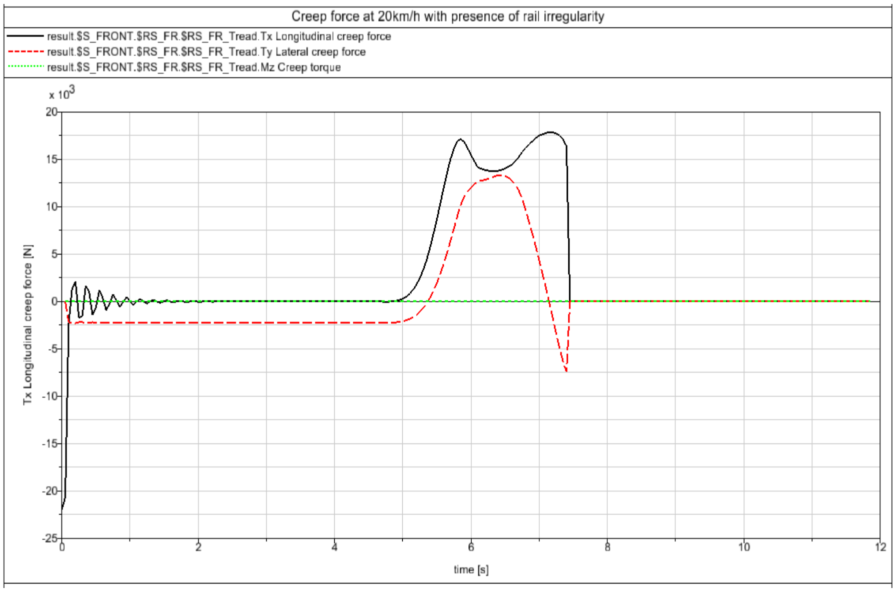

Figure 5. 13 Creep force at 20km/h with presence of rail irregularity

The result generated for the creepage is shown on the following graphs.

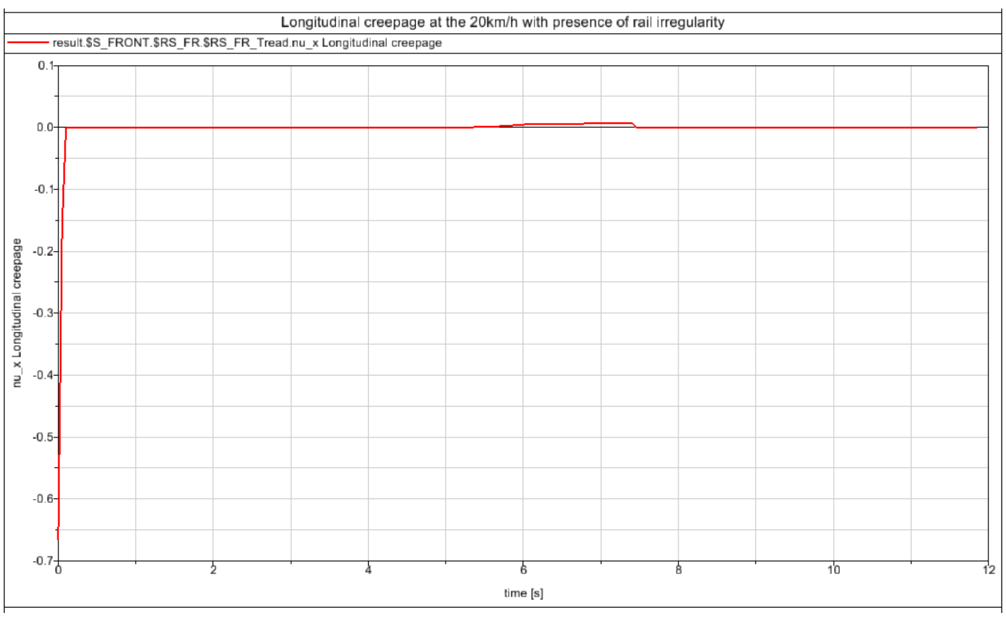

Figure 5. 14 Longitudinal creepage at 20km/h of vehicle speed with presence of rail irregularity

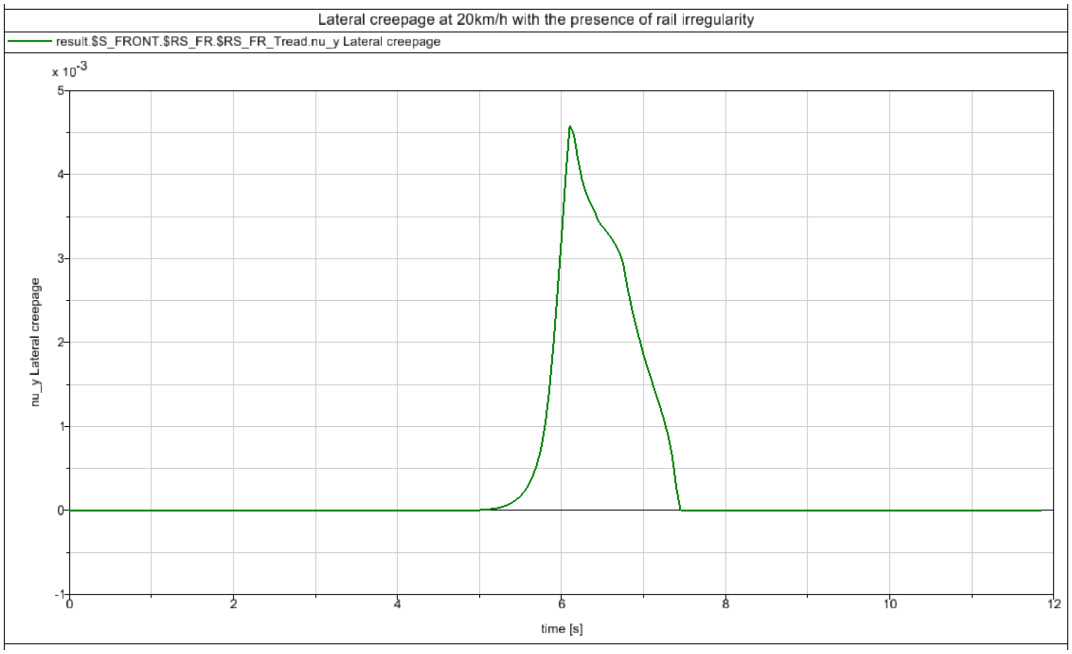

Figure 5. 15 Lateral creepage at 20km/h of vehicle speed with presence of rail irregularity

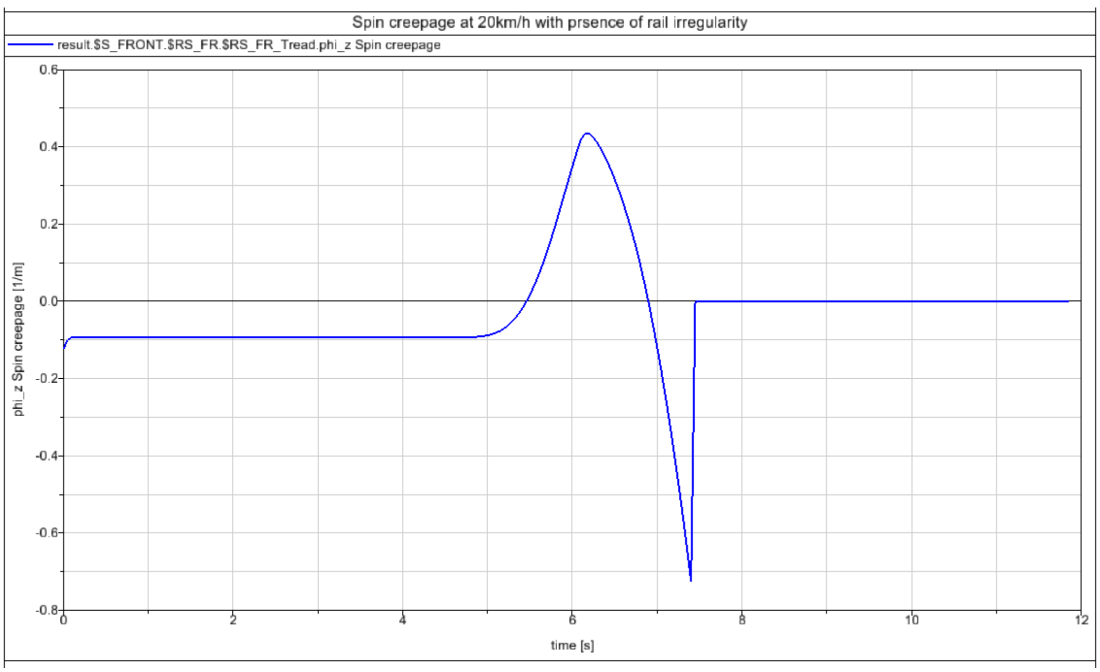

Figure 5. 16 Spin creepage at 20km/h of vehicle speed with presence of rail irregularity

For the adhesion coefficients the results are generated as the below graphs.

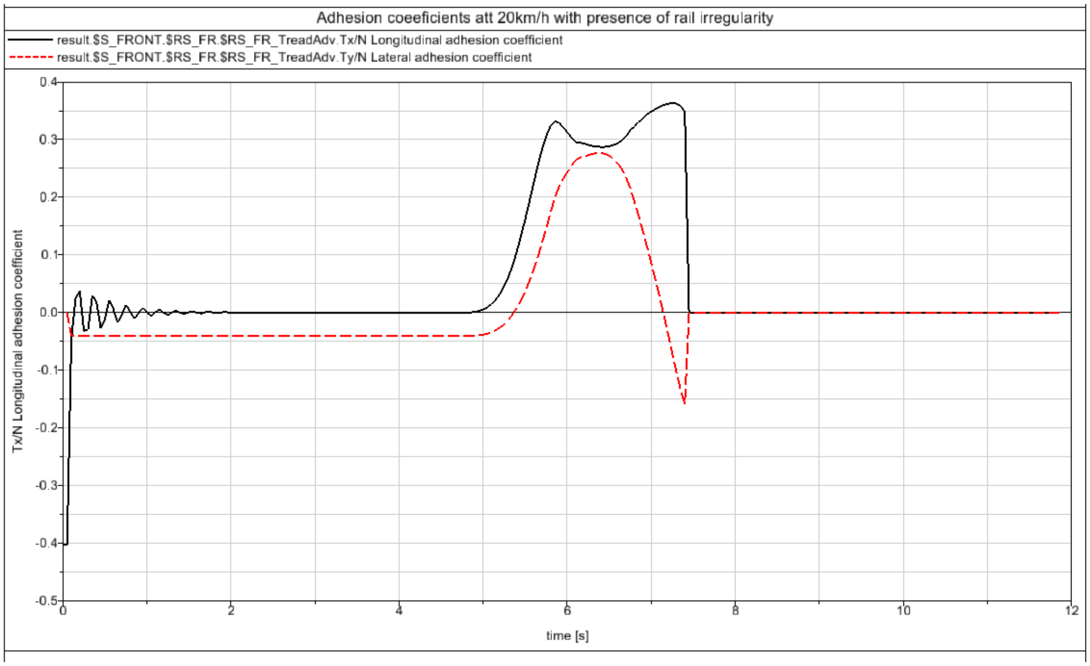

Figure 5. 17 Adhesion coefficients at 20km/h with presence of rail irregularity

When comparing the effects of rail irregularities on creepage, creep forces, and adhesion at different speeds, such as 40km/h and 20km/h, several differences can be observed. At a higher speed, such as 40km/h, the creepage is generally greater compared to a lower speed like 20km/h. This is because the difference in circumferential speeds between the wheel and the rail is larger at higher speeds. Similarly, creep forces, which are the forces acting between the wheel and the rail due to their contact, are also influenced by the vehicle speed. At 40km/h, the presence of rail irregularities can cause fluctuations in the contact pressure and lead to higher creep forces compared to 20km/h. The higher speed increases the dynamic loading on the contact area, exacerbating the effect of irregularities.

Adhesion, the frictional force between the wheel and the rail, is crucial for maintaining traction and ensuring efficient vehicle movement. Rail irregularities can reduce the contact area and negatively impact adhesion. However, the effect of irregularities on adhesion more pronounced at higher speeds. At 40km/h, the risk of wheel slip due to reduced adhesion is greater compared to 20km/h.

The results generated without the rail irregularity

The following graphs are the results of the creep force, creepage and adhesion coefficients generated without the presence of the rail irregularity.

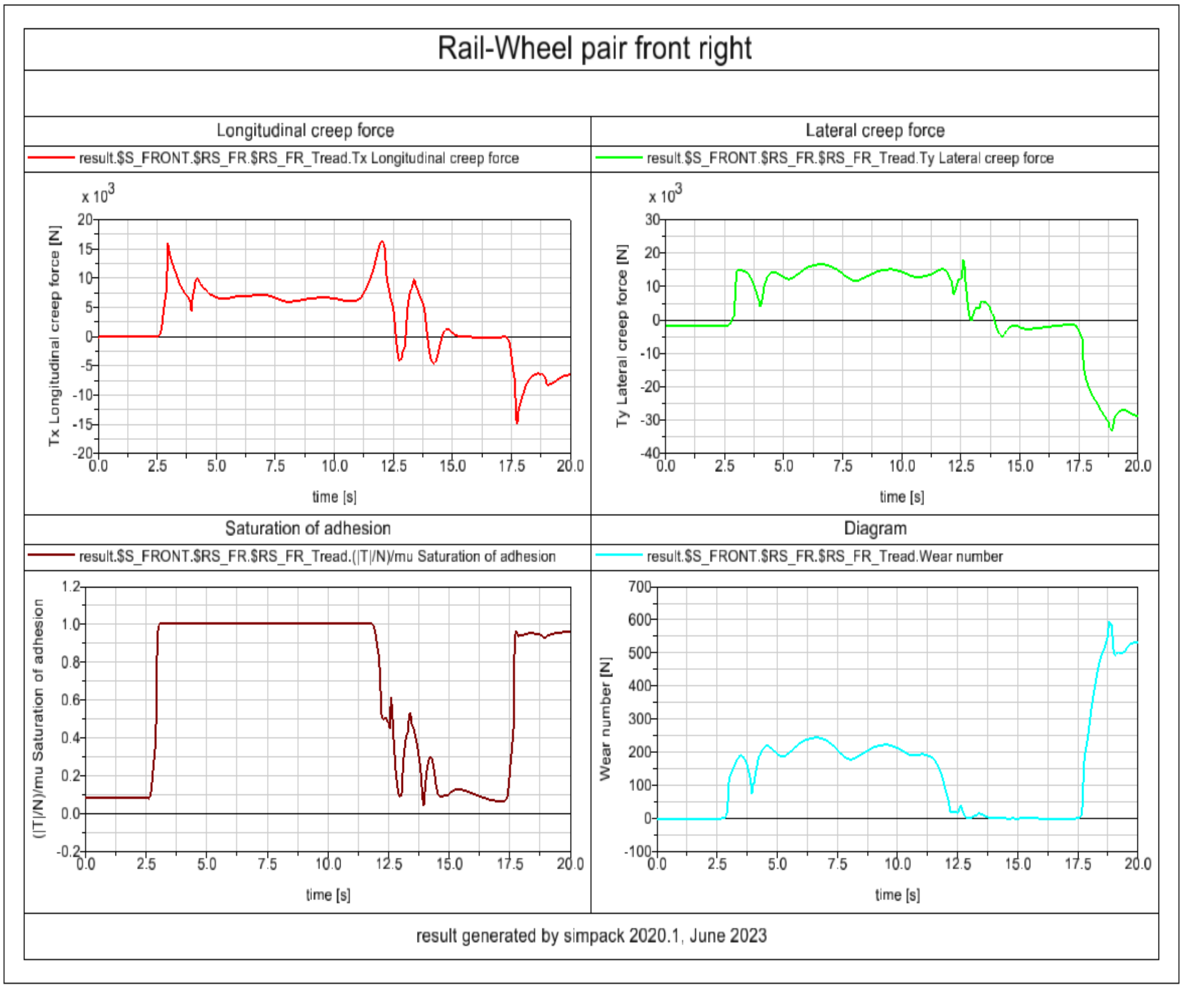

Figure 5. 18 Creep forces without the presence of rail irregularity

For the creepage the result is generated without any presence rail irregularity as the following figure.

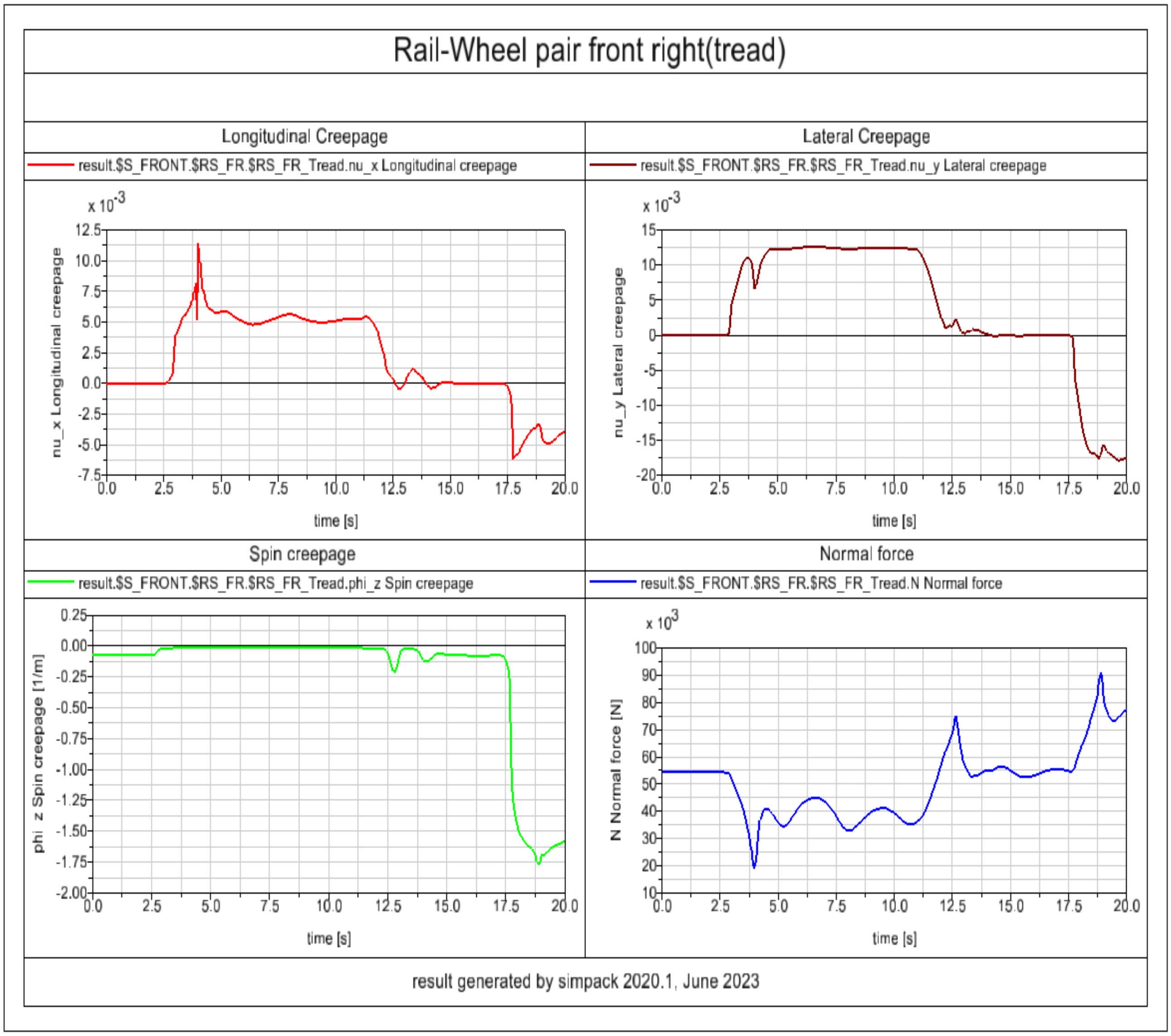

Figure 5. 19 Creepage without the presence of rail irregularity

The result generated for the adhesion coefficients without the presence of rail irregularity

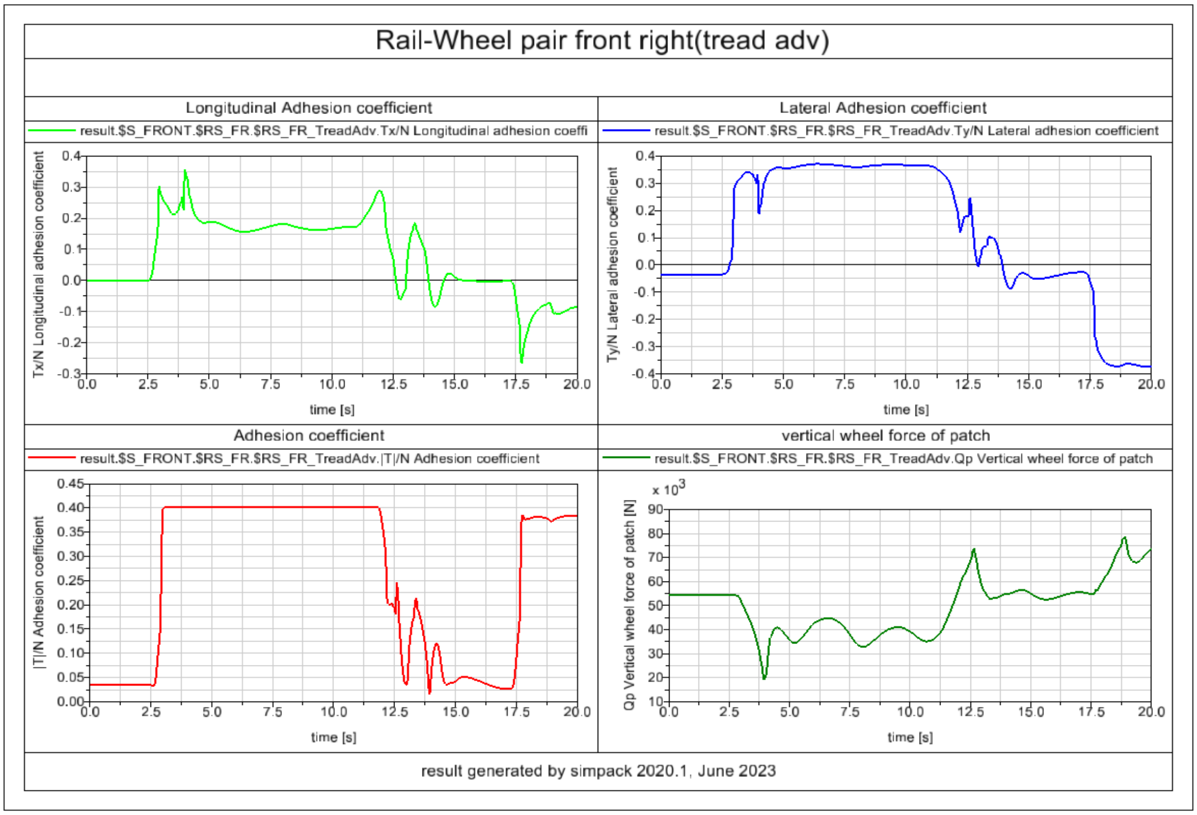

Figure 5. 20 Adhesion coefficients without the presence of rail irregularity

When comparing the effects of rail irregularity on creepage, creep forces, and adhesion with and without the presence of rail irregularity, several differences can be observed. Without any rail irregularity, the creepage is primarily influenced by factors such as wheel design and track geometry. The absence of irregularity allows for a smoother and more consistent interaction between the wheel and the rail, resulting in relatively lower creepage. Without any irregularity, the contact pressure between the wheel and the rail tends to be more uniform, resulting in lower creep forces. The absence of irregularity minimizes variations in the contact pressure and ensures a more stable interaction between the wheel and the rail. The contact area between the wheel and the rail is relatively consistent, allowing for optimal adhesion. The absence of irregularity ensures that the contact area remains intact and provides sufficient friction for good adhesion.

The result generated for the adhesion coefficients of 0.3

For the above results the maximum value of adhesion is 0.4. So, when the value adhesion coefficient is reduced to 0.3, then the results generated are discussed as the following graphs.

The following results of creepage and creep forces are generated when the value of adhesion coefficient is 0.3. The graph for the creep force is shown as follow.

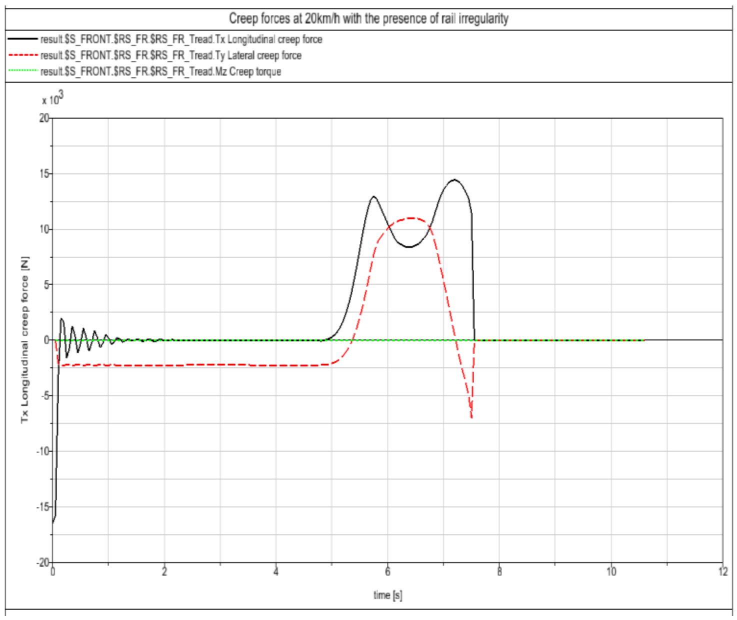

Figure 5. 21 Creep forces and creep torque when the adhesion coefficient is 0.3

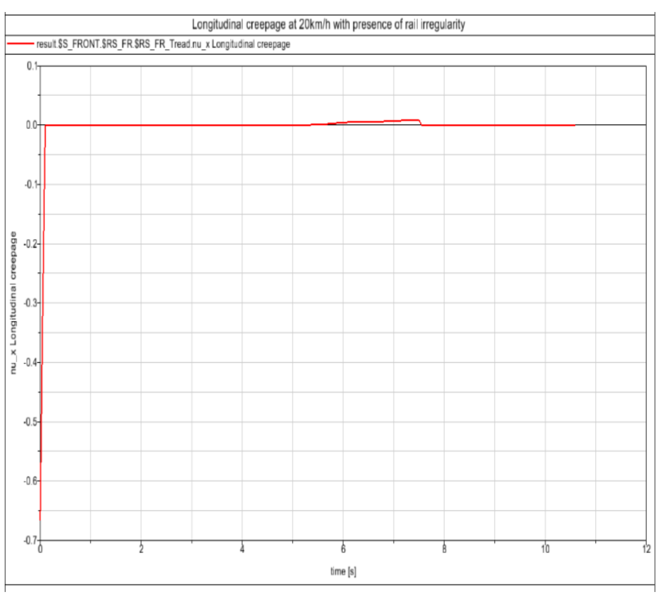

Figure 5. 22 Longitudinal creepage when the adhesion coefficient is 0.3

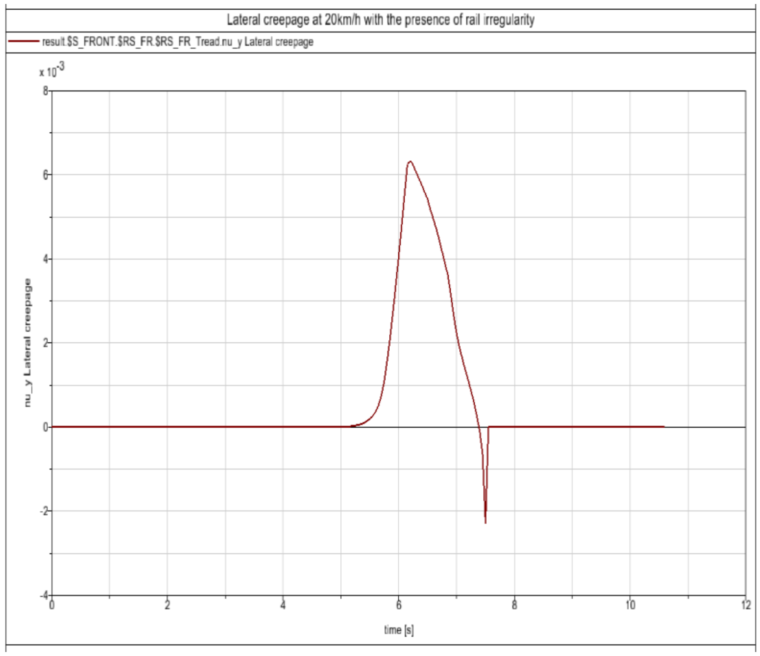

Figure 5. 23 Lateral creepage when the adhesion coefficient is 0.3

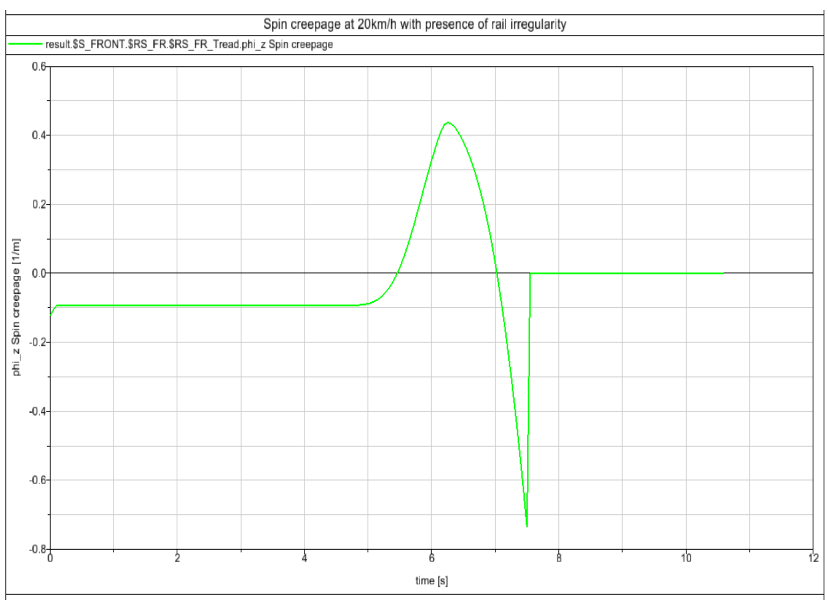

Figure 5. 24 The result of spin creepage generated with the adhesion coefficients of 0.3

The result is compared to the result generated for the adhesion coefficients of 0.4. Different adhesion coefficients, such as 0.3 and 0.4, can influence the creepage and creep forces. A higher adhesion coefficient, such as 0.4, indicates better traction and grip between the wheel and the rail, resulting in lower creepage and creep forces. Conversely, a lower adhesion coefficient, such as 0.3, it leads to higher creepage and creep forces due to reduced friction and grip.

In summary, the presence of rail irregularities affects creepage, creep forces, and adhesion differently at different speeds. Higher speeds generally result in greater creepage, higher creep forces, and a more significant impact on adhesion due to the increased dynamic loading. Therefore, the effects of rail irregularities on these factors are generally more pronounced at 40km/h compared to 20km/h. The presence of rail irregularity significantly affects creepage, creep forces, and adhesion. It increases the creepage due to variations in circumferential speeds, results in higher creep forces due to fluctuating contact pressures, and reduces adhesion by disrupting the contact area. Without any rail irregularity, these effects are minimized, allowing for smoother wheel-rail interaction, lower creepage, lower creep forces, and optimal adhesion. The presence of rail irregularity increases creepage and creep forces, while their absence results in lower values. Higher velocities generally generate greater creepage and creep forces compared to lower velocities. The adhesion coefficient plays a crucial role in determining the level of creepage and creep forces, with higher values associated with lower creepage and creep forces.

CHAPTER SIX

CONCLUSION AND RECOMMENDATION

6.1 Conclusion

Creepage at the wheel-rail interface is a critical phenomenon that affects the performance and safety of railway systems. It refers to the relative motion between the wheel and rail when the sliding force overcomes the adhesion force. Creepage can occur in various operating conditions, such as during acceleration, deceleration, braking, and when encountering rail irregularities.

This study aims to analyze the effects of creepage and creep force under different scenarios to gain insights into their behavior and improve the understanding of their impact on rail dynamics. The analysis of creepage and creep force with rail irregularity is crucial as it helps identify the response of the system when the wheel encounters unevenness and irregularities on the track. Rail irregularities can lead to changes in creepage behavior, affecting vehicle stability and ride quality. Understanding these effects can guide the design of railway infrastructure and maintenance practices, ultimately improving passenger comfort and safety.

On the other hand, analyzing creepage and creep force without rail irregularity allows for the investigation of the fundamental mechanisms governing creepage behavior. By eliminating external factors like rail irregularity, this analysis provides insights into the inherent characteristics of the wheel-rail interface and helps evaluate the efficiency of adhesion forces.

Furthermore, considering creepage and creep force with velocity variation enables us to explore the relationship between velocity and the occurrence of creepage. Different velocities induce changes in the contact forces and lead to variations in creepage behavior. Understanding the effect of velocity is crucial for optimizing vehicle operations.

Lastly, analyzing creepage and creep force with adhesion coefficients allows for the assessment of the influence of adhesion properties on creepage behavior. The adhesion coefficient determines the maximum amount of friction between the wheel and rail, impacting the occurrence and extent of creepage. Studying the effects of different adhesion coefficients provides valuable insights for optimizing vehicle control systems, particularly during braking and acceleration phases.

In summary, this study aims to investigate the phenomenon of creepage at the wheel-rail interface by examining its behavior with and without rail irregularity, with velocity variation, and with varying adhesion coefficients. By analyzing these specific objectives, a comprehensive understanding of creepage and creep force can be achieved, leading to improved safety, efficiency, and performance of railway systems.

6.1.2 Recommendations

Still, the rail way system needs more works on the bogie stability, the effect of lubrication on wheel and rail, wheel and rail surface irregularities, causes of corrugation, noise, body stability and the effect of braking and accelerating on the material removal and dynamic behavior of the vehicle. In general, the consideration of acceleration, braking and traction of the vehicle is significant for wheel-rail interface in the case of railway systems. The wheel-rail interface is a critical area in the case of rail vehicles. Because the wheel and rail contact have a vital role in the vehicle performance.

Future Work

Further research in this area is essential to enhance braking efficiency, improve vehicle dynamics, and reduce wear at the wheel-rail interface. Some interested areas are also mentioned below.

- Experimental study of the creepage zone when vehicle starts and stops
- Creepage zone on the small sliding of the wheel on the rail
- Analysis of the wear and adhesion by considering the distance between each station.
- Analysis of amount of material removed from the rail and wheel at each station during starting and braking.

Reference

[1] M. S. Sichani, R. Enblom, and M. Berg, *Non-Elliptic Wheel-Rail Contact Modelling in Vehicle Dynamics Simulation*, vol. 3, no. 3. 2014. doi: 10.4203/ijrt.3.3.5.

[2] A. Alonso, A. Guiral, L. Baeza, and S. Iwnicki, “Wheel-rail contact: Experimental study of the creep forces-creepage relationships,” *Veh. Syst. Dyn.*, vol. 52, no. SUPPL. 1, pp. 469–487, 2014, doi: 10.1080/00423114.2014.907923.

[3] F. Yang, Z. Wei, X. Sun, C. Shen, and A. Núñez, “Wheel-rail rolling contact behavior induced by both rail surface irregularity and sleeper hanging defects on a high-speed railway line,” *Eng. Fail. Anal.*, vol. 128, no. July, 2021, doi: 10.1016/j.engfailanal.2021.105604.

[4] Y. Qian, P. Wang, J. Chen, G. Bethel Lulu, J. Xu, and B. An, “Numerical investigation of the influence of the creep curve on the wheel–rail contact damage in high-speed railway turnouts,” *Proc. Inst. Mech. Eng. Part F J. Rail Rapid Transit*, vol. 233, no. 9, pp. 926–936, 2019, doi: 10.1177/0954409718819574.

[5] A. L. George, “THEORETICAL AND NUMERICAL INVESTIGATION ON TRACTION FORCES FOR HIGH ADHESION LOCOMOTIVES,” no. July, 2015.

[6] J. F. Aceituno, P. Wang, L. Wang, and A. A. Shabana, “Influence of rail flexibility in a wheel/rail wear prediction model,” *Proc. Inst. Mech. Eng. Part F J. Rail Rapid Transit*, vol. 231, no. 1, pp. 57–74, 2017, doi: 10.1177/0954409715618426.

[7] E. Meli, L. Pugi, and A. Ridolfi, “An innovative degraded adhesion model for multibody applications in the railway field,” *Multibody Syst. Dyn.*, vol. 32, no. 2, pp. 133–157, 2014, doi: 10.1007/s11044-013-9400-9.

[8] T. Jendel and M. Berg, "Prediction of wheel profile wear: Methodology and verification," in *Vehicle System Dynamics*, Swets en Zeitlinger B.V., 2003, pp. 502–513. doi: 10.1080/00423114.2002.11666258.

[9] A. Anyakwo, C. Pislaru, and A. Ball, "A new method for modelling and simulation of the dynamic behaviour of the wheel-rail contact," *Int. J. Autom. Comput.*, vol. 9, no. 3, pp. 237–247, 2012, doi: 10.1007/s11633-012-0640-6.

[10] C. Chang, B. Chen, Y. Cai, and J. Wang, "An experimental study of high speed wheel-rail adhesion characteristics in wet condition on full scale roller rig," *Wear*, vol. 440–441, p. 203092, 2019, doi: 10.1016/j.wear.2019.203092.

[11] H. Alturbeh, J. Stow, G. Tucker, and A. Lawton, "Modelling and simulation of the train brake system in low adhesion conditions," *Proc. Inst. Mech. Eng. Part F J. Rail Rapid Transit*, vol. 234, no. 3, pp. 301–320, Mar. 2020, doi: 10.1177/0954409718800579.

[12] X. Liu, C. Xiao, and P. A. Meehan, "The effect of rolling speed on lateral adhesion at wheel/rail interface under dry and wet condition," *Wear*, vol. 438–439, no. August, p. 203073, 2019, doi: 10.1016/j.wear.2019.203073.

[13] N. Jima, "Design and implementing of Passenger Information System at stations of AALRT," 2017.

[14] K. Oldknow, "Wheel-Rail Friction Management," 2022.

[15] SILABHADRA DAS, "Rail Wheel," *TradeBoss*, 2021, [Online]. Available: https://www.tradeboss.com/default.cgi/action/viewproducts/productid/258498/productname/Rail_wheel_railway_wheel_railroad_wheels_train_wheels_AAR_wheels/

[16] B. Dirks, *Simulation and measurement of wheel on rail fatigue and wear*, no. June 2015.

2015.

[17] Y. Zhu, *Adhesion in the wheel-rail contact*. 2013.

[18] N. Bosso, A. Gugliotta, M. Magelli, I. F. Oresta, and N. Zampieri, "Study of wheel-rail adhesion during braking maneuvers," *Procedia Struct. Integr.*, vol. 24, pp. 680–691, 2019, doi: 10.1016/j.prostr.2020.02.060.

[19] W. Yan and F. D. Fischer, "Applicability of the Hertz contact theory to rail-wheel contact problems," *Arch. Appl. Mech.*, vol. 70, no. 4, pp. 255–268, 2000, doi: 10.1007/s004199900035.

[20] T. Telliskivi and U. Olofsson, "Contact mechanics analysis of measured wheel–rail," *Rail Rapid Transit*, vol. 215, no. 2, pp. 65–73, 2005.

[21] J. Santamaria, E. G. Vadillo, and J. Gomez, "Influence of creep forces on the risk of derailment of railway vehicles," *Veh. Syst. Dyn.*, vol. 47, no. 6, pp. 721–752, Jun. 2009, doi: 10.1080/00423110802368817.

[22] D. J. Fourie, P. J. Gräbe, P. S. Heyns, and R. D. Fröhling, "Analysis of railway wheel-squeal due to unsteady longitudinal creepage using the complex eigenvalue method," *Notes Numer. Fluid Mech. Multidiscip. Des.*, vol. 139, pp. 57–69, 2018, doi: 10.1007/978-3-319-73411-8_3.

[23] Q. Wu, C. Cole, and M. Spiryagin, "Train braking simulation with wheel-rail adhesion model," *Veh. Syst. Dyn.*, vol. 58, no. 8, pp. 1226–1241, 2020, doi: 10.1080/00423114.2019.1645342.

[24] N. Bosso, M. Magelli, and N. Zampieri, "Investigation of adhesion recovery phenomenon using a scaled roller-rig," *Veh. Syst. Dyn.*, vol. 59, no. 2, pp. 295–312, 2021, doi:

10.1080/00423114.2019.1677922.

[25] S. C. Lim, M. F. Ashby, and J. H. Brunton, "Wear-rate transitions and their relationship to wear mechanisms," *Acta Metall.*, vol. 35, no. 6, pp. 1343–1348, 1987, doi: 10.1016/0001-6160(87)90016-2.

[26] I. Robla Sánchez, "Wheel Wear Simulation of the Light Rail Vehicle A32".

[27] Z. Lei and Z. Wang, "Contact and creep characteristics of wheel–rail system under harmonic corrugation excitation," *JVC/Journal Vib. Control*, vol. 27, no. 17–18, pp. 2069–2080, 2021, doi: 10.1177/1077546320953358.

[28] G. Tao, Z. Wen, G. Chen, Y. Luo, and X. Jin, "Locomotive wheel polygonisation due to discrete irregularities: simulation and mechanism," *Veh. Syst. Dyn.*, vol. 59, no. 6, pp. 872–889, 2021, doi: 10.1080/00423114.2020.1737148.

[29] E. Vollebregt, K. Six, and O. Polach, "Challenges and progress in the understanding and modelling of the wheel–rail creep forces," *Veh. Syst. Dyn.*, vol. 59, no. 7, pp. 1026–1068, 2021, doi: 10.1080/00423114.2021.1912367.

[30] Y. Yang, L. Ling, C. Wang, Z. Liu, K. Wang, and W. Zhai, "Wheel/rail dynamic interaction induced by polygonal wear of locomotive wheels," *Veh. Syst. Dyn.*, vol. 60, no. 1, pp. 211–235, 2022, doi: 10.1080/00423114.2020.1807572.

[31] T. M. Godie, "Analysis of Wear Resistance of Wheel-Rail Contact Surface Materials: In the Case of Addis Ababa Light Rail Transit," vol. 21, no. 1, pp. 1–9, 2020.

[32] Z. T. Birhan, "Effects of the Radius of Curved Rail and Vehicle Speed on Rail Friction and Wear," 2013.

[33] T. Atalay, “Shape Optimization of AALRT Wheel Profile,” no. June, 2018.

[34] D. Fekadu, “Investigating the wheel wear of Addis Ababa Light Rail Transit (AALRT),” no. December, p. 94, 2014.

[35] A. Negash, “Analysis of Wheel / Rail Contact Geometry and Applied Load Conditions on the Analysis of Wheel / Rail Contact Geometry and Applied Load Conditions on the Rail Head Surface,” 2012.

[36] G. Aklilu, “Investigation on the Contact Fatigue of Railway Wheel Using a Critical Plane Model,” p. 83, 2021, [Online]. Available: https://www.researchgate.net/publication/357673122_Investigation_on_the_Contact_Fatigue_of_Railway_Wheel_Using_a_Critical_Plane_Model

[37] “Operation and Maintenance Manual for 70% Low Floor Light Rail Vehicle Project in Addis Ababa, Ethiopia,” vol. Volume VIII, 2014.

[38] D. Thompson and G. Squicciarini, “Rail vehicle dynamics,” *Transp. Sustain.*, vol. 14, pp. 133–147, 2022, doi: 10.1108/S2044-994120220000014008.

Appendices

Formulas

$v = \sqrt{v_\xi^2 + v_\eta^2}$ = the net creepage

$v_\xi = \frac{v_\xi}{v}$ = longitudinal creepage

$v_\eta = \frac{v_\eta}{v}$ = lateral creepage

$\emptyset = \frac{\omega}{v}$ = spin creepage

$T_t = m \cdot a \cdot r = 4T_y$ = barking torque

$T_{tb} = m \cdot a \cdot r = 6T_b$ = total barking torque

$f_i = \frac{F_{x,i}}{N_i}$ = adhesion coefficient

$F_{x,i} = \frac{2}{d_w}(T_{b,i} - I_{w,yy}\dot{\omega}_{w,i})$ = longitudinal force

$V_{wear} = k_i \frac{sN}{H}$ = wear volume

S = $|\bar{v}_s| \frac{\Delta x}{V_v}$ = sliding distance

Wheel and rail geometry

The following figure shows the wheel and rail geometry

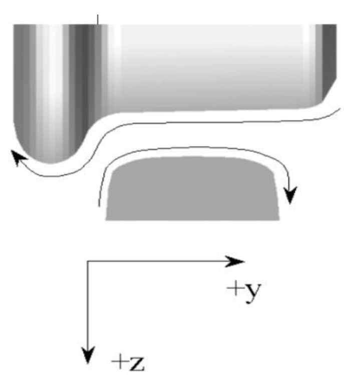

Wheel-Rail interface Inner profile side

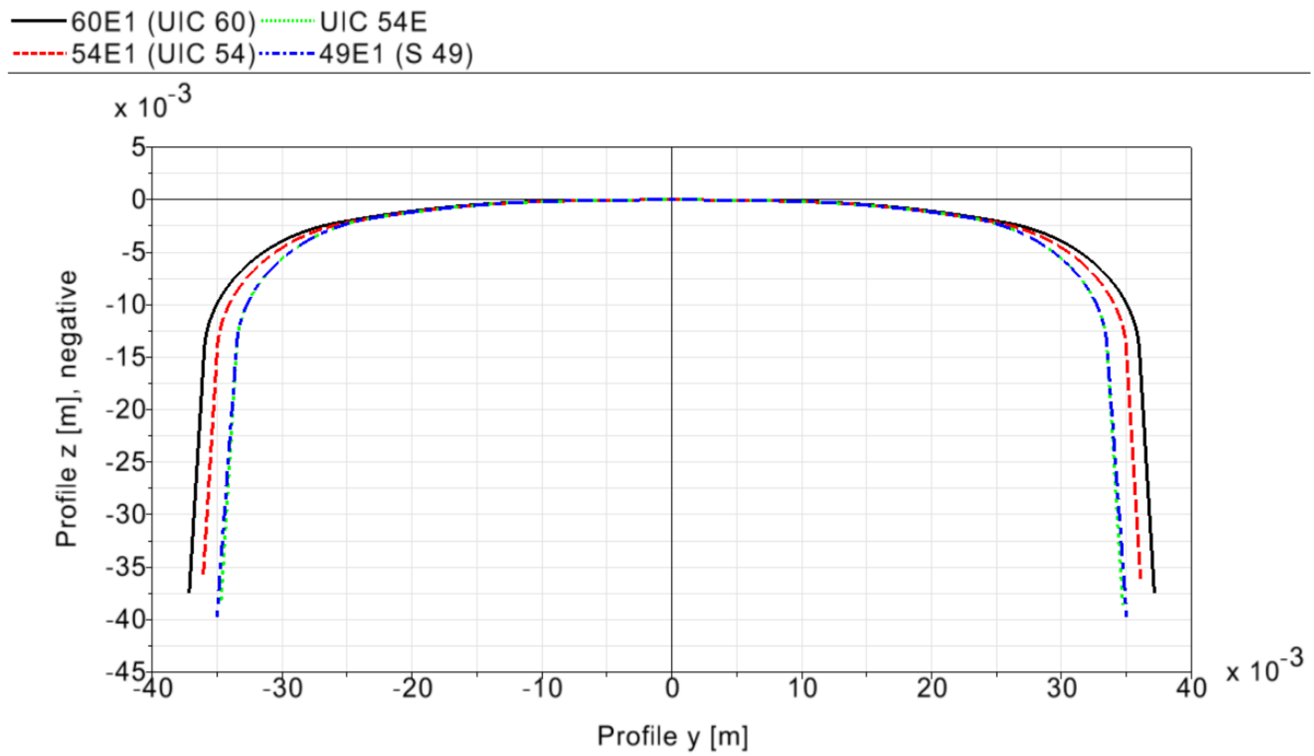

Standard rail profile

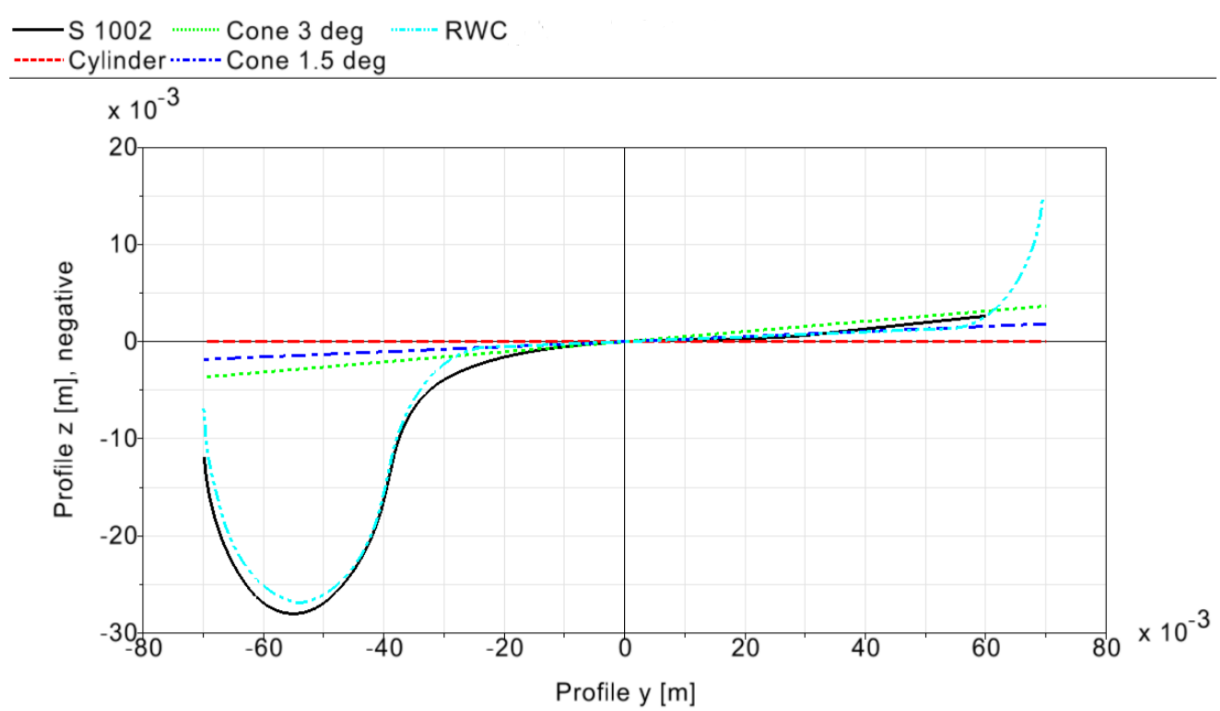

Standard wheel profile

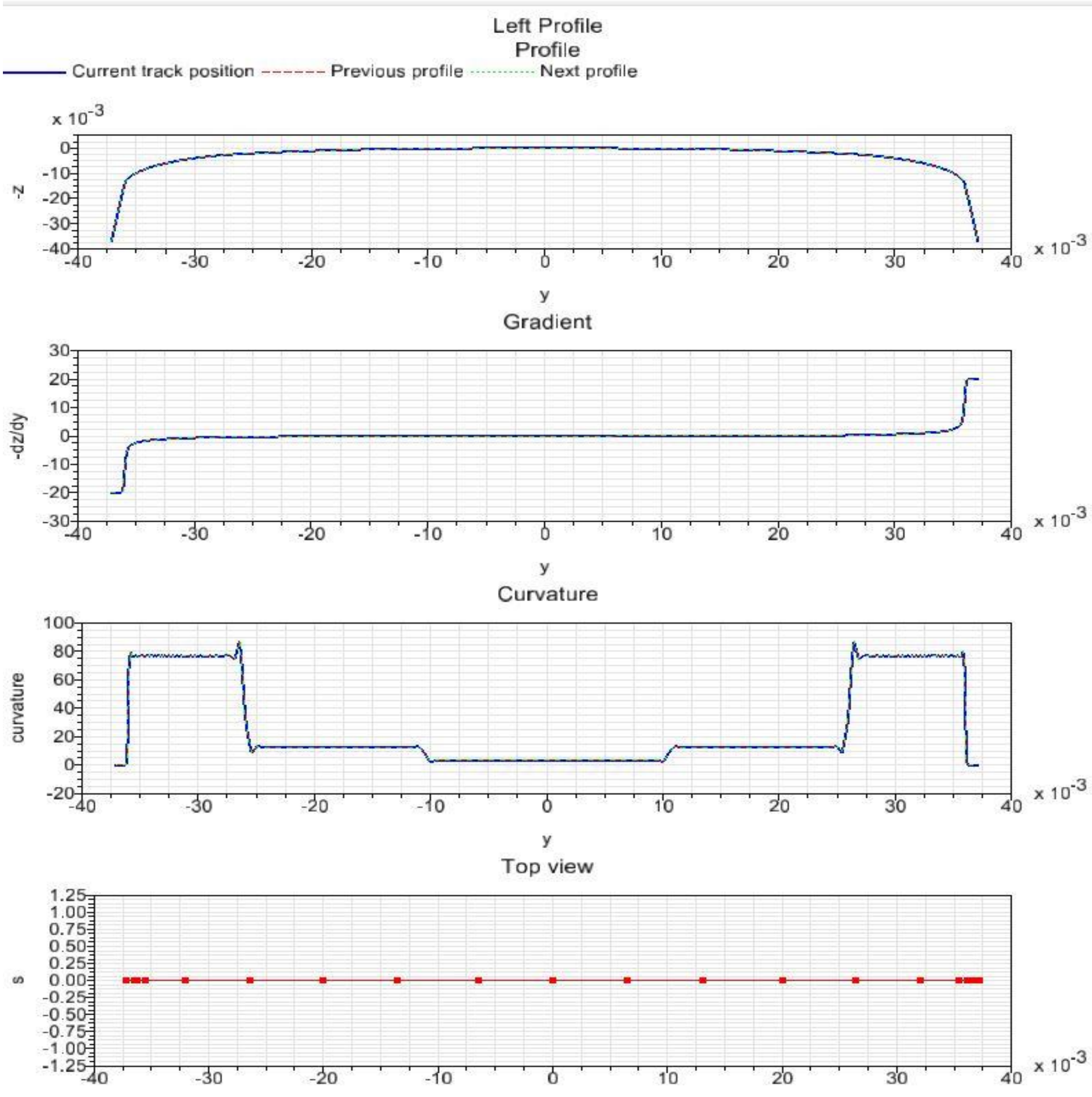

Left rail profile

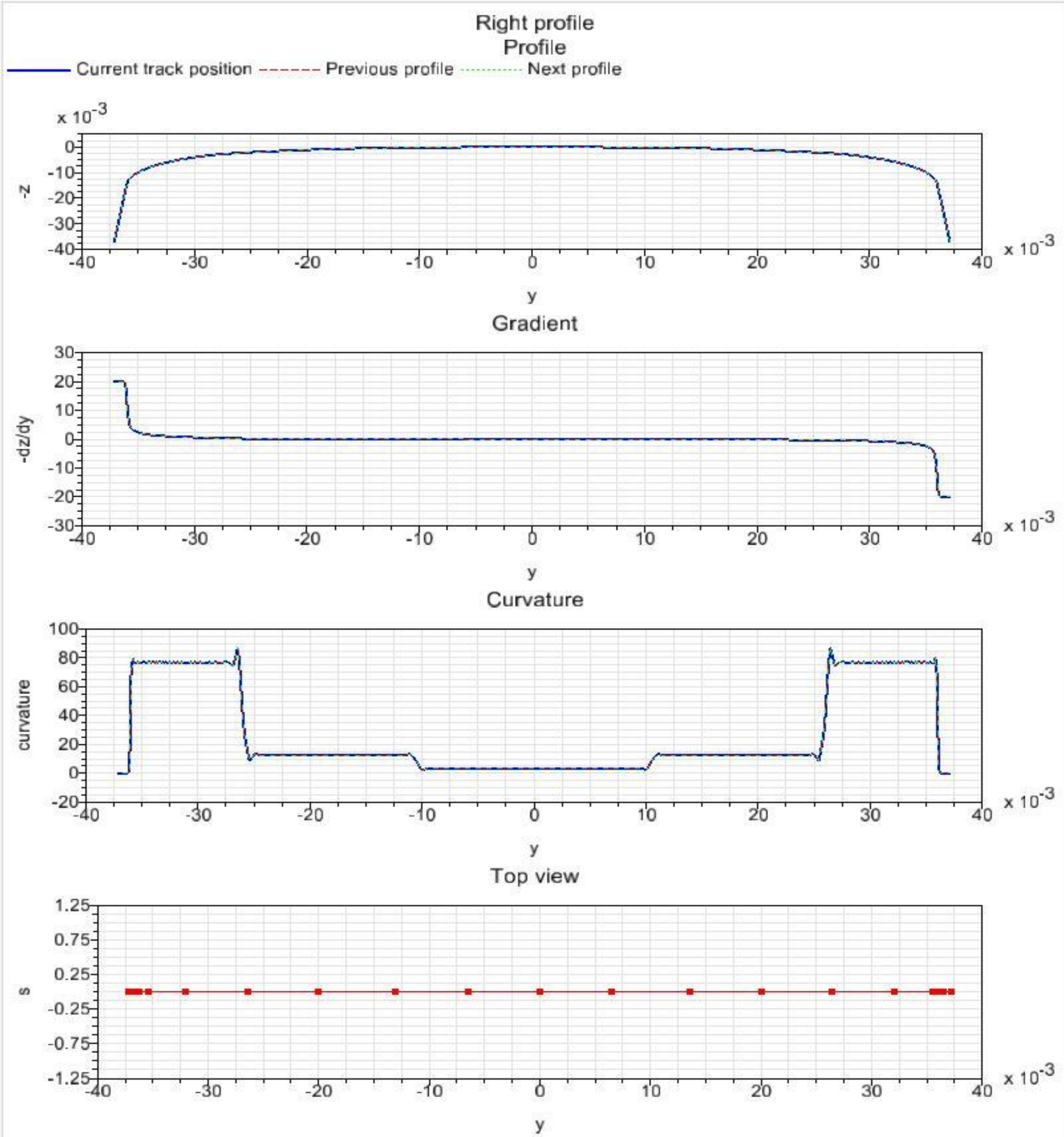

Right rail profile

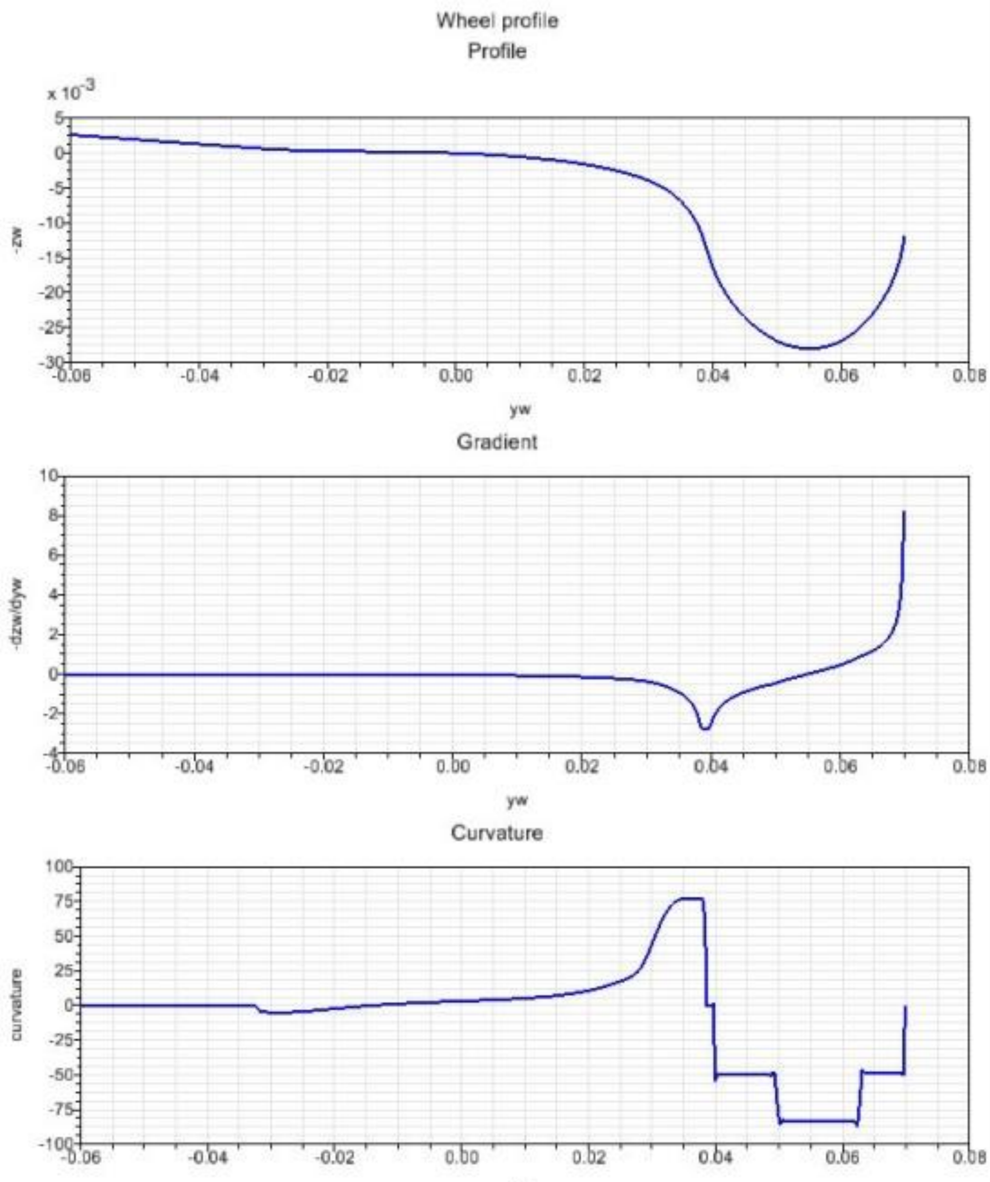

Rear left wheel profile

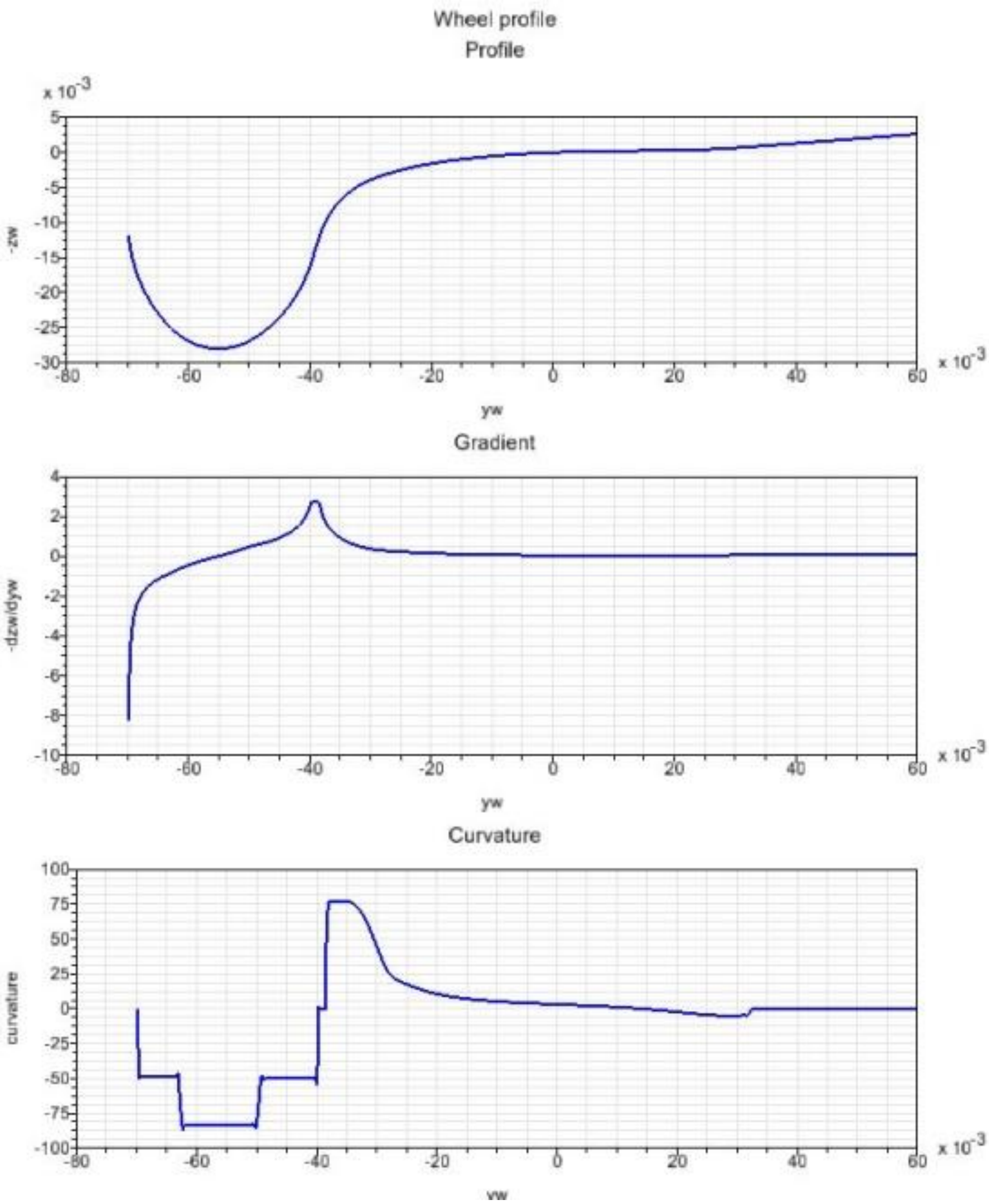

Rear right wheel profile

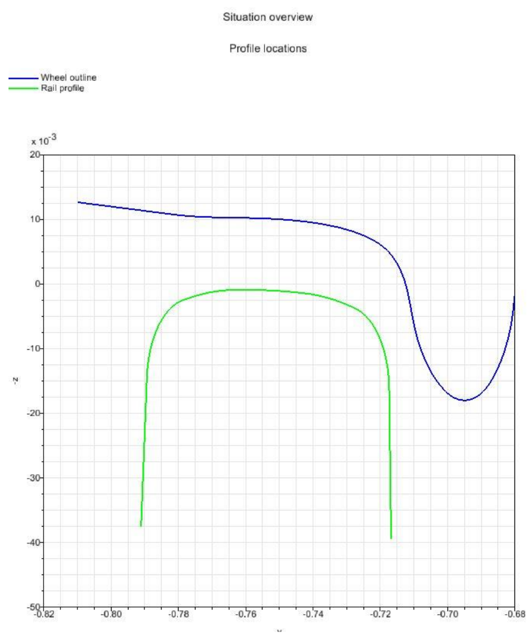

a

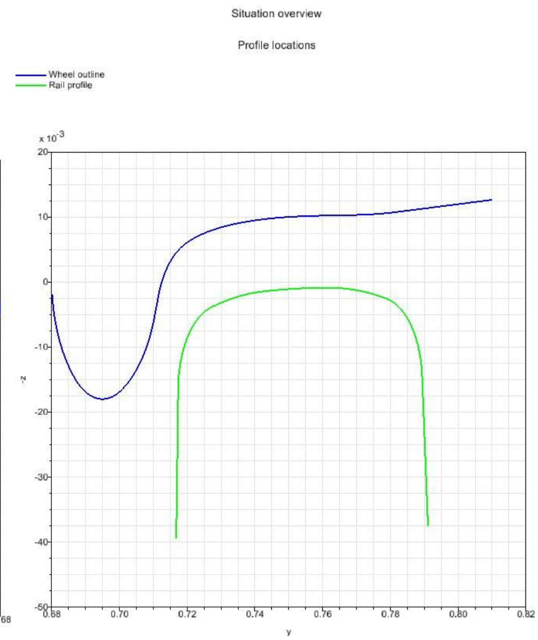

b

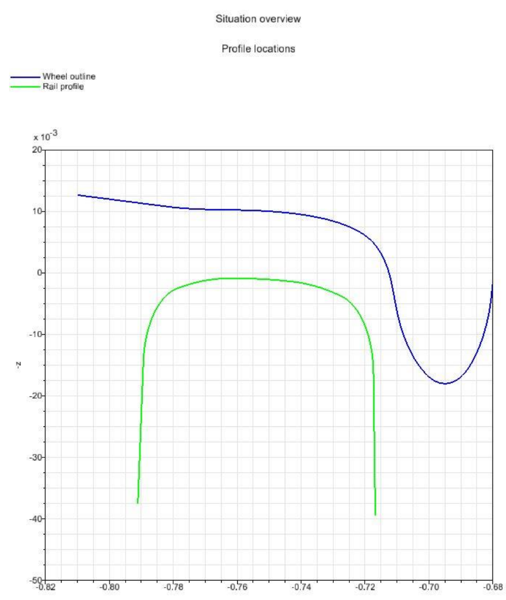

c

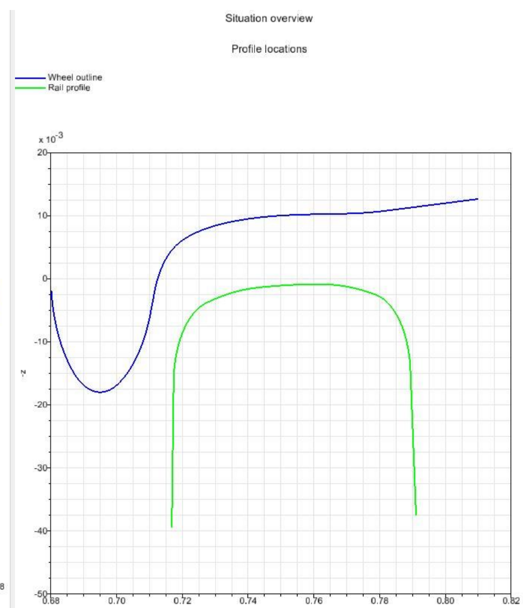

d

Situation over view profile location of a) front left, b) front right, c) rear left, and d) rear right

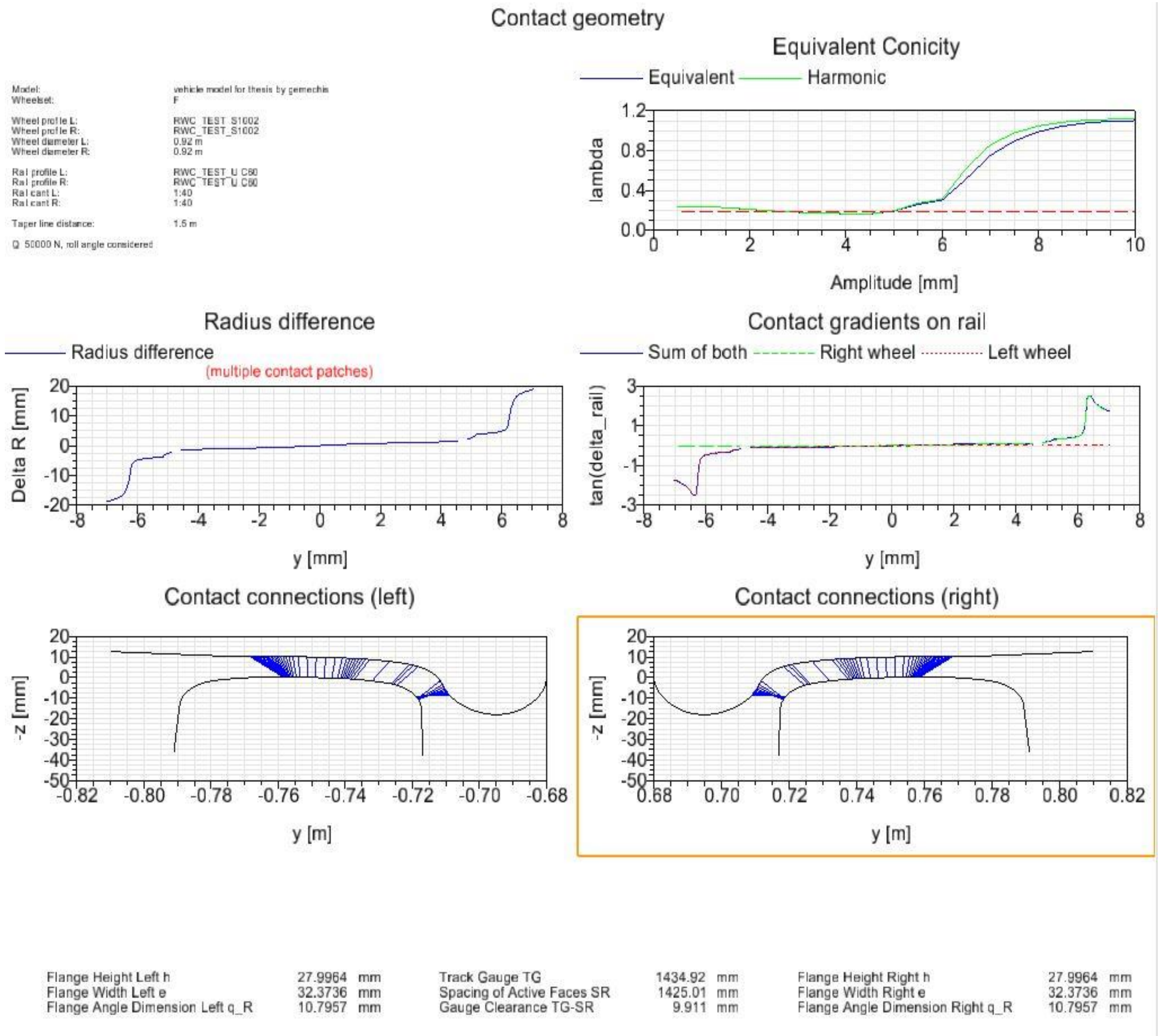

Wheel and rail profile (wheel-rail contact geometry)

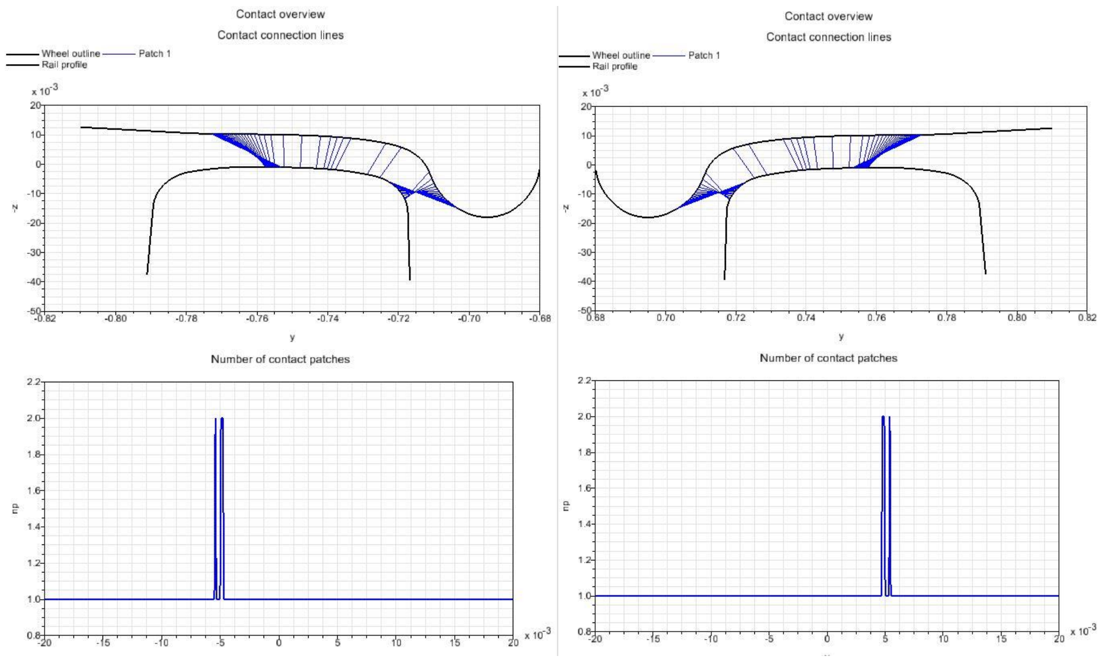

Contact over view contact connection line front left and front right (wheel-rail pair)

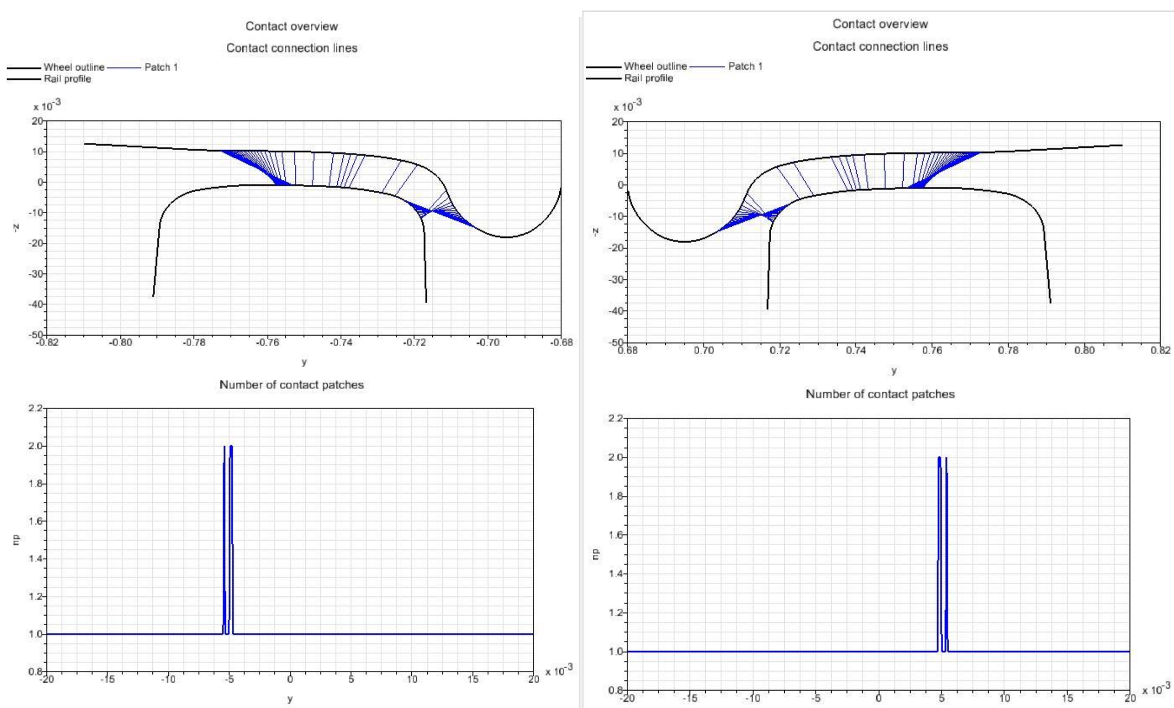

Contact over view contact connection line rear left and rear right (wheel-rail pair)

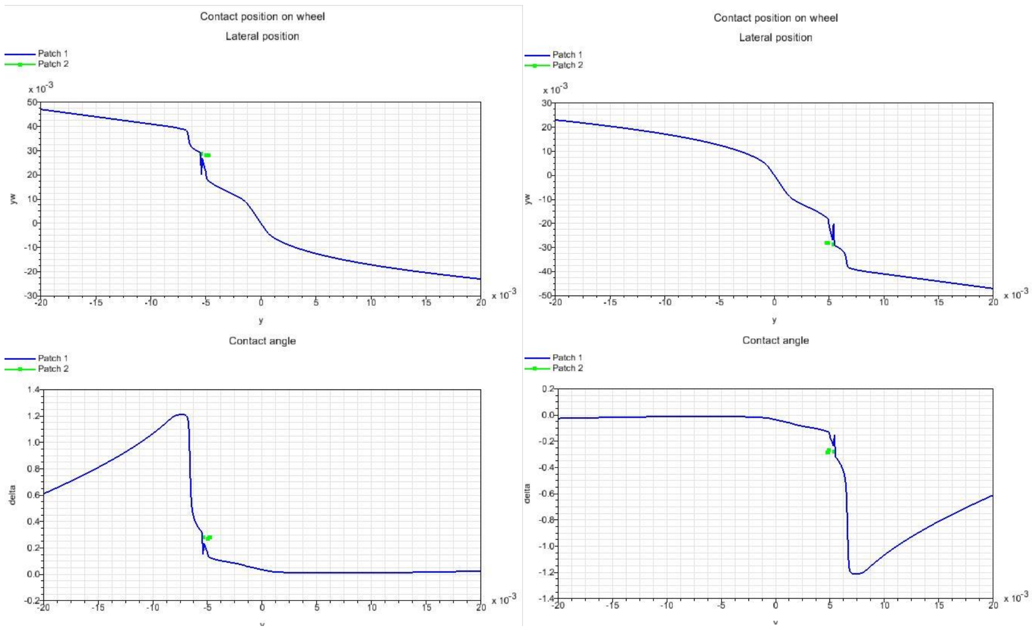

Contact position (lateral position) on front left and front right wheel

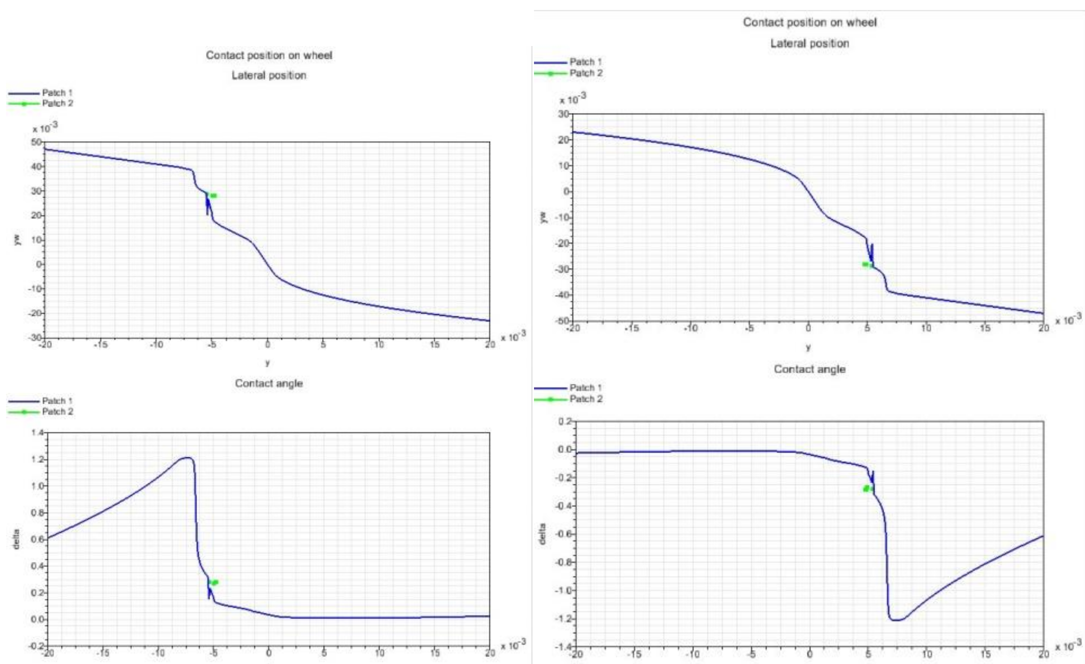

Contact position (lateral position) on rear left and rear right wheel

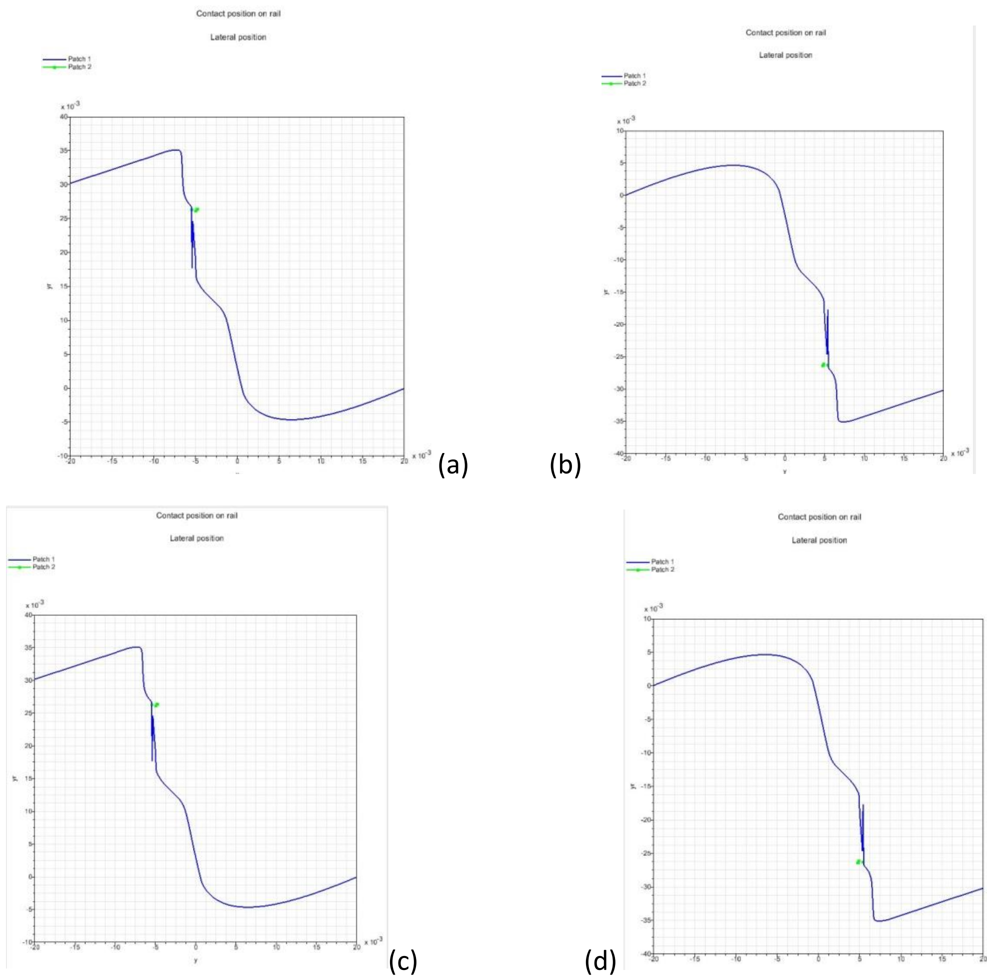

Contact position (lateral position) on (a) front left, (b) front right, (c) rear left, (d) rear right rail

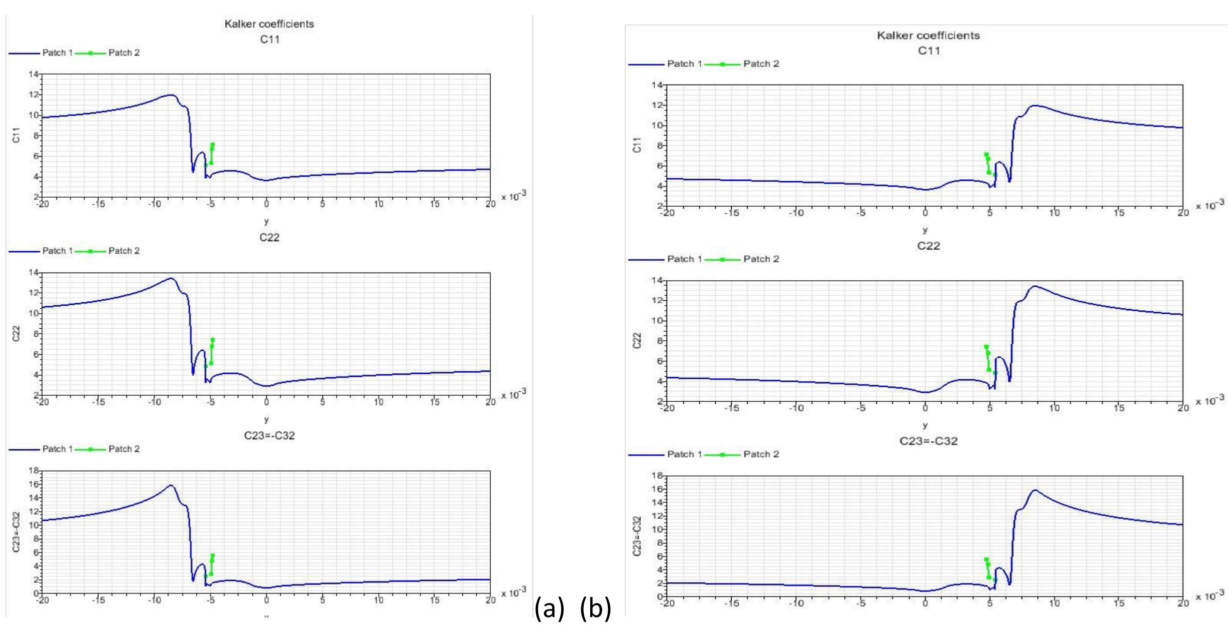

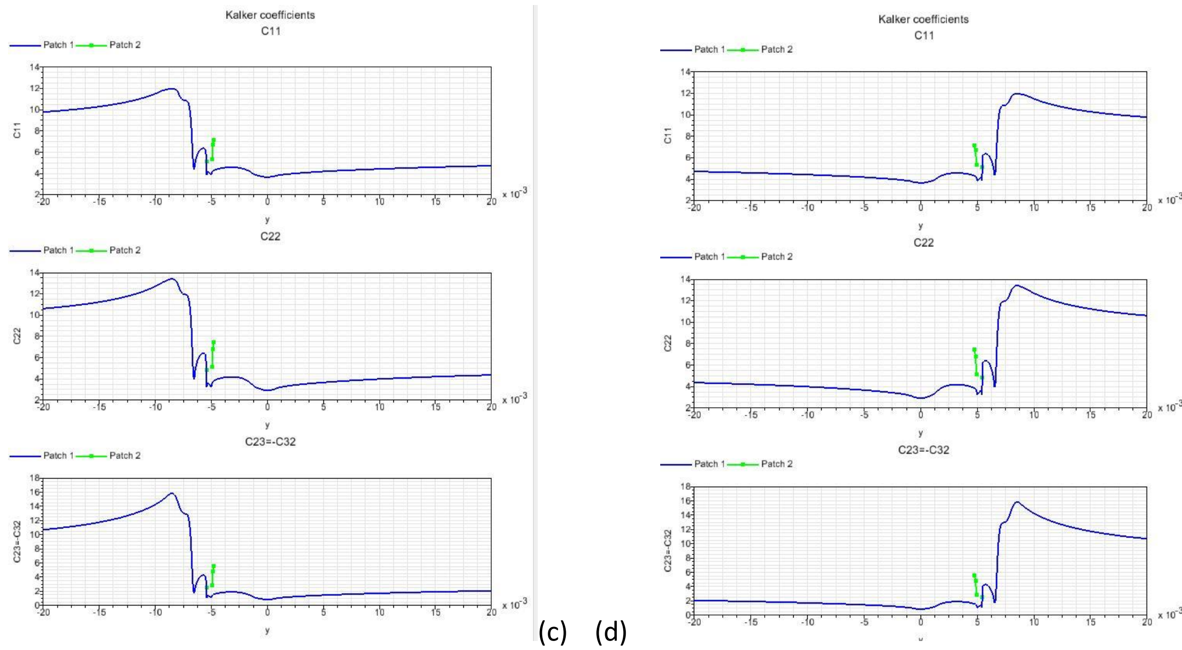

(c) (d)

Kalker coefficients (a) front left, (b) front right, (c) rear left, (d) rear right

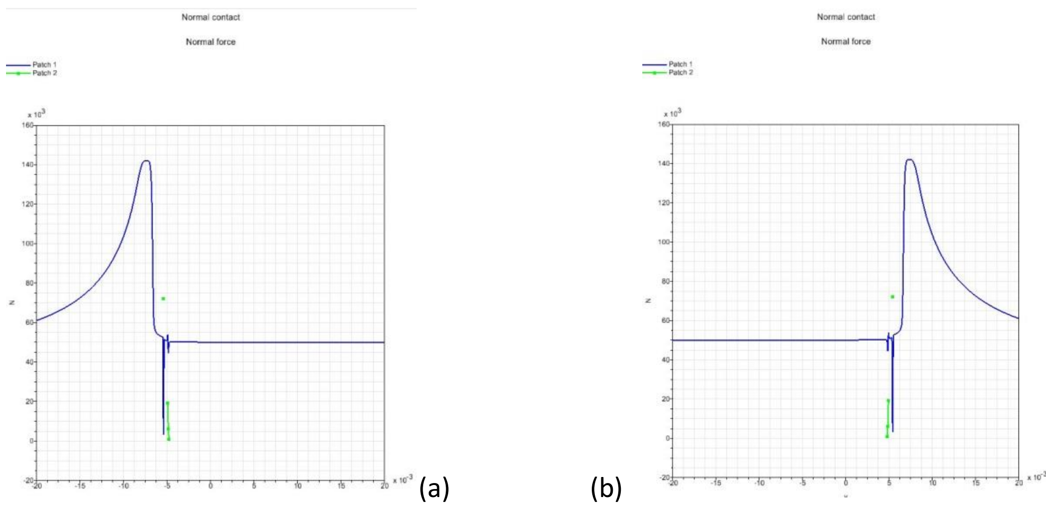

(a) (b)

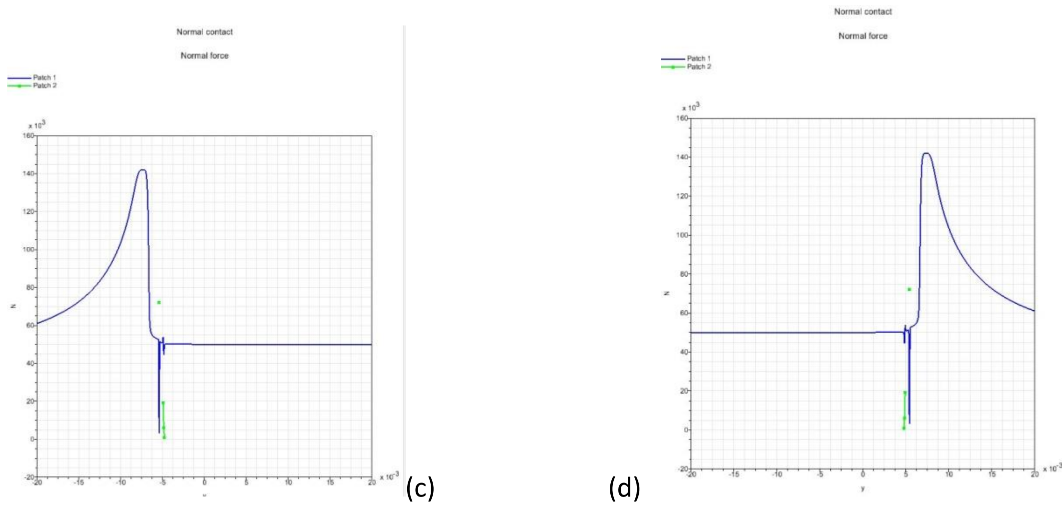

Normal contact force (a) front left, (b) front right, (c) rear left, (d) rear right

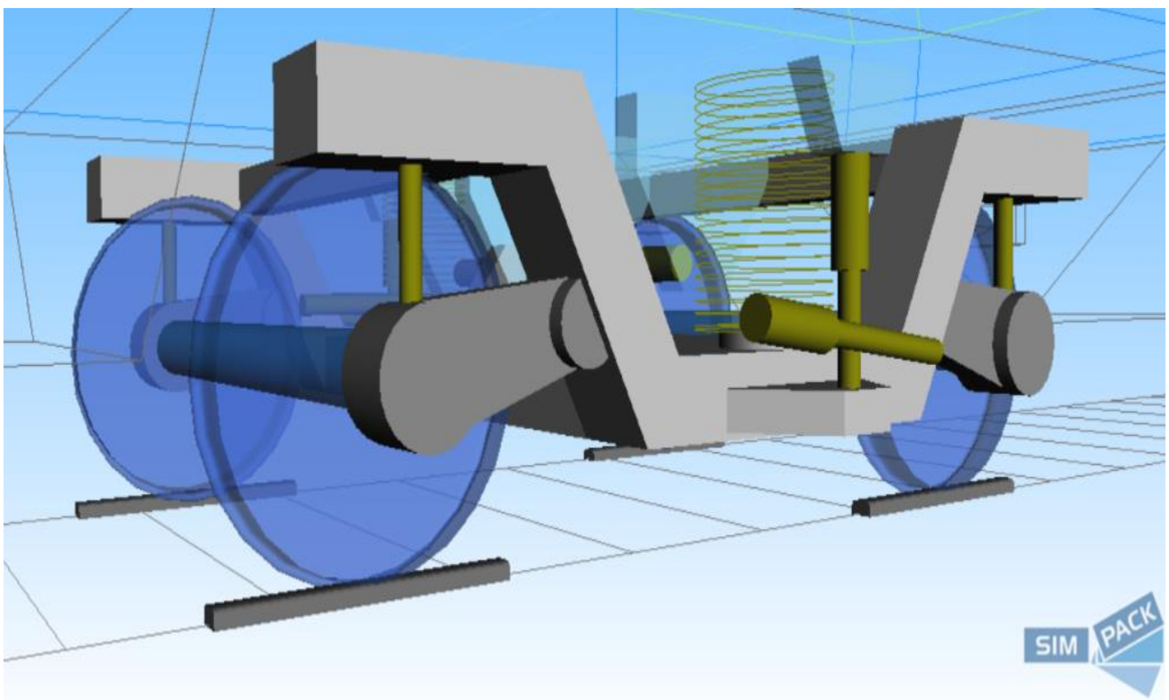

Detail view of the bogie (truck) with rail-wheel profiles

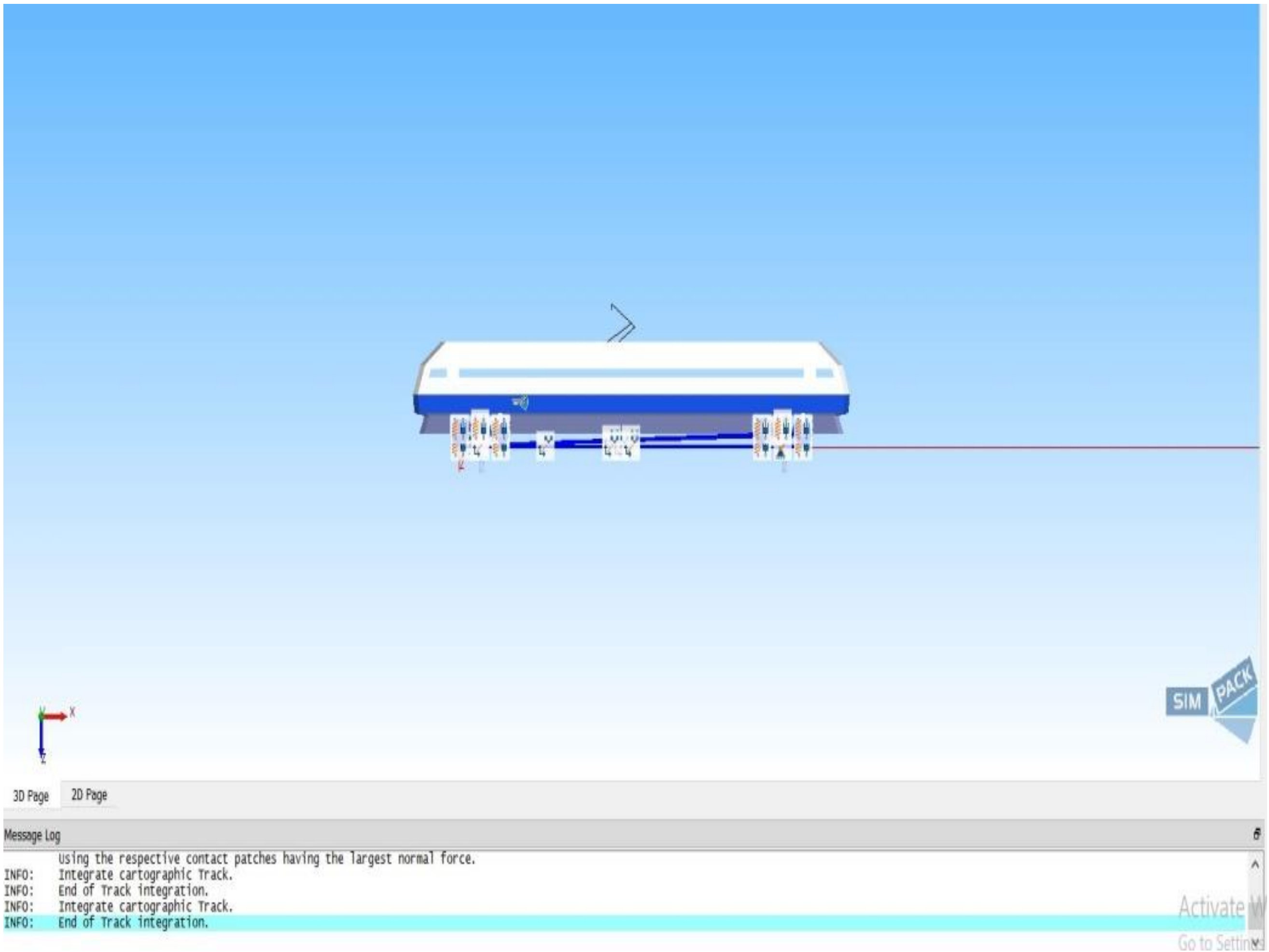

Side view of the rail vehicle

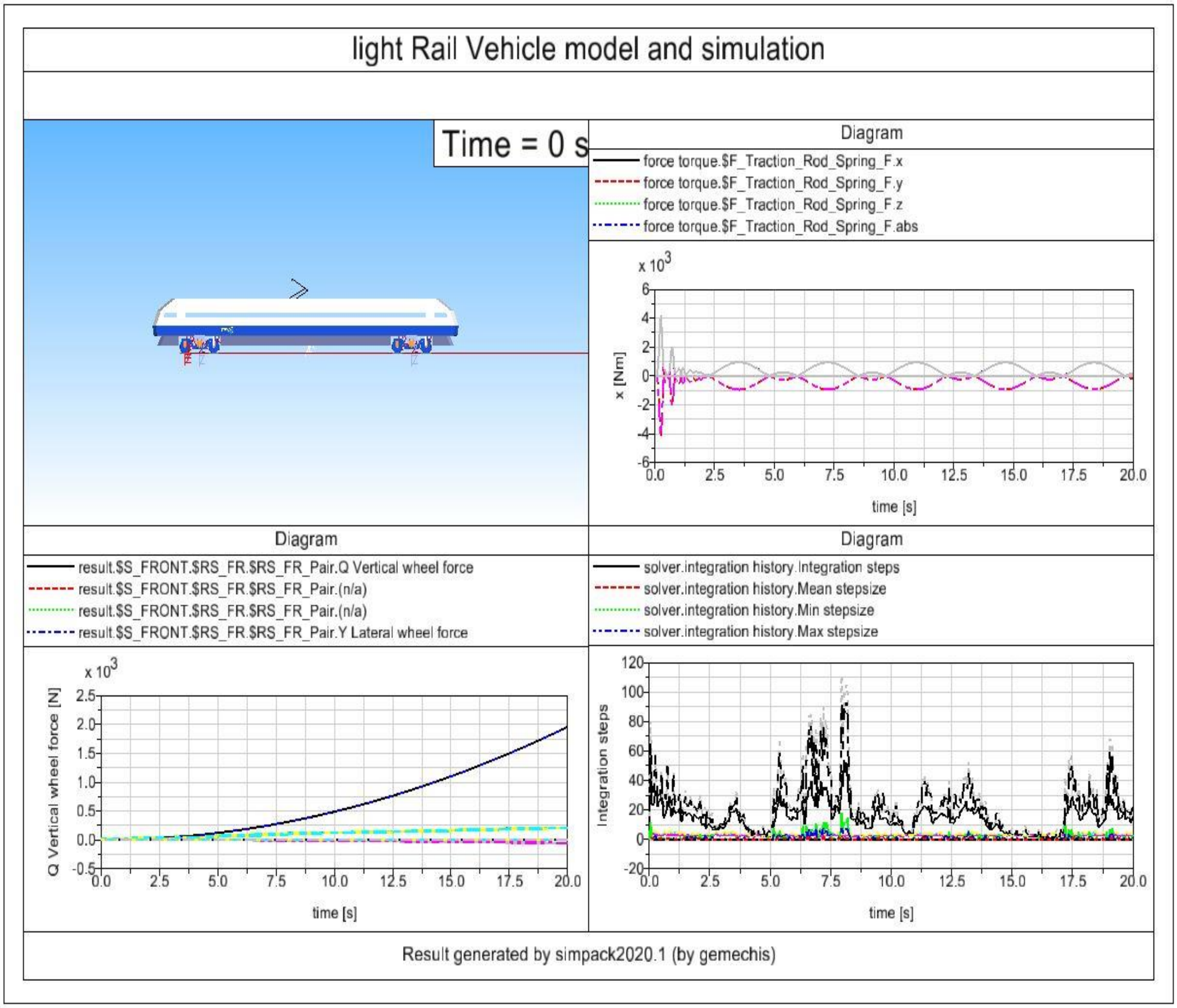

Figure 1. Light rail vehicle model and simulation

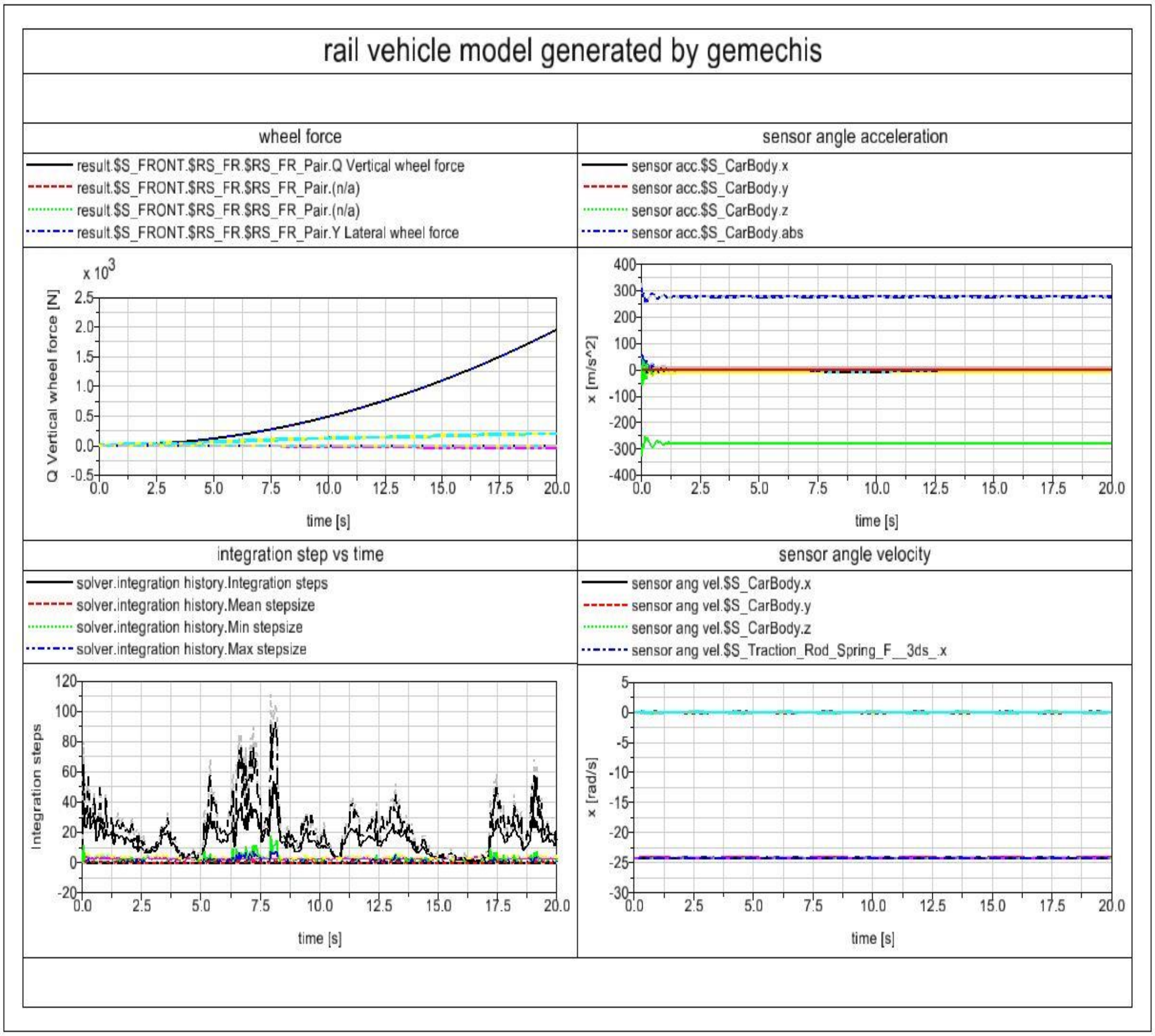

Integration vs time graph